# Significance of white matter anatomy in interpreting features and behaviour of low-grade gliomas and implications for surgical treatment.

FRANCESCO LATINI

Dissertation presented at Uppsala University to be publicly examined in C11, Rudbeckssalen, Rudbeck entréplan, Dag Hammarskjölds Väg 20, 752 37, Uppsala, Friday, 4 June 2021 at 13:00 for the degree of Doctor of Philosophy (Faculty of Medicine). The examination will be conducted in English. Faculty examiner: Professor Lorenzo Bello (University of Milan, Italy).

**Abstract**

Latini, F. 2021. Significance of white matter anatomy in interpreting features and behaviour of low-grade gliomas and implications for surgical treatment. *Digital Comprehensive Summaries of Uppsala Dissertations from the Faculty of Medicine* 1744. 112 pp. Uppsala: Acta Universitatis Upsaliensis. ISBN 978-91-513-1189-0.

Diffuse gliomas are extremely heterogeneous tumours characterized by slow growth but extensive infiltration. Their kinetic features reflect the complex interaction over time with the surrounding brain, influencing treatment planning and outcome. Indeed, resection of diffuse gliomas present a surgical challenge due to their invasiveness and the preferential location in eloquent regions. White matter bundles are the main eloquent limit to surgical resection, but this anatomical-functional information cannot be predicted preoperatively on the individual level. The incomplete description of the human brain connectome, the complex application of pathological/lesion model to the brain connectomic organization, and the underestimated role of white matter anatomy in radiological classification systems are among the major limitations for the comprehension of the glioma/white matter interaction. The overall aim of this thesis was to explore a new approach and new techniques to study the glioma/white matter interaction. A combination of white matter dissection and diffusion tensor tractography (DTT) was used to describe the connectomic organization of two major temporo-occipital connections, the inferior and the middle longitudinal fasciculus. This information was applied to patients with diffuse gliomas, demonstrating how white matter analysis was important to decode patient specific cognitive and language impairment. A new classification system for diffuse gliomas, the Brain-Grid, was created, merging local radiological anatomy with a DTT atlas for infiltration analysis. This standardized radiological tool provided information on subcortical extension (tumour invasiveness), speed, and preferential direction of glioma progression. Applied to a larger cohort of patients, differences were detected between diffuse gliomas subtypes. Tumour invasiveness and the preferential location, type, and extent of white matter involvement differed, impacting overall survival. Regional differences in white matter infiltration were detected among five major white matter bundles, and possible favourable morphological and diffusion features were investigated with transmission electron microscopy and DTT. Fibre diameter, myelin thickness, and the organization of the white matter fibres were different in regions with high infiltration frequency, providing a possible link to the preferential location of diffuse gliomas. Finally, the white matter connectivity, tumour-induced neuroplasticity, clinical and demographic information, preoperative assessment (neuropsychological and language evaluation) were compared with intraoperative findings during awake surgery. Neuropsychological impairment was associated with more invasive tumours and a higher risk of the intraoperative finding of eloquent tumour. The pattern of early cortical neuroplasticity seemed exhausted at the time of diagnosis, with age as a factor predicting the neuroplasticity potential. The combined use of these new techniques revealed new insights into the glioma/white matter interaction. The results provided in this thesis, describe a new way to structure the multidisciplinary perioperative management of these patients. This new information may improve the functional outcome at the individual level, resulting in prolonged survival for adults with diffuse gliomas.

*Keywords:* White matter; Cerebral gliomas; DTI; Brain-Grid; Brain mapping; Human connectome project

*Francesco Latini, Department of Neuroscience, Enblad: Neurosurgery, Akademiska sjukhuset, ingång 85 2 tr, Uppsala University, SE-751 85 Uppsala, Sweden.*

*Dedicated to my parents*

# List of Papers

This thesis is based on the following papers, which are referred to in the text by their Roman numerals.

I.     **Latini F**, Mårtensson J, Larsson EM, Fredrikson M, Åhs F, Hjortberg M, Aldskogius H, Ryttlefors M. (2017) Segmentation of the inferior longitudinal fasciculus in the human brain: A white matter dissection and diffusion tensor tractography study. Brain Res. 2017 Nov 15; 1675:102-115.

II.    **Latini F**, Trevisi G, Fahlström M, Jemstedt M, Alberius Munkhammar Å, Zetterling M, Hesselager G, Ryttlefors M. (2021) New insights into the anatomy, connectivity, and clinical implications of the middle longitudinal fasciculus. Front. Neuroanat. 2021. 14:610324.

III.    **Latini F**, Fahlström M, Berntsson SG, Larsson EM, Smits A, Ryttlefors M. (2019) A novel radiological classification system for cerebral gliomas: The Brain-Grid. PLoS One. 2019 Jan 24;14(1): e0211243.

IV.    **Latini F**, Fahlström M, Hesselager G, Zetterling M, Ryttlefors M. (2020) Differences in the preferential location and invasiveness of diffuse low-grade gliomas and their impact on outcome. Cancer Med. 2020 Aug;9(15):5446-5458.

V.    **Latini F**, Fahlström M, Beháňová A, Sintorn IM, Hodik M, Staxäng K, Ryttlefors M. The link between gliomas infiltration and white matter architecture investigated with electronic microscopy and diffusion tensor imaging. Submitted.

VI.    **Latini F**, Axelson H, Fahlström M, Jemstedt M, Alberius Munkhammar Å, Zetterling M, Ryttlefors M. (2021) Role of Preoperative Assessment in Predicting Tumor-Induced Plasticity in Patients with Diffuse Gliomas. J. Clin. Med. 2021, 10, 1108. https://doi.org/10.3390/jcm10051108

Reprints were made with permission from the respective publishers.

# Contents

# Abbreviations

| | |
|---|---|
| AD | Axial diffusivity |
| AF | Arcuate fasciculus |
| AC | Anterior commissure |
| ATR | Anterior thalamic radiation |
| BG | Brain-Grid |
| Ci | Cingulum |
| CC | Corpus callosum |
| CNS | Central nervous system |
| CSF | Cerebrospinal fluid |
| CST | Cortico-spinal tract |
| DG | Diffuse gliomas |
| DLGG | Diffuse low-grade gliomas |
| DSI | Diffusion spectrum imaging |
| DTI | Diffusion tensor imaging |
| DTT | Diffusion tensor tractography |
| DWI | Diffusion-weighted imaging |
| EOR | Extent of resection |
| FA | Fractional anisotropy |
| FACT | Fibre assignment by continuous tracking |
| FAT | Frontal aslant tract |
| FLAIR | Fluid attenuated inversion recovery |
| Fo | Fornix |
| HCP | Human connectome project |
| HGG | high-grade gliomas |
| IC | Internal capsule |
| ILF | Inferior longitudinal fasciculus |
| IFOF | Inferior fronto-occipital fasciculus |
| LGG | Low-grade gliomas |
| MD | Mean diffusivity |
| MdLF | Middle longitudinal fasciculus |
| MRI | Magnetic resonance imaging |
| OR | Optic radiation |
| OS | Overall survival |
| PET | Positron emission tomography |
| PFS | Progression free survival |
| PS | Penfield Stimulation |

rCBV Regional cerebral blood volume
RD Radial diffusivity
ROI Region of interest
SLF Superior longitudinal fasciculus
SMA Supplementary motor area
SSS Sagittal stratum of Sachs
STG Superior temporal gyrus
STS Short train Stimulation
TE Echo time
TEM Transmission Electron Microscopy
ThR Thalamic radiation
TR Repetition time
UF Uncinate fasciculus
VOF Vertical occipital fasciculus
WHO World health organization
WM White matter

Native space = patient-specific space

Montreal Neurological Institute (MNI) space = space defined by the MNI template

Spatial normalization = the process by which images are transferred from native to the MNI space

# 1. Introduction

## 1.1. Study of White Matter Anatomy

### 1.1.1. Historical background

Since Galen of Pergamum, who first described the corpus callosum and fornix in animals, the study of cerebral white matter (WM) has aroused the interest of anatomists of every century [1–3]. Many different techniques for specimen preparation and ex vivo dissection have been used during the centuries in an effort to understand the complex WM architectural organization of the brain [1,2,4]. The major credit for the description of the modern anatomy of WM pathways falls to Meynert (1833–92), who was the first to recognize the important functional role played by fibres connecting different parts of a single hemisphere, which he termed association fibres. He was also the first to classify WM fibres into three groups: projection fibres (the ascending or descending pathways arising and terminating in the cortex), commissural fibres (which connected cortex in both hemispheres) and association fibres (which connected cortical regions within a hemisphere) [5,6].

However, it was the contribution of Joseph Klingler that permitted 3-dimensional (3D) visualization of the trajectories of certain WM fasciculi, making the study of WM more feasible and widely undertaken [1,4,7]. Klingler developed a new method of brain fixation, which consisted of freezing already formalin-fixed brains before dissection [7,8]. The water crystallization induced by freezing disrupts the structure of the grey matter (which has a high-water content), making it possible to peel off the cortex from the brain surface. The freezing process also spreads along the WM fibres, inducing separation between them, which facilitates dissection by progressive peeling of the fibres [1,3,4,9]. With his work, Klingler's preparations won the attention of neurologists and neurosurgeons, but they have also resulted in advances in the study of the inner topography of the brain. Dissection methods and descriptions, however, are necessarily invasive and therefore unsuitable for the study of living human subjects in a clinical environment.

One of the most important advances in modern neuroscience regarding the study of WM came with the development of magnetic resonance imaging (MRI) and diffusion tensor imaging (DTI) based on the differences in self-diffusivity of water in different regions of the brain[10]. With this technique it was possible to extrapolate the self-diffusivity of water in grey matter (which

appears to be the same in all directions, i.e., "isotropic"), the self-diffusivity of cerebro-spinal fluid (CSF) in the ventricles (the same in all directions but increased compared to the grey matter), and the diffusivity in WM (much less hindered along the long axes of ordered axons than perpendicular to the long axes, where molecules take a more tortuous route, i.e., "anisotropic") [10,11]. Basser et al. [12,13] showed how this self-diffusion tensor could be estimated noninvasively in each voxel of a MR image data set, with a technique called diffusion tensor MRI (DT-MRI). For each voxel, it is possible to calculate the trace that provides a rotationally invariant estimate of diffusivity [12]; various measures of diffusion anisotropy [12,14,15], which reflect the degree of tissue structure; and the orientation of the diffusion tensor [14,15], which has been shown to be parallel to the dominant orientation of anisotropic structures in vivo. Makris et al. [16] used colour-coded fibre orientation images (derived from DT-MRI data), combined with a priori knowledge of the location and pathways of WM fasciculi, to produce a series of 2-dimensional coronal images within which the major fasciculi could be identified. However, visualization was still 2-dimensional with consequent difficult orientation. The more advanced DT-MRI fibre tracking or "tractography" [13,17–19] aimed to reconstruct the 3D trajectories of WM tracts by following a continuous path of greatest diffusivity (i.e., least hindrance to diffusion) through the brain from an initial set of "seed points." Diffusion tractography is nowadays the only non-invasive technique for localizing cerebral WM fibre tracts in humans, and it is widely used in both clinical practice and research to evaluate fibre tract pathways [20]. On the other hand, DTI-based tractography oversimplifies fibre tract anatomy because it only considers a single direction of diffusion per voxel [21]. Although tractography has been used for pre-operative planning and per-operative navigation in patients with cerebral tumours [22,23], it can suffer from a lack of reliability [24,25]. Diffusion tractography relies on complex acquisition methods and post-processing mathematical models that provide anatomical information indirectly and therefore need to be validated. Since a good correlation between WM dissection and diffusion tractography is generally accepted [21], direct comparison between human anatomy with Klingler's technique and human MR tractography is often utilized as the gold standard combination for confirmation of complex cerebral anatomy [21,26–29].

## 1.1.2. Connectomic organization of brain circuits and surgical implications

In the past decades, a significant progress in understanding the anatomic and functional organization of the brain has been achieved thanks to important conceptual and methodological advances. New reliable biological models have been formulated regarding the basis of brain processing and have contributed to a clarification of the relationship between anatomy and function

[5,6,30,31]. It is accepted that the central nervous system (CNS) is organized as a complex, large-scale, and dynamic global network [5,6,10,30–33]. The basic concept underlying the modern view of cognitive neurosciences is brain connectivity, which in anatomical terms, corresponds to the axonal extensions of neurons [34,35]. According to this principle, the CNS is organized in a complex network of multiple distinct neural circuits, the connectome, with higher brain functions being the result of their interactions [30,36–40]. In this view, a pathological process not only concerns the anatomic region directly affected by the tumour, but also affects the global and regional nature of the structural and functional architecture of the brain. The result is that each brain lesion may affect cognitive functions in different ways in accordance with the inter-individual anatomic and functional variability and natural history of that lesion[30,41]. Recent methodological advances in anatomic subcortical characterization have highlighted the important role of the WM in clarifying how cortical skills are combined in the short and long term. Consequently, in the economy of brain processing, the functional contribution of a given area depends on its integration with the activity of anatomically interconnected regions. The global cognitive result arises from a large-scale orchestration between topography (study of cortical functional epicentres) and hodology (study of connectivity between areas)[30,42,43]. This so-called hodotopic framework includes grey and WM as parts of the same interactive process [6,32,43–46]. According to this concept, complex, multimodal, and integrated parallel distributed networks form the architecture of the CNS, with cognitive processes consisting of a continuous and often redundant stream of information dynamically modulated by experience and the external environment [47]. In hodotopic terms, a given cortical region can be supported by four main types of connectivity: (1) loco-regional WM connectivity, mediated through U-fibres, which influences the phenomenon of functional perilesional compensation; (2) subcortical WM connectivity, which connects different regions of both hemispheres through the association pathways (horizontal connectivity); (3) interhemispheric WM connectivity, which ensures the connection between anatomically similar or different regions of the two hemispheres through commissural fibres; and (4) the vertical WM connectivity, mediated by projection fibres, which allows the modulation of cortical processing by deep grey nuclei and the brain stem [5,30,43]. Applying this framework to preoperative, intraoperative, and postoperative mapping techniques, the neurosurgeon is able to explore the individual anatomical-functional brain architecture, including higher neurocognitive aspects[30,32,41]. Thus, it is finally possible to adapt the surgical approach specifically to each patient and to each lesion according to its individual organization. A better comprehension of the anatomical-functional architecture of the brain opens up the possibility of removing regions traditionally considered inoperable without inducing permanent deficits and the potential use of these areas as a safe passage to deeper territories [33]. One major limitation exists for the universal application of this method: the incomplete understanding of the

brain connectome. Not all the identified WM networks and connections have been described in detail and/or are fully understood. Several major WM bundles, already described by anatomical studies, have only recently been decoded in functional terms [26,46,48]. The study of the WM connectivity through dissection and neuroimaging is, therefore, of paramount importance for the deeper comprehension of the relationship between brain and mind.

# 1.2. Diffuse gliomas

## 1.2.1. 2016-WHO classification of diffuse gliomas

Diffuse gliomas (DGs) are primary brain tumours which comprise approximately 30% of all primary CNS tumours and 80% of malignant brain tumours [49,50]. According to the 2016-WHO classification of brain tumours [51], DGs (whether astrocytic or oligodendroglial) are grouped together, based not only on their growth pattern and behaviours, but also more pointedly on the shared genetic driver mutations in the *IDH1* and *IDH2* genes.

In this recent classification, the DGs include WHO grade II and grade III astrocytic tumours, grade II and III oligodendrogliomas, and grade IV glioblastomas (GBMs). WHO grade II diffuse astrocytomas and WHO grade III anaplastic astrocytomas are divided into the following categories: IDH-mutant, IDH-wildtype, and Not Otherwise Specified (NOS) (when IDH status is not available). The diagnosis of oligodendroglioma and anaplastic oligodendroglioma requires the demonstration of both an IDH gene family mutation and combined whole-arm losses of 1p and 19q (1p/19q codeletion). In the absence of testing capabilities or in the setting of inconclusive genetic results, a histologically typical oligodendroglioma should be considered as NOS.

However, in this thesis GBMs (either primary or secondary) are not considered due to their different natural course, different interaction with the brain, and different functional effects on brain structure in comparison with other gliomas [52,53], and therefore only WHO grade II and III gliomas are included because they represent the best model to study brain plasticity and WM/gliomas interaction. In this thesis the term DGs refers to astrocytic or oligodendroglial tumours (WHO grade II and WHO grade III and NOS). The term diffuse low-grade gliomas (DLGGs) refers specifically to WHO grade II astrocytic or oligodendroglial tumours.

## 1.2.2. Epidemiology and natural history of DLGG

DLGGs are WHO grade-II tumours, characterized by slow growth but extensive infiltration. The incidence of DLGGs is estimated to be 1/100 000 persons/year [54]. They occur mainly in young and middle-aged adults, with a peak

incidence around 30–35 years of age [55]. The clinical course of DLGG is diverse, but all tumours eventually recur or transform into high-grade gliomas (HGGs) and will ultimately lead to death [51,56–58]. The median survival from diagnosis is approximately 7 years [55,59,60].

The natural course of DLGGs consists of a silent period, followed by a symptomatic period and a subsequent progressive phase [57,61]. During the silent period, the slow growth of the tumour allows cortical adaption mechanisms enabling functional and morphologic reorganization of the brain, and neurologic deficits are usually absent at disease onset [62]. However, incidental DLGGs have growth dynamics similar to symptomatic DLGGs, and they continue to grow even during symptom-free intervals [58]. Over time, the tumour tends to interfere with normal brain function by disrupting the functional connectivity of brain networks within peritumoral and distant brain areas, promoting seizure activity [63,64] or impairment of high cognitive functions [65–67]. During the symptomatic phase, diagnosis is, however, based on radiological findings that identify a suspected lesion with specific MRI characteristics that depend on hyperintensity in fluid-attenuated inversion recovery (FLAIR) sequences and/or contrast enhancement [57,68–70]. Several studies have shown that DLGGs continue to grow during symptom-free intervals [56,58]. The continuous growth during the low-grade phases (either treated or untreated) leads to malignant transformation in the progressive stage of the disease, ultimately leading to recurrent tumours or death [56,58]. The time to malignant transformation differs considerably between patients, but it strongly affects the overall survival [71,72], with a median survival of 1 to 2 years for those patients who display features of high-grade gliomas. The differences in growth rate, the complex growth patterns, preferential locations, and the resilience of gliomas also suggest that these lesions do not behave as randomly organized and diffuse cell masses [73].

Several studies have described DLGGs as being located preferentially in "secondary" functional areas (immediately near the so-called primary eloquent regions), especially within the SMA (supplementary motor area) and the insular lobe. This preferential localization has been explained as being due to developmental, cyto- and myeloarchitectonic, neurochemical, metabolic, and functional reasons [68,74,75]. Other studies have suggested differences in the molecular biology of DLGGs as the reason for differences in tumour location [76–78], with a higher rate of 1p deletion in the anterior part of the brain (in particular in the frontal lobe) [78] and a lower rate in the insula [77], or the absence of IDH1 mutation within the insula [76] and its presence in tumours located within the frontal lobe [79].

The combination of clinical parameters with molecular tumour markers is now improving our comprehension of the heterogeneity of DLGGs. However, their heterogeneity, their interaction with the brain connectome, and their variable

clinical presentation make DLGGs among the most challenging lesions to treat.

## 1.2.3. Radiological assessment in Diffuse gliomas

MRI is fundamental to the characterization of brain tumours, guides the surgical strategy, and it is required to monitor treatment response. A conventional MRI protocol consisting of T2-weighted (T2W), T2 Fluid attenuated inversion recovery (T2-FLAIR) (in low slice thickness ($\leq 3$ mm) to facilitate volumetric assessment), diffusion sequences (DWI) and pre- and post-contrast T1-weighted (T1W) has been recommended as standard glioma imaging practices [80,81]. Morphological MRI sequences (volumetric T1W, T2W, and T2-FLAIR) are used in clinical practice to assess brain tumour location, tumour volume and heterogeneity, mass effect, contrast enhancement, and the presence of multiple brain lesions [80–82].

Using morphological sequences, the standard radiological classification of gliomas is based on the nomenclature of the major lobes invaded and less often by their subcortical extension [57,70,83]. These sequences are also used to observe glioma kinetics with 3D-volume segmentation by comparing tumour progression on MRI at different times (in the absence of or after specific treatment) [57,58,84,85].

Diffusion sequences (DWIs) show the normal or abnormal displacement of water molecules reflecting tissue microstructure [18,20]. DWIs can non-invasively contribute to estimating tumour cellularity and grade [86–88] and support the assessment of therapy response, although as a single modality its accuracy appears limited for the distinction of tumour and radiation effects [89,90].

Perfusion sequences can be useful to assess the blood flow through tissues and vessels, thereby revealing barrier damage [91–93]. With this technique, HGGs can be differentiated from DLGGs using regional cerebral blood volume (rCBV) values, with high (95%) sensitivity but with relatively low (70%) specificity [94,95].

Among the advanced imaging methods, DTI studies have led to important advances in the non-invasive diagnosis of gliomas' infiltration/dislocation of WM tracts [96–100]. However, there are still important limitations (operator-dependent variables, scan dependent, algorithm related, peritumoral tissue abnormalities, post-radiation WM abnormalities) to the standardization and clinical integration of tractography for neurosurgical decision-making [99,101–104].

Positron emission tomography (PET) is a valuable nuclear medicine imaging technique based on positron emission from radioactive nuclei in which the number of protons exceeds the number of neutrons [105,106]. This technique with labelled amino acid tracers has been widely used to capture the biological activity of DGs. The most commonly used amino acid tracers in brain tumour imaging are 18F-fluoro-ethyl-l-tyrosine and 11C-methyl-l-methionine [107]. In spite of the widespread use of PET in the diagnosis of DLGGs, there is no

consensus regarding evidence for the clinical benefit in terms of diagnostic and prognostic capabilities in patients with these lesions [108].

## 1.2.4. Treatment Modalities

### 1.2.4.1. Surgery

The diffusely infiltrative nature of DGs and their tendency to invade preferential eloquent locations poses a critical challenge to the ability of neurosurgeons to perform gross total tumour resection[68,109,110]. Overcoming this challenge would have major prognostic value, especially since the most-important independent spontaneous factor for a poor prognosis is a large tumour, and larger tumours tend to expand into central/eloquent areas of the cortex, thus hindering their gross total resection [68,70,110,111]. Despite the relatively high risk of incomplete resection, surgery remains a significant first-line treatment option [111,112]. Several studies have shown that early extensive resection can influence the natural history of this disease, prolonging both overall survival (OS) and progression-free survival (PFS) and postponing or even avoiding malignant transformation [113–116]. To avoid postoperative neurological deficits, the use of intraoperative electrical mapping during awake craniotomy has increased during the past 20 years. This technique has been shown to increase the extent of resection (EOR), improve the quality of life postoperatively, and prolong the OS in patients with supratentorial DLGGs and allow for the mapping and preservation of language function intraoperatively [32,41,110,117–119].

### 1.2.4.2. Radiotherapy

Adjuvant therapy (radiotherapy and chemotherapy) can be deferred initially at the time of diagnosis in low-risk patients who are in good condition if monitored meticulously with serial MRI investigations. However, they are strongly recommended in high-risk patients older than 40 years or those having undergone incomplete resections [112,120]. Because of the risk for post-radiation effects, the currently applied dose of radiation, comprising 50–54 Gy given in fractions of 1.8 Gy, was agreed upon after the recent implementation of two randomized trials [121,122]. Regarding the timing for radiotherapy, two major studies compared early postoperative radiotherapy with an observation-based "wait-and-see" approach (i.e., radiation given at the time of progression). Both studies found that PFS increased slightly with no change in OS in those who received early treatment [121,123]. On the other hand, the effects of radiotherapy on cognitive functions have been addressed by many authors using different scales to measure cognitive performance and impairment. The evidence suggests that leukoencephalopathy and long-term memory decline are more severe in patients who had received early radiotherapy postoperatively [124–126].

#### 1.2.4.4. Chemotherapy

Although the mainstay of treatment for DLGGs consists solely of surgery and radiation, there has been increasing evidence that chemotherapy may have beneficial effect on OS [127–129]. Several reports have mentioned that chemotherapy administered to patients with DLGGs may have clinical benefits, including improved seizure control, neurologic function, and quality of life [130]. The two primary chemotherapeutic agents used in the treatment of patients with DLGGs, PCV (procarbazine, lomustine, and vincristine) and temozolomide (TMZ), yield comparable objective response rates (45%–62%) and duration of response (10–24 months) [116,131]. The PCV combined therapy in addition to radiotherapy was the preferred treatment choice for patients with newly diagnosed high-risk DLGGs [128]. However, TMZ seems to be better tolerated, with reduced myelotoxicity and greater dose intensity [116,131]. The optimal timing of chemotherapy in relation to surgery and radiation and the group of patients which may receive the greatest benefit remain to be determined [127].

## 1.3. Considerations regarding the significance of white matter in gliomas

From a clinical as well as tumour biological prospective, gliomas are extremely heterogeneous tumours. Their kinetic features reflect the complex dynamic interaction over time with the surrounding brain [73,132]. Bio-mathematical modelling has provided important insights regarding the glioma progression, identifying mainly two phenomena: proliferation and infiltration [73,133–137]. Differences in cortical subcortical infiltration and dislocation patterns are related to the histological origin and may depend on the permissive nature of neighbouring structures around the tumour. When proliferation is the predominant phenomenon, the effects of tumour infiltration do not affect tumour shape, which is grossly bulky with sharp radiological borders, whereas diffusively infiltrating tumours with low proliferation will lead to a complex shape with digitations along the deep WM fibres [73,135,137–139].

Several studies have confirmed the anisotropic invasion of glioma cells along WM fibres [73,135,137,139,140]. Hence, since WM architecture plays such an important role in the progression of gliomas, the natural evolution in their description should be the direct correlation with the WM architecture involved in such biological phenomena. This information seems essential to understand and classify gliomas. However, gliomas are still described based on the nomenclature of major lobes invaded despite their subcortical extension [57,70,83]. For bulky tumours, it seems reasonable to describe the location by naming the pathological lobe. However, favoured directions of extension during tumour evolution would be expected to follow the WM bundles. One natural solution to investigate the relationship between WM and the pattern of glioma invasion

would be the use of MR tractography, which has been done in several clinical and experimental studies [96–100]. Unfortunately, because of the technical limitation of this technique in clinical practice, it is not always possible to reconstruct in detail the regional WM architecture and understand the most probable path of invasion/diffusion in time-comparable MRI [99,101–104]. The use of DTI atlases, which represented a milestone for the localization of the WM bundles in both physiological and pathological conditions [10,20,141,142], seems also limited in daily clinical practice due to a few reasons. First, the necessity to analyse MRI sequences in a normalized space (not patient-specific) and the lack of landmarks in the deep WM for longitudinal comparison in time on a millimetric scale. An accurate classification able to predict tumour behaviour and to tailor individual treatment strategies is still lacking. Gliomas' tendency to preferentially infiltrate eloquent areas is still not fully understood despite developmental, cyto- and myeloarchitectonic, neurochemical, metabolic, and functional theories [68,69,74,75,143]. However, many of the studies investigating the radiological location of gliomas included both HGGs and DLGGs or different subtypes, with no evidence suggesting specific differences between them [68,69,75,110]. Dissemination of astrocytic tumours seems to be confined to the WM near the cortex or deep grey nuclei, which, under certain circumstances, act as barriers to the invasion of some gliomas [134,144,145]. This phenomenon is less prominent in oligodendrogliomas, which will frequently invade the cortex and are less likely to respect anatomic boundaries [146]. The implications of the exact location and histological correlation are extremely important for the treatment planning and thus for the outcome, but this crucial correlation is still poorly understood. Moreover, from the surgical perspective, DGs are challenging lesion to operate on because of their infiltrative features and their preferential location into areas of brain that are not resectable without inflicting a functional neurological impairment for the patient. All together, these highly eloquent areas are defined "minimal common brain", and they represent the surgical limit for tumour resection based on intraoperative functional mapping [109,147]. WM bundles are the main eloquent component of this "minimal common brain". There is, however, no possibility to predict this anatomical-functional data preoperatively on an individual level and according to different degrees of glioma infiltration.

The individual mechanisms behind the clinical heterogeneity in glioma phases and clinical onset are still not clear. It is commonly accepted that, initially, the slow growth of DLGGs allows for cortical adaptor mechanisms that enable functional and morphologic reorganization of the brain. In a second phase, the tumour tends to interfere with normal brain function by disrupting the functional connectivity of brain networks within peritumoral and distant brain areas, thereby promoting positive symptoms such as seizure activity[61,148]. Standard morphological MRI investigations alone do not provide enough information about the specific WM bundle involved, nor about the possible grade of resectability. Intraoperative electrical stimulation mapping

of the cortex and WM tracts in awake patients undergoing surgery for tumour or epilepsy showed an important anatomical-functional variability [32,41,149], huge at the cortical level, very low at the subcortical level.

Hence, a better understanding of how gliomas invade the WM bundles would improve our comprehension of biological tumour kinetics, of neuro-plasticity/reorganization induced by the tumour kinetics, and of resectability of these lesions. Finally, we might be able to predict the risk for functional deficits induced by total or subtotal surgical resection. This should theoretically be applied in clinical practice for all possible tumour locations, on an individual level but with a standardized model.

# 2. Aims

## 2.1. General aims

The overall aim for the work presented in this thesis was to investigate the interplay between brain WM connectivity and gliomas. Different techniques for the study of WM and new tools for a better classification of gliomas and for a better comprehension of the mechanisms behind the interaction tumour-WM architecture were used. These investigations may improve the preoperative planning, the surgical technique, and finally the functional outcome, thereby helping to prolong survival for adults with brain tumours.

## 2.2. Specific aims

Study I
To investigate the connectomic organization and the possible clinical/functional implications of a poorly described WM bundle, the inferior longitudinal fasciculus (ILF), merging WM dissection and diffusion tensor imaging.

Study II
To establish the connectomic organization and clinical implications of the middle longitudinal fasciculus (MdLF) based on fibre dissections, in-vivo DTI tracking, and two clinical cases of patients harbouring gliomas that invade into MdLF territories.

Study III
To create an anatomically standardized grid system (the Brain-Grid) to merge local radiological anatomy, WM architecture, morphology, and kinetics of gliomas into one radiological classification system.

Study IV
To investigate preferential locations of WHO-II astrocytomas and WHO-II oligodendrogliomas and identify whether specific radiological or topographical differences between the histological types could affect the outcome.

Study V
To investigate whether gliomas' preferential infiltration of specific WM pathways may be linked to intrinsic architectural and diffusion proprieties of the WM bundles such as fibre density, diameter, or myelin thickness.

Study VI
To investigate whether a correlation exists between clinical variables at the radiological diagnosis and intraoperative findings of eloquent tumour from brain mapping.

To identify possible mechanisms of local tumour-induced plasticity/reorganization analysing tumour extension and the presence of intratumoral and peritumoral eloquent spots at brain mapping.

# 3. Material and Methods

## 3.1 Anatomical dissection

### 3.1.1. Subjects and preparation technique (Studies I, II and V)

Thirty-six normal cerebral hemispheres (18 right and 18 left) obtained from human cadavers (age range 49–96) donated to the Department of Medical Cell Biology, Section for Anatomy Studies at Uppsala University, Sweden, were studied (14 for Study I; 12 for Study II, and 10 for Study V). All individuals donating had given written consent for use of the whole cadaver for biomedical research and education in a testimonial donation letter. The study protocol was filed with the application for ethical vetting of research involving humans to the Regional Ethical Vetting Board in Uppsala, Sweden (Dnr 2014/468). Each brain was fixed with an intra-carotidal injection of 12% formalin solution within the first week after death (in Study V, the mean post-mortem interval was $1.6 \pm 0.4$ days). After the left or right common carotid artery was exposed and opened at the neck, a pressure transducer was placed within the carotid artery and 2 l of 12% formalin was injected into the intracranial compartment with a perfusion pressure of 200 kPa. The whole duration of the process was approximately 15–20 min. The procedure was considered complete once the ocular bulbs of both sides showed signs of formalin infiltration. After this procedure, the brain was considered fixed after 48 h. The brains were carefully extracted and put in 10% formalin for 24 h.

For Studies I and II, the specimens were prepared with a modified fibre dissection technique in respect to the technique described by Klingler [3,150,151]. The pia mater, arachnoid membrane, and vascular structures were carefully removed after fixation under microscopic magnification. Then, the hemispheres were frozen at −15 to−20∘C for 6–10 days, then slowly defrosted for 12 h. Before the start of dissection, the superficial anatomy of the sulci and gyri was studied in detail. The specimens were dissected in a stepwise manner, from lateral surface to the medial structures and from the basal surface to the ventricle [3,150]. Microscopic metal dissectors and thin wooden spatulas were used in the initial steps of the dissection to split or partially peel away the brain cortex, preserving the most superficial intra-cortical and subcortical fibres of the lateral and basal brain surfaces. Sub-cortical U-fibres and intra-lobar, associative, and projection fibres were exposed until the basal ganglia region

was reached in each specimen. The dissections were performed under micro-scopic magnification (up to 10×). Between each dissection session, the speci-mens were placed in 5% formalin.

## 3.1.2. Sample collection (Study V)

The brains were dissected, and the samples collected without freezing the specimens in preparation for transmission electron microscopy (TEM) analy-sis. Ten WM regions were collected for each hemisphere. Two samples were collected from each of the following WM bundles: the corpus callosum (CC), the cingulum (Ci), the arcuate fasciculus (AF), the inferior fronto-occipital fasciculus (IFOF), and the cortico-spinal tract (CST). The dissections and sample collections were performed under microscopic magnification (up to 10x). All the blocks had a relatively large areal size of up to 0.5 and 0.8 cm$^2$. The first block was sampled from the genu of CC (Ge), identified on the sag-ittal mesial surface of all hemispheres. Microscopic metal dissectors and mi-cro blades were used for the dissection of WM to split or partially peel away the brain cortex, preserving the most superficial intra-cortical and subcortical fibres of the lateral and basal brain surfaces. Following the fibres from the CC to the callosal radiation, a second block was collected deep in the frontal WM in continuity with the callosal radiation ($Ca_R$). The cortex of the cingulum in its frontal component at the level of the SMA/Pre-SMA was dissected, and the underlying WM of the cingulum was collected as a third block ($Ci_F$). The tem-poral-occipital portion of the cingulum was then identified on the mesial brain surface and the cortex was peeled away to reveal the WM, which was sampled as the fourth block ($Ci_T$). The last block was sampled from the anterior cere-bral peduncle of the mesencephalon where all the CST fibres converged after escaping from the internal capsule region ($CST_{BS}$).

On the lateral surface of the brain, the Sylvian fissure was opened at the posterior insular point. The deep cortex of the supramarginal gyrus/temporo-parietal operculum was removed under magnification. The first WM bundle identified at this level was the vertical segment of the superior longitudinal component posteriorly [3,152,153]. The vertical fibres of the arcuate fasciculus were identified medially in respect to the vSLF and sampled as $AF_{TP}$. The ventral premotor cortex was then dissected, revealing the intermediate subcor-tical WM fibres, and then the AF fibres were identified as a compact bundle of WM running medial compared with the indirect anterior component of the superior longitudinal fasciculus (hSLF) and lateral compared with corona ra-diata fibres, which run perpendicular to the AF fibres. The AF was then sam-pled in this region as $AF_F$. Deep in the Sylvian fissure, at the intersection be-tween AF fibres and longitudinal fibres from the middle longitudinal fascicu-lus, the anterior portion of the sagittal stratum of Sachs was identified. A deeper layer with respect to the MdLF was sampled afferent to the inferior

fronto-occipital fasciculus (IFOF$_{SSS}$). A dissection at the level of the limen insula was then performed to reveal first the uncinate fasciculus and then the IFOF fibres running through the external capsule region in its anterior part. The IFOF was then sampled as IFOF$_F$. The central sulcus was identified and dissected from its dorso-lateral surface (hand area). Deeper WM was identified in respect to the U-fibres between motor and sensory cortices. Vertical fibres originating from the hand area and directed to the corona radiata-capsular region were sampled as the cortico-spinal tract (CST$_F$).

### 3.1.3. Transmission electron microscopy

#### 3.1.3.1. Preparation

A part of the tissue from each block was cut off and used for embedding for TEM. Samples were rinsed in 0.1 M maleate buffer for 10 min prior to 1 h incubation in reduced osmium tetroxide in 0.1 M maleate buffer. After a further rise in 0.1 M maleate buffer, samples were dehydrated in graded alcohols (70%–99.9%) for 1 h in total, followed by 5 min incubation in propylene oxide. The tissue samples were then placed in a mixture of Epon resin and propylene oxide (1:1) for 1 h, followed by two changes of 100% resin, the first for 2–4 h and the last o/n. Subsequently, samples were embedded in capsules in newly prepared Epon resin and left for 1 h and then polymerized at 60°C for 48 h. The specimens were cut into semi-thin sections (1–2 microns), stained in toluidine blue and examined in LM to control for the presence of cross-sectioned axons. The block was trimmed and ultrathin sections (60–70 nm) were cut in a Leica UCT ultramicrotome and placed on a grid. The grids were contrasted in 5% uranyl acetate and 3% Reynolds lead citrate for 10 and 2 minutes. Grids were examined by TEM (FEI Tecnai G2) operated at 80 kV. For each sample 10–12 images were taken from two areas with the best-preserved morphology at 4200x magnification.

#### 3.1.3.2. TEM measurement of white matter features

High resolution pictures from electron microscopy preparation were uploaded in parameters measurement (PM), a dedicated in-house developed software based on Matlab® (version R2020a, The MathWorks, Inc., Natick, MA, USA). PM is a software for the interactive measurements of myelinated axons in WM. A scale of 5 μm were utilized in all the pictures as reference for measurement. The area analyzed for each specimen was formed by the two best images (each with an area of 186 μm$^2$) with a total area for each specimen of 372 μm$^2$. A sampling area was discarded and replaced by another only if, at high magnification, it turned out that a glia cell body or a blood vessel was captured (because it would fill a large part of the sampling area).

The fibres diameter was measured starting with the inner diameter, defined as the straight line starting from inner borders from the myelin sheath (thus

excluding the myelin sheath itself). Then the outer diameter was measured. Since profiles are often not circular but elliptic or elongated, depending on the angle with the plane of section, the largest diameter perpendicularly to the long axis of the profile was measured, parallel to the inner diameter [154,155]. The g-ratio, defined as defined as the ratio between the inner and the outer diameter of the myelin sheath [156] was automatically calculated by the software. Profiles of myelinated axons extending over the image borders were discarded, as were those with an awkward/irregular shape in which a diameter could not be defined and those with profiles which ran in parallel to the section. Profiles which could not be identified with high probability as axons/fibres were also discarded. In the few remaining questionable cases, the following additional criteria were applied: profiles with only a very thin dark membrane and no internal structure were excluded, as were profiles in which the membrane could not be clearly delimited from internal structures. An illustration of the measurement procedure is presented in Figure 1.
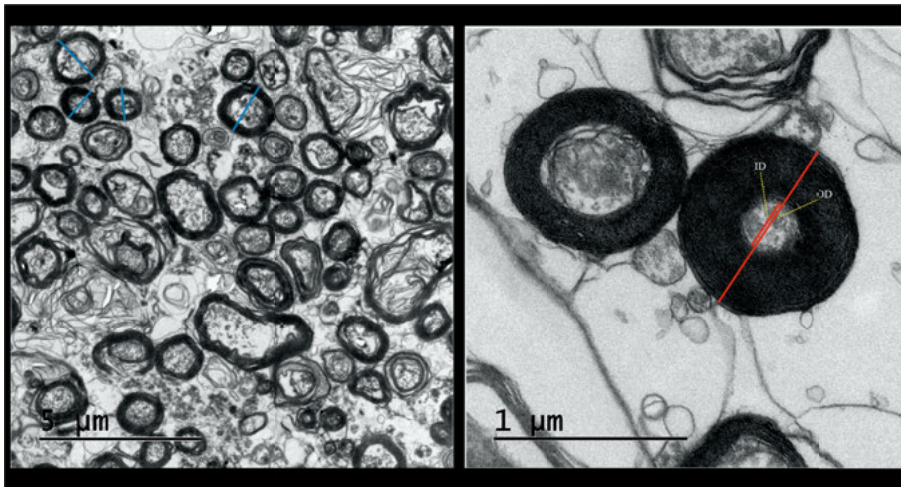


*Figure 1.* Illustration of the interactive TEM image analysis of one $CST_{BS}$ sample. The left image shows one of several TEM images of the sample in which the myelinated fibres were measured (scalebar 5 µm). As a visual aid to avoid failing to measure some fibres, blue lines indicate fibres that have already been measured. The right image shows a myelinated fibre in the displayed close-up (scalebar 1µm) used for measuring the inner diameter (ID) and the outer diameter (OD). The g-ratio was automatically calculated by the software

## 3.2. Subjects and patient populations

### 3.2.1. Study I

Thirty healthy human subjects were included in this study. The participants were aged 21–28 years; 24 were right-handed and 6 were left-handed. All the

participants had a high level of education (17 high school, 13 university) and matched the following inclusion criteria: (1) age range between 18 and 30 years, (2) no previous history of head injury, (3) no history of neurological or psychiatric disorders, and (4) no current psychotropic medication. Informed consent was obtained from all participants, and the study was approved by the Regional Ethical Vetting Board in Uppsala (Dnr 2013/500). Only right-handed subjects were analysed in this study to avoid differences in lateralization of WM bundles dependent on the subjects' handedness.

## 3.2.2. Study II

Clinical and radiological data of two patients were retrospectively analysed in this study. The patients underwent surgery at the Department of Neurosurgery, Uppsala University-Hospital, Uppsala, Sweden, because of suspected DG involving the MdLF territories (superior temporal gyrus, STG). The patients were also selected because of an extensive pre- and postoperative neuropsychological and speech evaluation as a part of a larger research project that included subjects with suspected DGs. The regional ethics committee approved the study protocol (Dnr 2015/210). Data were collected anonymously, and informed consent from patients included in this study was acquired.

Twenty-four subjects (14 females and 10 males; age groups 26–30, 31–35, and 36+) were acquired from the Human Connectome Project (HCP) database; the 1200 Subjects Release diffusion data acquisition and pre-processing are included in the 1200 subjects release and are summarized below. The subjects were selected because of the similar older age group and high-quality structural images including T1 and T2 sequence and high angular resolution diffusion imaging (dMRI).

## 3.2.3. Study III

Thirty-nine patients (>18 years) presenting with a radiological diagnosis of suspected DG were consecutively recruited at the Department of Neurosurgery, Uppsala University-Hospital, Uppsala, Sweden, and enrolled in the study between February 2010 and September 2015 [157]. The study was approved by the local ethics committee (Dnr 2010/015), and written informed consent was obtained from all patients prior to participation. The capacity to consent was ascertained through clinical and mental status evaluation at the time for inclusion in the study. Inclusion criteria were morphological MRI findings with high signal intensity on T2- FLAIR sequence and a 3D T1-weighted sequence with no or minimal (patchy and faint) contrast enhancement suggestive of a DG.

### 3.2.4. Studies IV and V

One hundred and two adult patients (>18 years) with a radiological and histological diagnosis of DLGG (WHO II), who had undergone surgery between February 2005 and December 2015, were included in this study and reclassified according to the WHO 2016 classification [51]. Molecular verification including the IDH status (either IDH1/IDH2 mutant, IDHm/IDH wildtype, IDHwt) and LOH1p19q codeletion were recollected in all the available cases. The regional ethics committee approved the study protocol (Dnr 2015/210).

For study V, 20 subjects (12 females and 8 males; age groups 31-35, and 36+) were also acquired from the Human Connectome Project (HCP) database the 1200 Subjects Release for DTI analysis. The subjects were selected because of their age groups were closer to the age of DLGG patients, and they provided high-quality structural images including T1 and T2 sequences and high angular resolution diffusion imaging (dMRI).

### 3.2.5. Study VI

Thirty-six patients (>18 years) presenting with a radiological diagnosis of suspected DG were consecutively recruited at the Department of Neurosurgery, Uppsala University-Hospital, Uppsala, Sweden, and enrolled in the study between August 2014 to August 2020. Exclusion criteria for this study were previous resection for brain tumours, previous radio-chemotherapy, severe respiratory diseases, history of psychiatric diseases or psychiatric contraindication, severe language impairment. The study was approved by the regional ethics committee (Dnr 2015/210/2). Informed consent was obtained prior to surgery.

## 3.3. Neuroradiological assessment of patients with DGs

### 3.3.1. Studies II, III, IV, V and VI

Magnetic resonance imaging (MRI) were performed on a 1.5 T or 3T MRI scanner (Philips Achieva, Best, the Netherlands), including a conventional MRI protocol consisting of T2W, T2-FLAIR (slice thickness ranged between 1 mm and 5 mm and axial resolution was 0.5–2 mm.); diffusion sequences and pre- and post-contrast T1W were acquired according to our standard glioma imaging practice[80,81]. Morphological MRI sequences (volumetric T1W, T2W, and T2-FLAIR) were used to assess brain tumour location and heterogeneity, mass effect, radiological border (sharp or diffuse), contrast enhancement, and the presence of multiple brain lesions [80–82]. T2 turbo spin echo or T2 FLAIR images in Vue picture archiving and communication system (PACS) software (version 11.1.0, Carestream Health Inc., Rochester, NY, USA) were used to

segment the lesions both pre- and postoperatively with the aid of a semiautomatic method (Livewire Algorithm)[158]. The software is supported by an algorithm that uses an active contour model to evolve and segment the lesions. In defining the volume of the surface voxels, a clear difference in pixel contrast (black/white) assisted the operator, increasing the ability to better adapt or correct the contour line even where it was less defined. As radiological variables, the tumour borders were considered sharp, with well-defined margins (without any finger-like hyperintense signals on T2 TSE or T2 FLAIR sequences), while tumour margins with unclear and irregular signal intensity on T2 FLAIR sequences were considered diffuse.

## 3.3.2. Advanced Neuroradiological processing

### 3.3.2.1. The Brain-Grid (Studies III, IV and VI)

A standardized grid based on previously chosen anatomical landmarks was created intersecting longitudinal lines on the axial, sagittal, and coronal planes on a T1-weighted average brain in the Montreal Neurological Institute (MNI) space. Superficial and consistent cortical/gyral anatomical landmarks were chosen based on their bilateral symmetry and their relationship with subcortical WM architecture. The sulcus between cingulum cortex and corpus callosum, the mammillary bodies, superior temporal sulcus, middle frontal sulcus, the midline, the parieto-occipital sulcus, the temporal-occipital junction, and the anterior and posterior insular points were selected as clear and consistent landmarks. The Brain-Grid was constructed by 3 axial lines, 2 coronal lines, and 3 sagittal lines, whereas the intersection of these lines creates 48 grid voxels. Each voxel could be identified using simple nomenclature with radiological orientation. In the axial (A) plane, voxels are labelled 1–4, right to left direction. In the coronal (C) plane, voxels are labelled 1–3, cranio-caudal direction. In the sagittal (S), voxels are labelled 1–4, anterior-posterior direction. A stepwise instruction describing the placement of the Brain-Grid classification system according to morphological landmarks and both the MNI and Talairach atlas coordinates can be found in Figure 2.
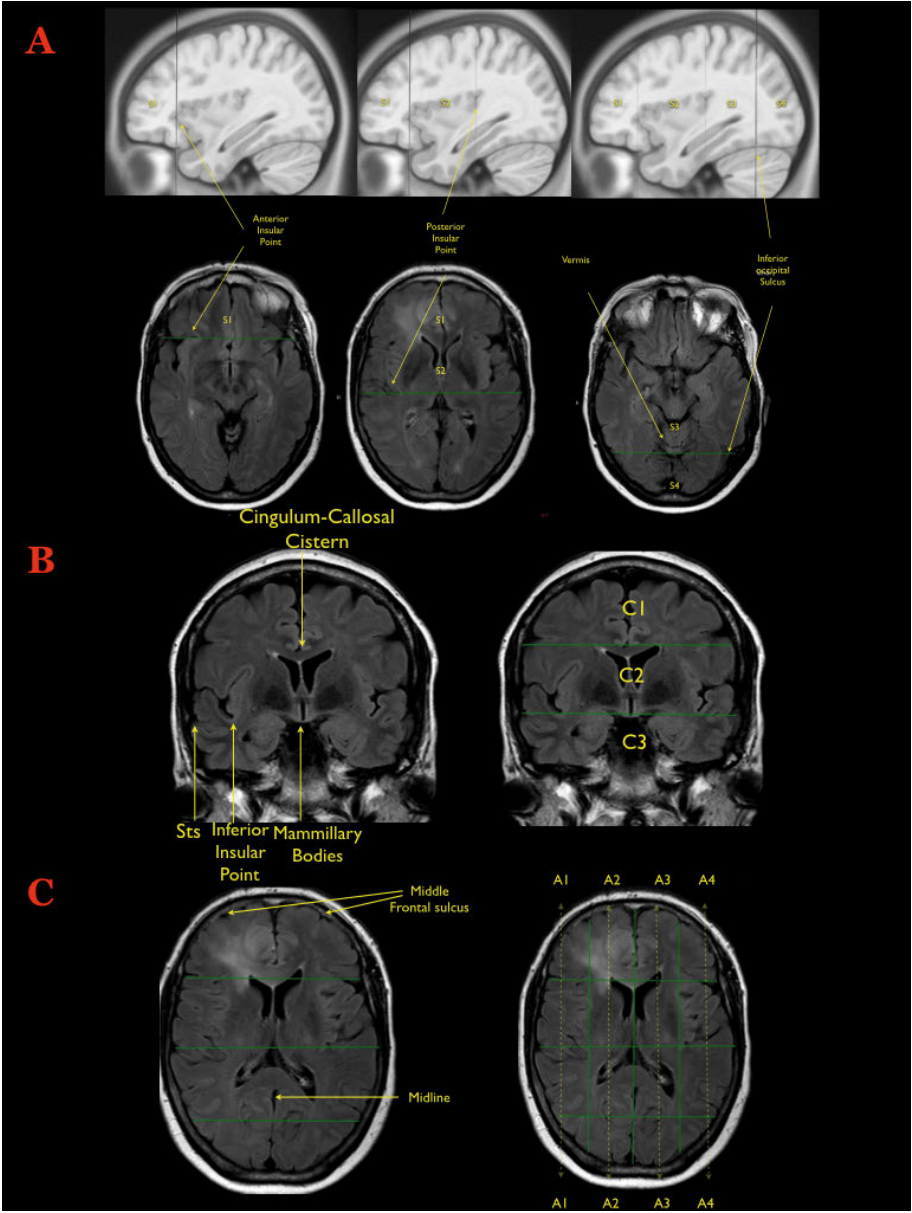
*Figure 2.* The MRI sequences were oriented according to the anterior commissure-posterior commissure line. **A)** The first step during the creation of the Brain-Grid is illustrated on the sagittal or axial slices: the anterior insular point (the most anterior landmark of the insular sulcus) is identified on both sides and the first line is drawn on the sagittal plane (MNI: Y 28, Talairach: Y25). The second line (drawn as well on the sagittal plane) is parallel to the previous one, crossing the posterior insular point (MNI: Y-23; Talairach: Y-24). On the midline (with sagittal view) the point where the calcarine fissure (V1) meets the most anterior portion of the parieto-occipital sulcus should be identified to track the third parallel line on the sagittal plane (MNI: Y-68; Talairach: Y-66). The same line crosses the temporo-occipital junction between the posterior portion of the fusiform gyrus and the inferior occipital sulcus more basally on the axial plane. The three lines on the sagittal plane will segment the whole brain into four grid voxels. The S1 voxel is the pre-insular/prefrontal portion of both hemispheres. The S2 is enclosed within the anterior insular point and posterior insular point (landmark for the second sagittal line). The S3 includes the retro-insular region and the parietal lobe, and the S4 includes primarily the occipital lobe and the border with the parieto-occipital sulcus. **B)** The second step during the creation of the Brain-Grid system is the identification of the right slice on the coronal plane (into the MNI space: Y-5; Talairach Y -7). The first of the two parallel lines crosses the inferior insular point (the lowest limit of the insular sulcus) and the floor of the third ventricle that leads to the rounded shape of the mammillary bodies. In most patients, this horizontal line usually crosses the superior temporal sulcus on both sides (MNI: X0, Y-5, Z-13; Talairach: X0, Y-7, Z-7). The second line passes through the cistern/space between the Cingular gyrus and the callosal body in the midline (MNI:X0, Y-5, Z33; Talairach: X0, Y-4, Z 31). **C)** Third step: Once the coronal segments and the sagittal segments are created, one should identify the middle frontal sulcus bilaterally, which is easily recognizable on the axial slice that shows the level of the lateral ventricle on the coronal reference (shown on the side). The two lines should be parallel to the midline, connecting this sulcus with the middle occipital gyrus crossing the WM of the external capsule without invading the periventricular ependyma (right line, MNI: X33; Talairach: X32. left line, MNI:X-33; Talairach: X-32). The third and last line follows the midline along the falx and/or the septum pellucidum (MNI: X0; Talairach: X0). In this way four longitudinal segments are created, termed A1 to A4, from the right lateral side to the left lateral side.

The application of the Brain-Grid classification system in patients was performed using T2 turbo spin echo (TSE) or T2-FLAIR images in the Vue PACS software (version 11.1.0, Carestream Health Inc., Rochester, NY, USA.) (in Study III). Multiplanar reconstructions were performed to orient the image in relation to the anterior commissure-posterior commissure line. If there was infiltration/dislocation of the anatomical landmarks, the contralateral landmark was identified to track the grid lines. High signal intensity on T2 FLAIR or T2 TSE images was used to delineate the tumour using PACS. The borders were drawn at the transition between high signal intensity and normal parenchymal signal intensity based on visual evaluation. The number of grid voxels involved in the tumour extension was registered based on the defined tumour lesion. Registered grid voxels were also compared to the WM architecture, defining fibre tracts involved by tumour extension. The distance between the

grid line and the visible tumour border was recorded and compared in patients with multiple MRI scans during the follow-up period. Furthermore, to confirm consistency between patient-specific measurement and normalized space, MRI images of 10 patients were chosen (randomly selected, independently of volume or location) and spatially normalized to the MNI space using the SPM12 toolbox (Wellcome Trust Centre for Neuroimaging, London, UK). Applying the Brain-Grid classification system using the FSLeyes software (https://fsl.fmrib.ox.ac.uk/fsl/fslwiki/FSLeyes) in the MNI space, the number of voxels involved in the tumour was counted and compared to a correspond-ing value from the Vue PACS in the patient-specific space. The Brain-Grid system was reconstructed directly into MNI space in Studies IV and VI.

### 3.3.2.2. Probabilistic and frequency maps (Study IV and V)

FLAIR images of all the patients were normalized to MNI space using the built-in normalizing software in DSI studio (DSI Studio, http://dsi-studio. lab-solver.org/download-images). The non-linear registration box included an af-fine registration component and a diffeomorphic mapping method, contour driven match (CDM); standard parameters (resolution 2, smoothness 0.30 and 60 steps) were chosen for the registration. FLAIR-T2 slice thickness ranged between 1 mm and 5 mm and axial resolution was 0.5-2 mm. In those cases with 5 mm thickness, a volumetric T1 was also co-registered in MNI space to increase the quality of adjustment of the FLAIR registration. The registration was systematically checked in all the cases before the next step with adjust-ment registration box. The corpus callosum and fourth ventricle were used as anatomical landmarks for sagittal slices, lateral ventricles, and the contour of fronto parietal cortices were used as anatomical landmarks on the axial slices and body of corpus callosum and third ventricle were used as references on coronal slices. Translocation, scaling, shearing, and rotation were then used to manually adjust the match and re-run the registration.

Tumour lesions were successively manually segmented on original FLAIR images within the MNI space [159]. Statistical maps of tumour location fre-quency were obtained by computing the cumulative number of observed le-sions for each voxel and dividing by the total amount of lesions [109].


# 3.4. Diffusion tensor imaging and tractography: image acquisition and tracking method

## 3.4.1. Study I

DTI was performed using a single-shot spin echo sequence with echo-planar imaging (EPI), 60 contiguous slices, voxel size 2 x 2 x 2 mm$^3$, Echo time (TE)/Repetition time (TR) of 77/6626 ms/ms, a diffusion-weighting factor b

= 1000 s/mm2 and diffusion encoding along 48 directions. Corrections for subject motion and eddy current induced geometric distortions of the DTI data were performed using ElastiX [160]. A linear least squares fitting was used for the tensor fitting procedure, diffusion parameter maps were calculated, and streamline tractography files with a fractional anisotropy (FA) threshold of 0.1 and an angular threshold of 45° were calculated using in-house developed software (Matlab, The Mathworks Inc, Natick, MA, USA). The diffusion parameter maps and the calculated DTT were evaluated using the software TrackVis (www.trackvis.org). TrackVis was used for the placement and drawing of regions of interest (ROIs) and of the anatomical landmarks. These manual ROIs were placed in FA maps with locations according to the anatomical findings in the WM dissection. The ILF fibres were identified when isolated from other WM bundles. Then each ILF occipital termination was identified using an additional one-ROI approach in each cortical/subcortical territory based on the anatomical findings in cadaver dissection. For each identified subcomponent of the ILF, the diffusion parameters and their interhemispheric symmetry were analysed. To demonstrate the connectivity of the ILF subcomponents, we investigated their peripheral endpoints closest to the cortical surface of each gyrus/sulcus. The occipital terminations were matched with a standard anatomical gyral classification, while the temporal region anterior in respect to the temporal horn was subdivided on the coronal plane into five territories: superior temporal gyrus (T1), middle temporal gyrus (T2), inferior temporal gyrus (T3), lateral occipito-temporal gyrus (T4), parahippocampal gyrus (T5).

## 3.4.2. Study II

HCP diffusion data were acquired using a Siemens Skyra 3.0 T with a 32-channel head coil (Siemens Healthineers, Erlangen, Germany) according to the HCP Study Protocol [161]. A multi-shell diffusion scheme was used (*b*-values 1000, 2000, and 3000 s/mm$^2$), each shell with 90 diffusion sampling directions. The in-plane resolution and slice thickness were 1.25 mm, TE/TR of 89/5500 ms/ms. All HCP diffusion datasets were pre-processed to remove EPI distortions, eddy-current-induced distortions, and subject motion and to correct for gradient-nonlinearities [162–164]. Pre-processed HCP diffusion data were reconstructed using the generalized q-sampling imaging approach [165] with a diffusion distance ratio of 1.2. The full technical documentation, describing the method in more depth, can be found freely downloadable at https://db.humanconnectome.org.

We performed deterministic fibre tracking using DSI Studio software (DSI Studio, http://dsi-studio.labsolver.org), which utilizes a generalized streamline fibre tracking method [166]. Parameters selected for fibre tracking included a step size of 0.2 mm, a minimum fibre length of 20 mm, and a turning angle

threshold of 45°. For progression locations containing >1 fibre orientation, the fibre orientation most congruent with the incoming direction and turning angle <45° was selected to determine subsequent moving direction. Each progressive voxels' moving directional estimate was weighted by 20% of the previous voxels incoming direction and by 80% of its nearest fibre orientation. This sequence was repeated to create fibre tracts. Termination of the tracking algorithm occurred when the quantitative anisotropy [166] dropped below a subject-specific value: when fibre tract continuity no longer met the progression criteria or when 100,000 tracts were generated. DSI Studio was used to place and draw ROIs and anatomical landmarks. These manual ROIs were placed on T1-weighted maps with locations according to the anatomical findings in the WM dissection. The whole cortical subcortical connectivity of the temporo-parieto-occipital region was then revealed to virtually dissect the MdLF and its sub-segments. The MdLF fibres were identified and isolated from other WM bundles. Each MdLF temporal termination was identified using an additional one-ROI approach in each cortical/subcortical territory based on the anatomical findings in the cadaver dissection.

The Harvard-Oxford Cortical Atlas [167,168] was spatially normalized to subject-specific space for each subject using the built-in normalization software in DSI Studio. Streamline counts, i.e., number of reconstructed streamlines between two given regions, were generated by the Connectivity Matrix function in DSI Studio. Average normalized percentage streamline counts, and standard deviations were calculated. Average normalized percentage streamline counts were used to generate connectograms for the left and right posterior segment of MdLF (pMdLF), anterior segment of MdLF (aMdLF), and whole MdLF using CIRCOS (http://mkweb.bcgsc.ca/tableviewer/visualize/). Tract metrics (volume; length; fractional anisotropy FA; mean diffusivity, MD; axial diffusivity, AD; and radial diffusivity, RD) were also calculated using DSI Studio.

## 3.4.3. Study III

A standard template, the HCP-488 atlas, was created averaging the reconstructed data of the 488 subjects (199 males, 289 females, average age 29.15 years, standard deviation 3.47 years) enrolled in the HCP [161]. The diffusion data were acquired using a Siemens 3.0 T Skyra scanner with a 2-dimensional spin-echo single-shot multiband echo planar imaging sequence, a multiband factor of 3, and monopolar gradient pulse. The spatial resolution was 1.25 mm isotropic, repetition time was 5500 milliseconds, and echo time was 89 milliseconds. A multishell diffusion scheme was used: b values were 1000, 2000, and 3000 s/mm2. The total number of diffusion sampling directions was 270.

The diffusion data were reconstructed in the MNI space using q-space diffeomorphic reconstruction [165] with DSI Studio. A deterministic fibre tracking algorithm was used for the brain fibre tracking [166].

We applied a knowledge-based multiple ROIs approach in which the tracking algorithm was initiated from user-defined seed regions. The anatomical placement of the ROIs was selected by using the most validated DTI atlases [10,11,20,141] as references. Thirty-four major WM bundles/structures were reconstructed and merged with the Brain-Grid lines normalized into MNI space to create Brain-Grid tractography atlas (Figure 3).
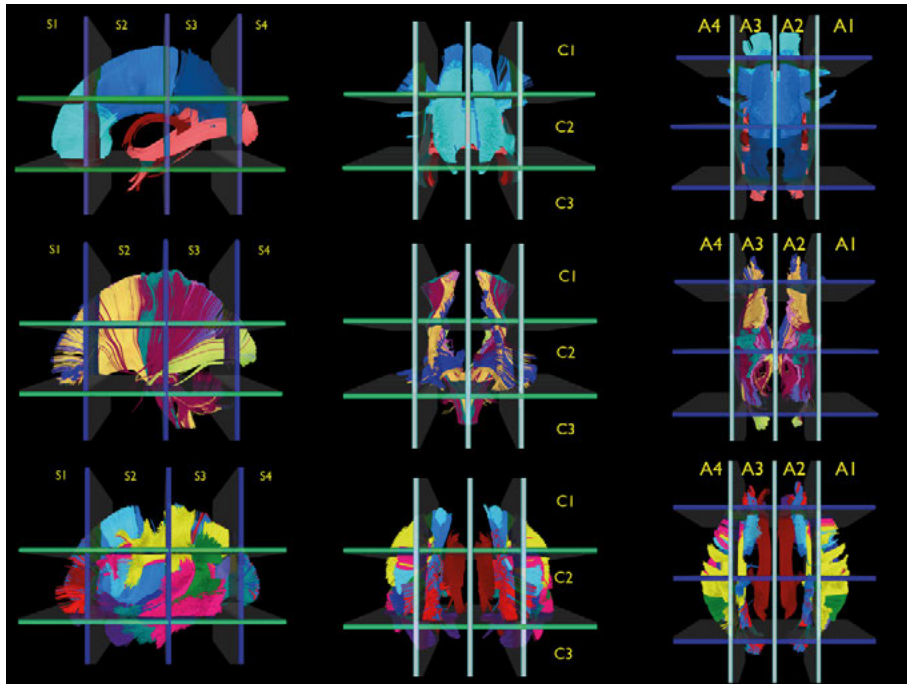


*Figure 3*. The illustration shows the reference WM atlas reconstructed from the HCP template and analysed with the Brain-Grid system. The major commissural (corpus callosum, CC, three nuances of blue; anterior commissure, AC, salmon; and fornix, Fo, cayenne; first row), projection pathways (cortico-spinal tract, CST, teal colour; internal capsule, IC, lemon and maroon colours; optic radiation, OR, honeydew colour; thalamic radiation, ThR, blueberry and grape colours; second row), and associative pathways (cingulum, cayenne colour; components of superior longitudinal fasciculus SLF, lemon, moss, and strawberry colours; vertical occipital fasciculus, VOF, orchid colour; ILF, teal colour; MdLF, blueberry colour; IFOF, red colour; uncinate fasciculus, UF, grape colour; and frontal aslant tract, FAT, sky colour; third row) of both hemispheres are displayed in a left sagittal view (first column), anterior coronal view (second column), and superior-axial view (third column). The WM bundles were tracked from the HCP-488 template within the MNI space and then analysed using the Brain-Grid system with the number and letters for the grid voxels displayed for each projection.

### 3.4.4. Study IV

A group average template was constructed from a total of 1021 subjects, the HCP 1021 dataset. A multishell diffusion scheme was used. The b-values were 990, 1985, and 2980 s/mm$^2$, and the number of diffusion sampling directions were 90, 90, and 90. The in-plane resolution and the slice thickness were 1.25 mm. The diffusion data were reconstructed in the MNI space using q-space diffeomorphic reconstruction [169] to obtain the spin distribution function [170]. A diffusion sampling length ratio of 2.5 was used, and the output resolution was 1 mm. The restricted diffusion was quantified using restricted diffusion imaging [171]. Major projection, commissural, and association WM pathways were reconstructed within the HCP 1021 template following the anatomical criteria previously described for the Brain-Grid DTT reference atlas [172] and matched with gradient maps for tumour frequency.

### 3.4.5. Study V

HCP diffusion data were reconstructed in DSI Studio (http://dsi-studio. lab-solver.org) using the generalized q-sampling imaging approach [165] with a diffusion distance ratio of 1.2. Prior to reconstruction, all included datasets were thoroughly examined to ensure the quality and integrity of diffusion data using the built-in quality control in DSI studio and by visual examination [173]. Deterministic fibre tracking was performed in DSI Studio, using a generalized streamline fibre tracking method [166]. Five selected WM tracts were reconstructed in all the subjects following the anatomical criteria previously published with the Brain-Grid DTT reference atlas [172]. Ten squared ROIs were acquired matching the probabilistic infiltration weighted gradient map and the anatomical sampling criteria for TEM analysis for each hemisphere. A total of 400 regions was acquired. DTI-based parameters including FA, mean diffusivity (MD), AD, and RD were acquired for each region and for each WM bundle.

### 3.4.6. Study VI

DTI was performed using a single-shot spin echo sequence with echo-planar imaging, 60 contiguous slices, voxel size 2 x 2 x 2 mm3, Echo time/repetition time of 77/6626 ms/ms, a diffusion-weighting factor b = 1000 s/mm$^2$, and diffusion encoding along 48 directions. Motion and eddy current correction of acquired DTI data was automatically performed in BrainEx (version 2.3.6. NordicNeuroLab AS, Bergen, Norway). The parametric maps of FA, AD, and RD were calculated and merged on T2-FLAIR volumetric sequences. Streamline tractography was performed with a fractional anisotropy threshold of 0.1, an angular threshold of 45°, and minimum length of 20 mm. BrainEx was used for the placement and drawing of ROIs and regions of avoidance (ROAs). The

anatomical placement of the ROIs and ROAs was manually performed using the most validated DTI atlases as references [10,20,141]. Using a two-ROIs approach, IFOF, superior longitudinal fasciculus (both horizontal indirect component hSLF and vertical indirect component vSLF), AF, CST, FAT, and optic radiation (OR) were reconstructed in each patient on the interested hemisphere.

## 3.5. Neuropsychological and language assessment (Studies II and VI)

Patients were assessed by a speech therapist and a neuropsychologist before surgery. Also, 3- and 12-month postoperative evaluations are included in our standard protocol for functional assessment of DGs but not reported in this thesis. The linguistic evaluation contained confrontation naming, language comprehension, phonological and semantic word fluency, tests of reading and writing, and phonological ability. The neuropsychological assessment contained tests of attention and working memory, processing speed, learning, and long-term memory (verbal and visual), visuospatial construction, executive functioning, and self-reported anxiety and depression. (see Appendix, Electronic Supplementary material 1, Studies II and VI for the test choices).

## 3.6. Surgical and stimulation technique (Studies II and VI)

In Study II, the patients underwent surgery under general anaesthesia, and no intraoperative mapping was performed.

In study VI, the anaesthetic technique was according to an asleep-awake-sedation/asleep protocol. The surgical resection aimed to reach functional limits and/or crucial anatomical structures such as basal ganglia or anterior perforate substance. For the cortical and subcortical mapping, we utilized a combination of bipolar and monopolar cortical-subcortical stimulation, as described in other studies [174–176]. Cortical electrical stimulation (60 Hz, biphasic pulses with a 1 ms duration for 3 seconds) was performed using a bipolar probe with an interelectrode distance of 5 mm (Dr. Langer Medical GmbH, Waldkirch, Germany) according to the Penfield stimulation technique (PS)[177]. The required stimulation intensity for cortical mapping was established by stimulating either the ventral premotor or primary motor cortex while observing corresponding clinical effects (i.e., speech arrest during counting or tonic muscle contractions). The corticectomy started after the cortical mapping, and the resection of subcortical structures was continuous until functional limits

were detected, leaving the pathological tissue in situ. This reduced the possibility of anatomical shift between the cortical and subcortical eloquent points. The PS intensity was the same for cortical and subsequent subcortical stimulation. Language-related tests (e.g., picture naming, reading, or repetition) were performed by a speech therapist or a neuropsychologist during electrical stimulation. A custom-made system was used for intraoperative testing of language and other cognitive functions. Language test-related images were displayed on a PC monitor and presented to the patient at a constant pace. The electrical stimulation was controlled from a neuromonitoring device (Cadwell Industries, Kennewick, WA, USA) that also monitored cortical EEG, free-running EMG, and motor evoked potential (MEP). Stimulus-induced muscle contractions were also monitored by clinical inspection. MEP recordings were used for subcortical motor mapping. Cortical EEG was recorded from two separate one-by-four strip electrodes (Ad Tech Medical Instruments, Racine, WI, USA) to detect seizure activity or after-discharges. Stimulation results/effects were documented intraoperatively and video captured for postoperative review. At the subcortical level, we also used continuous (3 Hz) cathodal short-train stimulation (STS) (5 monophasic pulses, 4 ms interpulse interval and 0.5 ms pulse duration) delivered via the tip of a specially designed suction probe (Inomed, Emmendingen, Germany). Language interference and other clinical effects from STS were compared with those produced by PS (feasibility and reliability of continuous STS are explored in an ongoing separate study). Anatomical sites that were positive at PS (cortical or subcortical) or consistently positive at 5 mA with STS (subcortical) were considered eloquent and acquired on the neuronavigation system. After registration of the eloquent spots, the rest of the tumour was resected with an ultrasonic dissector to reveal the medial or deep functional limit of the resection. In case of brain-shift, the intraoperative navigated ultrasound (Flex focus 800, BK Medical, Denmark) probe was used to adjust the navigation accuracy, as described by other authors [178–180].

## 3.7. Postoperative analysis (study VI)

The linear distance between the 3-D defined eloquent points acquired intraoperatively and the tumour margins was measured postoperatively (Brainlab software, Munich, Germany). Tumours containing eloquent points within areas defined by hyperintensity on FLAIR sequences (cortical or subcortical) were considered eloquent. Eloquent points within 5–10 mm from the FLAIR signal margin were considered peritumoral, while those acquired beyond 10 mm from the FLAIR signal were considered outside the tumour area. Pre- and

postoperative images (acquired within 48 hours and 3 months after the operation) were merged to detect and spatially locate the presence of eventual residual tumour.

# 3.8. Statistical analysis

## 3.8.1. Studies I-II

For descriptive analysis, means and standard deviations were calculated for tract volume, tract length, and tract diffusion parameters for all tracts and visualized through box plots that included mean value, 25th and 75th percentile, and min to max. Statistical analyses were conducted in Study I, using the *t*-test for independent samples for all measurements (volume, length, and FA) and ILF subcomponents for comparison of the left versus the right hemisphere for normally distributed data in Study I (24 subjects). In Study II (not normal distribution), a Mann–Whitney U-test for independent samples was used for comparison between groups for volume, length, FA, MD, AD, and RD. The symmetry coefficient of each tract metric and MdLF component was calculated, based upon the formula (L - R)/ (L + R), as reported in previous studies [181,182]. A *p*-value less than 0.05 was considered statistically significant. STATISTICA 12 software (Statsoft Inc. 2013. Tulsa, OK, USA) and statistical package SPSS 25.0 (SPSS, Inc., Chicago, IL, USA) were used.

## 3.8.2. Study IV

Frequency distributions and summary statistics were calculated for all the demographic, clinical, and radiological variables. The variables analysed were age, side of tumour location, description of radiological border (sharp or diffuse), preoperative volume, number of BG voxels, invasion of eloquent WM pathways [109], and EOR. To investigated possible differences between subgroups of astrocytomas and oligodendrogliomas according to their molecular status against the not confirmed groups (NOS, non-otherwise specified), we used the Kruskal–Wallis test for comparison between IDHm, IDHwt, and astrocytomas NOS for numerical variables. The Mann–Whitney U test for independent samples was used for comparison between confirmed oligodendrogliomas (LOH1p19q+) and oligodendrogliomas NOS for numerical variables. Pearson's chi-square test was used for categorical variables analysis between sub-groups. To investigate differences in variables distribution between astrocytomas and oligodendrogliomas, a Mann–Whitney U-test for independent samples was used for group comparison for numerical variables. Pearson's chi-square test was used for categorical variables. We calculated survival probability using the Kaplan–Meier method[183], performing comparisons with the log-rank test to assess the effect of variables on OS. OS was calculated

from dates of biopsy or surgical intervention to death or last follow-up. For the number of BG voxels and tumour volume, an optimal cut-off choice in two groups was made according to receiver operating characteristics curves (ROCs)[184]. We examined all variables in the proportional hazard analysis (Cox model [185]) to identify independent predictors of survival. Univariate OS analyses using proportional hazards models were used to assess the prognostic significance of multiple variables. Forward stepwise proportional hazards modelling was performed to assess the relative and independent prognostic capacity of each parameter. A second block was used for interaction analysis between the more relevant categorical variables (infiltration of crucial WM, side, radiological border, IDH status in astrocytomas, and LOH status in oligodendrogliomas) and numerical variables (volume, number of BG voxels, EOR). All statistical analyses were performed at a significance level of $p <$ 0.05. For analyses involving multiple categories, to minimize the problem of overstatement of statistical differences resulting from multiple comparisons, individual comparisons were considered for statistical significance only if the overall test was statistically significant. The statistical analysis was performed using the statistical package SPSS 25.0 (SPSS, Inc., Chicago, IL, USA).

### 3.8.3. Study V

Descriptive statistics included mean and SD for both histological variables (fibre density, inner diameter, outer diameter of fibres, and g-ratio) and diffusion indices (FA, MD, AD, RD). The histological variables and the diffusion parameters were analysed in two steps. First: WM regions within the same bundles were compared using the Kruskal–Wallis test. Dunn's post-hoc test for multiple comparison was chosen as a not parametric test. Second, the sample regions were analysed based on the infiltrations risk in high infiltration frequency (HIF) vs low infiltration frequency (LIF) and analysed with the Mann–Whitney U test. A Spearman correlation analysis was then used to detect relationship between diffusion parameters and infiltration risk. The Shapiro–Wilk test for normal distribution was performed and demonstrated normal and non-normal distribution among all variables, hence all statistical tests are performed as non-parametric. Statistical tests were performed at a significance level of $p < .05$. The statistical analysis was performed using the statistical package SPSS 25.0 (SPSS, Inc).

### 3.8.4. Study VI

For descriptive analysis, mean values and standard deviation (SD) were calculated for age, volume, EOR, survival from diagnosis, and the number of eloquent spots detected intraoperatively at the cortical and subcortical level. Median and inter-quartile range (IQR) were calculated for the number of

Brain-Grid voxels. Total values and percentages were calculated for gender, epileptic onset, eloquent tumours, and preoperative neuropsychological or language impairment. Group comparison between eloquent and non-eloquent tumours and tumour subtypes and histology were performed with the Mann–Whitney U-test and Kruskal–Wallis test for all the variables analysed. A Shapiro–Wilk test was used to test normal distribution of the continuous variables. A Spearman correlation analysis was chosen for the more relevant continuous variables (age, tumour volume, BG voxels, number of eloquent points cortical/subcortical, intratumoral/peritumoral, resection grade). For the age, number of BG voxels, and tumour volume, an optimal cut-off choice in two groups was made according to ROCs to convert them in dichotomous variables. Pearson's chi-square test and contingency test were used for group correlation for categorical and dichotomous variables (gender, age cut-off, epileptic onset, preoperative NPS, and language impairment, eloquent tumours, radiological border, volume cut-off, number of BG voxel cut-offs, histology, tumour grade). A group comparison between younger patients and older patients was performed post-hoc with the Mann–Whitney test for the following variables: histology, tumour grade, tumour volume, tumour location, BG voxels, clinical variables, and intraoperative variables including the number of eloquent spots.

A binary logistic regression model was used to investigate the relationship between clinical variables (epileptic onset, NPS impairment and language impairment) considered as dependent variables, the intraoperative variables (eloquent spots, cortical, subcortical, intratumoral, peritumoral), and the most often infiltrated BG voxels. Finally, a multivariate binary logistic regression model was used to identify independent predictors of eloquent tumours. Forward stepwise proportional hazards modelling was performed to assess the relative and independent prognostic capacity of each parameter. All statistical analyses were performed at a significance level of $p < 0.05$ and confidence interval of 95%, using the statistical package SPSS 25.0 (SPSS, Inc., Chicago, IL, USA).

# 4. Results

## 4.1. Study I

The organization of the ILF was investigated with WM dissection and DTI analysis. The ILF fibre system was identified bilaterally in 14 normal human hemispheres by anatomical dissection of their subcomponents. The anatomical findings were used to create similar diffusion tensor tractography (DTT) reconstructed connectivity in 48 hemispheres. We found that the main structure of the ILF was composed of three constant components: the fusiform (Fu) (100% of the analysed hemispheres, 14 specimens and 48 in vivo), the lingual (Li) (100% of the analysed hemispheres, 14 specimens and 48 in vivo), and the dorso-lateral-occipital (DLOC) (98% of the analysed hemispheres, 14 specimens and 47 in vivo). The cuneal component (Cu) was inconstant (67% of the analysed hemispheres 12 specimens and 30 in vivo). Regarding anatomical relationships and cortical terminations, tractography and dissection results matched (Figure 4 A-B). The analysis of the biophysical parameters for each ILF subcomponent acquired from tractography showed a substantial inter-hemispheric symmetry. The analysis of the entire ILF showed a significant rightward lateralization of the total ILF volume only (Table 1).

Both post-mortem and in vivo analyses of the anatomical pattern of connectivity revealed that the Fu branch and the DLOC branches had the richest pattern of connectivity among the ILF subcomponents (Figure 4-C).
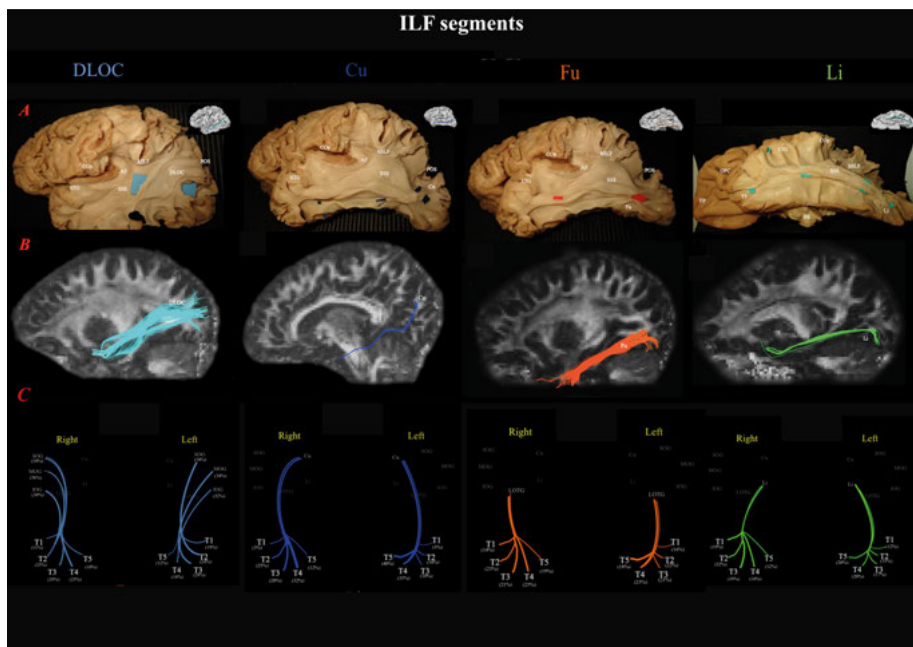
*Figure 4.* **A-B)** The illustration shows the match between anatomical findings from WM dissection and DTT for each sub-segment of ILF, dorso-lateral occipital (DLOC), cuneal (Cu), fusiform (Fu), and lingual (Li). **C)** Summary of the connectivity for each ILF subcomponent in the right-handed population (according to the closest subcortical endpoints at DTT reconstruction).

COp: Central operculum; STG: superior temporal gyrus; POS: parietal occipital sulcus; AF: arcuate fasciculus; hSLF: horizontal segment of superior longitudinal fasciculus; SSS: sagittal stratum of Sachs, TP: temporal pole; FP: frontal pole; OFC: orbito-frontal cortex; Occ: occipital cortical terminations; SO: superior occipital gyrus; MO: middle occipital gyrus; Cu: cuneal gyrus; LOT: lateral occipito-temporal gyrus (including fusiform region); Li: lingual gyrus. Temp: temporal cortical terminations; t1: superior temporal gyrus; t2: middle temporal gyrus; t3: inferior temporal gyrus; t4: lateral occipito-temporal gyrus; t5: parahippocampal gyrus.

Table 1. Summary of fractional anisotropy (FA), volume (Vol), and length (Len) of the inferior longitudinal fasciculus (ILF) and its subcomponents and statistical analysis in the right- handed population (24 subjects).

**Inferior Longitudinal Fasciculus (ILF) (Complete)**

|  | Side | Mean | SD | t | p |
|---|---|---|---|---|---|
| FA | L | 0.48 | 0.03 |  |  |
|  | R | 0.47 | 0.03 |  |  |
|  | Sym | 0.01 | 0.03 | 1.99 | 0.05 |
| Vol (ml) | L | 9.64 | 2.36 |  |  |
|  | R | 11.18 | 2.86 |  | * |
|  | Sym | -0.06 | 0.15 | -2.09 | <0.05 |
| Len (mm) | L | 79.41 | 8.82 |  |  |
|  | R | 78.21 | 12.93 |  |  |
|  | Sym | 0.01 | 0.07 | 0.70 | 0.48 |

| | | **Dorso-Lateral Occipital segment (DLOC)** | | | | **Fusiform segment (Fu)** | | | |
|---|---|---|---|---|---|---|---|---|---|
|  | Side | Mean | SD | t | p | Mean | SD | t | p |
| FA | L | 0.44 | 0.07 |  |  | 0.46 | 0.08 |  |  |
|  | R | 0.44 | 0.05 |  |  | 0.45 | 0.07 |  |  |
|  | Sym | 0.00 | 0.32 | 0.00 | 0.99 | 0.00 | 0.14 | 0.18 | 0.85 |
| Vol (ml) | L | 3.90 | 2.39 |  |  | 5.83 | 2.00 |  |  |
|  | R | 3.97 | 2.32 |  |  | 5.58 | 2.47 |  |  |
|  | Sym | -0.01 | 0.47 | -0.14 | 0.88 | 0.03 | 0.27 | 0.62 | 0.53 |
| Len (mm) | L | 81.77 | 11.68 |  |  | 75.91 | 10.50 |  |  |
|  | R | 82.48 | 15.95 |  |  | 72.15 | 12.99 |  |  |
|  | Sym | 0.00 | 0.32 | 0.02 | 0.98 | 0.02 | 0.08 | 1.70 | 0.10 |

| | | **Cuneal segment (Cu)** | | | | **Lingual segment (Li)** | | | |
|---|---|---|---|---|---|---|---|---|---|
|  | Side | Mean | SD | t | p | Mean | SD | t | p |
| FA | L | 0.43 | 0.09 |  |  | 0.47 | 0.09 |  |  |
|  | R | 0.46 | 0.06 |  |  | 0.49 | 0.08 |  |  |
|  | Sym | -0.13 | 0.72 | -0.86 | 0.39 | -0.01 | 0.17 | -0.45 | 0.65 |
| Vol (ml) | L | 1.98 | 1.65 |  |  | 3.13 | 1.29 |  |  |
|  | R | 3.68 | 2.81 |  |  | 3.31 | 1.71 |  |  |
|  | Sym | -0.15 | 0.75 | -0.94 | 0.35 | -0.06 | 0.22 | -1.29 | 0.20 |
| Len (mm) | L | 90.66 | 16.74 |  |  | 86.86 | 11.64 |  |  |
|  | R | 99.34 | 14.30 |  |  | 87.31 | 10.59 |  |  |
|  | Sym | -0.12 | 0.71 | -0.77 | 0.44 | -0.00 | 0.09 | -0.20 | 0.84 |

Sym: symmetry coefficient, from the formula (Left – Right)/ (Left + Right). A positive value reflects lateralization to the left side, while a negative value reflects lateralization to the right; zero (0) reflects that both sides were equal in the measured value. The *t*-statistic and p-value refer to a *t*-test of means against reference constant (0) applied to the symmetry index. Reference constant chosen to test the null hypothesis that the measured value of ILF and subcomponents would be equal in size in both hemispheres, thus equal zero. * *t*-test, ILF volume left (mean 9.64 ml) vs. ILF volume right (mean 11.18 ml) ($t = -2.03$, $p < 0.05$). L: left side; R: right side. SD: standard deviation.

## 4.2. Study II

The organization and the possible functional implications of the MdLF were investigated with WM dissection, DTI analysis, and spatial normalization of two clinical cases. The MdLF was consistently organized into two layers: an antero-ventral segment (aMdLF) connecting the anterior STG (including temporal pole and planum polare) and the extrastriate lateral occipital cortex, and a posterior-dorsal segment (pMdLF) connecting the posterior STG (including anterior transverse temporal gyrus, aTTG; and planum temporale, PT) and the superior parietal lobule and lateral occipital cortex. The results were found in 100% of specimens and subjects analysed and in both the left and right hemispheres (Figure 5 A-B-C). Both fibre dissection and fibre tracking confirmed an intimate anatomical relation of the MdLF with the AF/SLF, ILF, IFOF, and optic radiations within the sagittal stratum of Sachs.

The aMdLF connects the aSTG and the planum polare (PP) with 1) the superior portion of lateral occipital cortex (sLOC); 2) the inferior portion of the lateral occipital cortex (iLOC); 3) the occipital pole (OP) in both right and left hemisphere (Figure 5-D). A slight asymmetry was detected on the left side with higher connectivity between the PP and the iLOC.

The pMdLF displayed a constant connection between the posterior portion of the superior temporal gyrus (pSTG), the aTTG, and PT, and the parieto-occipital region. The most important connections were found between the aTTG and SPL bilaterally, between the PT and SPL bilaterally, and between the PT and sLOC. In the statistical analysis of tractography results, the whole MdLF or the MdLF sub-segments showed lateralization in terms of volume, length, FA, MD, AD, or RD (Table 2).

The two patients analysed for tumours harbouring in the MdLF territories displayed different patterns of symptoms linked to an altered connectivity of the superior temporal gyrus.

A WHO-II oligodendroglioma infiltrating the anterior portion of superior temporal gyrus (aSTG) and temporal pole (TP) on the right side was detected at the MRI when patient #1 experienced seizures and hallucinations, mostly

described as a form of focal epilepsy with "déjà vu" phenomena and auditory hallucinations (melodies) evoked by other sounds. The preoperative neuropsychological examination revealed impaired visuo-constructional ability but no deficits in learning and memory. A complete surgical resection of FLAIR signal hyperintensity was performed, and at the postoperative neuropsychological examination (3 months after the operation), the patient reported several psychiatric symptoms including obsessions (counting and finger tapping of rhythms or melodies) as well as compulsive behaviour. The retrospective analysis of WM bundles involved by the tumour area and postoperative resection revealed that the aMdLF was mainly involved within the aSTG, but even the most anterior portion of the ILF was invaded in the TP.

Patient #2 displayed cognitive impairment involving learning, memory, and concentration. An MRI investigation revealed WHO-II astrocytoma in the pSTG on the left side. At the neurological examination, he described an intermittent whistling sound inside his head that made it difficult to perceive sounds in the surroundings. Preoperative neuropsychological and language examination confirmed the impaired learning and concentration in the audioverbal domain. A radical surgical resection of the FLAIR-hyperintense signal was performed, and speech function tests 3 months after the operation revealed impairment in all the domains. The relevant auditory contributions being word mobilization, language understanding, and verbal working memory, while reading performance and spelling results improved. Neuropsychological examination was essentially unchanged compared with the preoperative results and showed impaired learning potential for verbal stimuli but not for visual stimuli. The analysis of WM from the tumour region revealed that the tumour affected mainly the pMdLF, with minor infiltration of the short fibres of the AF on the left side.
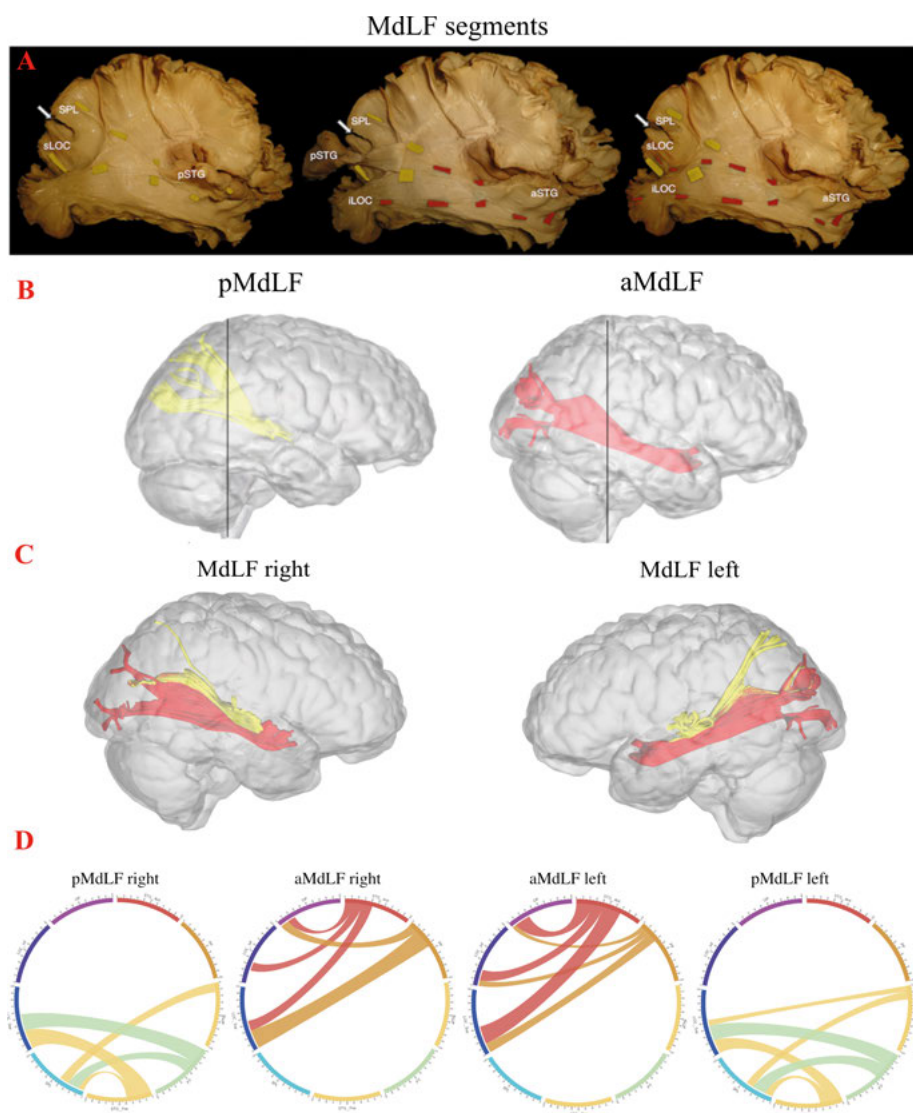
*Figure 5*. **A)** WM dissection of one right hemisphere, infero-lateral view. On the left side the anatomical course of the posterior middle longitudinal fascicle (pMdLF). Yellow tags underline the path of the pMdLF, which is the posterior, superficial branch of the MdLF: anterior terminations are in the posterior superior temporal gyrus (pSTG), namely Heschl's gyrus and the planum temporale; posterior terminations go across the parieto-occipital sulcus (POS; white arrow) at the superior parietal lobule (SPL) and at the superior lateral occipital cortex (sLOC). The central picture shows the anterior middle longitudinal fascicle (aMdLF). In this stage, pSTG has been disconnected and the stripped posteriorly along with pMdLF fibres, showing the deeper, anterior segment of the MdLF (aMdLF). Red tags show the path of the aMdLF from the anterior superior temporal gyrus (aSTG), including planum polare and temporal pole, to the LOC. On the right side, after the pSTG has been completely removed with the main fibres of the pMdLF, the aMdLF is uncovered. While

no fibres of the aMdLF were detected above the POS, we found that both the aMdLF and pMdLF had terminations at the level of the sLOC. Only the aMdLF showed cortical terminations at iLOC. **B)** Three-dimensional DTT reconstruction within a "glass-brain" of origin, course, and terminations of the pMdLF (yellow) and aMdLF (red) on the right-side hemisphere on sagittal projection.

**C-D)** Connectivity analysis at group level for the two subcomponents of the MdLF on both sides, with 3-dimensional reconstruction of the illustrative pathways and a circle diagram to show the connectivity between the selected regions from the Harvard-Oxford Cortical Atlas. The number associated to the cortical areas define the normalized number of streamlines (percentage) connecting the two regions with a cut-off of 3%. The aMdLF (red) was found to connect the anterior portion of the superior temporal gyrus (aSTG) and the PP on both sides with the occipital region only. Within the occipital region, three areas where consistently connected by the aMdLF: the superior portion of lateral occipital cortex (sLOC), which received 40% of the fibres on the left side and 45% on the right side; the inferior portion of lateral occipital cortex (iLOC), with 25% on the left side and 10% on right side; and the occipital pole (OP) receiving 25% of the fibres on the right side and 32% on the left side. The pMdLF (yellow) displayed a constant connection between the posterior portion of the superior temporal gyrus, the anterior temporal transverse gyrus (aTTG) and planum temporale (PT) with the parieto-occipital region. Fibres from the aTTG were found in connection with the superior parietal lobe (SPL) bilaterally (10% on the left side and 15% on the right side) and with sLOC on the left side only (10%). The PT displayed a connection with the SPL bilaterally (20% on the left side, 15% on the right side) and with the sLOC (25% on the right side and 22% on the left side). The posterior portion of the superior temporal gyrus (pSTG) displayed bilateral connections with the SPL (10% on the left side, 8% on the right side) and with sLOC (20% on the left side, 30% on the right side).

Table 2. Summary of descriptive results at group level with means, standard deviations (SD), and range for all the tract indices (upper part with volume, tract length, tract FA-value; lower part with MD, AD, and RD) for all subgroups. The Mann–Whitney U test for independent samples was used for comparison between groups for volume, length, FA, MD, Ad and RD. A *p*-value less than 0.05 was considered statistically significant.

SymCo: symmetry coefficient, from the formula (Left – Right)/ (Left + Right). A positive value reflects lateralization to the left side, while a negative value reflects lateralization to the right; zero (0) reflects that both sides were equal in the measured value. FA. Fractional anisotropy; MD: mean diffusivity, AD. axial diffusivity; RD: radial diffusivity; a.u: absolute unit.

**Table 1**

| | Indices | Volume | | | | Length | | | | FA | | | |
|---|---|---|---|---|---|---|---|---|---|---|---|---|---|
| | | [mm³] (SD) | Range | P | SymCo (SD) | [mm] (SD) | Range | P | SymCo (SD) | [a.u] (SD) | Range | P | SymCo (SD) |
| Tracts | Anterior Left | 6175 (3507) | 1885-14715 | 0.21 | 0.10 (0.21) | 86.78 (17.19) | 48.81-117.6 | 0.05 | 0.07 (0.10) | 0.76 (0.05) | 0.66-0.89 | 0.06 | 0.02 (0.04) |
| | Anterior Right | 4999 (2892) | 1238-13377 | | | 76.59 (18.58) | 23.25-108.8 | | | 0.73 (0.06) | 0.64-0.878 | | |
| | Posterior Left | 8084 (4120) | 2604-15324 | 0.66 | 0.01 (0.29) | 71.49 (14.63) | 36.68-101 | 0.65 | 0.05 (0.21) | 0.76 (0.04) | 0.66-0.88 | 0.18 | 0.05 (0.20) |
| | Posterior Right | 8628 (4306) | 1977-15996 | | | 69.64 (13.10) | 42.37-97.64 | | | 0.74 (0.05) | 0.64-0.87 | | |
| | MdLF Left | 11927 (5518) | 4197-24623 | 0.8 | -0.00 (0.15) | 78.65 (16.24) | 47.42-99.63 | 0.35 | 0.02 (0.05) | 0.67 (0.09) | 0.51-0.79 | 0.06 | -0.01 (0.03) |
| | MdLF Right | 12354 (6057) | 3680-23045 | | | 74.62 (13.07) | 50.48-94.88 | | | 0.69 (0.07) | 0.54-0.79 | | |

**Table 2**

| | Indices | MD | | | | AD | | | | RD | | | |
|---|---|---|---|---|---|---|---|---|---|---|---|---|---|
| | | [a.u] (SD) | Range | P | SymCo (SD) | [a.u] (SD) | Range | P | SymCo (SD) | [a.u] (SD) | Range | P | SymCo (SD) |
| Tracts | Anterior Left | 0.24 (0.01) | 0.2-0.26 | 0.06 | -0.01 (0.04) | 0.48 (0.02) | 0.42-0.51 | 0.14 | -0.01 (0.02) | 0.11(0.01) | 0.08-0.15 | 0.10 | -0.03 (0.09) |
| | Anterior Right | 0.24 (0.01) | 0.21-0.27 | | | 0.49 (0.01) | 0.46-0.53 | | | 0.12 (0.02) | 0.08-0.16 | | |
| | Posterior Left | 0.22 (0.01) | 0.19-0.26 | 0.13 | -0.01 (0.01) | 0.46 (0.02) | 0.41-0.49 | 0.09 | -0.01 (0.03) | 0.10 (0.01) | 0.07-0.14 | 0.13 | -0.03 (0.05) |
| | Posterior Right | 0.23 (0.02) | 0.18-0.26 | | | 0.47(0.02) | 0.4-0.5 | | | 0.11 (0.02) | 0.07-0.15 | | |
| | MdLF Left | 0.21 (0.02) | 0.14-0.26 | 0.11 | -0.03 (0.03) | 0.43 (0.05) | 0.32-0.5 | 0.14 | -0.02 (0.04) | 0.10 (0.01) | 0.07-0.14 | 0.11 | -0.03 (0.06) |
| | MdLF Right | 0.22 (0.02) | 0.15-0.26 | | | 0.45 (0.04) | 0.31-0.51 | | | 0.11 (0.01) | 0.07-0.15 | | |

## 4.3. Study III

One hundred and five MRI scans of 39 patients were used to investigate the differences between standard radiological/topographical classification of DG and the Brain-Grid classification system. The anatomical landmarks for the intersecting line placement were consistently identified in all the scans. We analysed findings according to the quantitative and qualitative involvement of grid voxels and considered tumour location, WM architecture, and longitudinal examinations. The mean number of infiltrated Brain-Grid voxels by the tumour in patients at the time of recruitment was 7.4 (range 1–16). The average number of grid voxels was lower in tumours with sharp radiological borders (5.1) and in grade II tumours (6.6) compared with diffuse (9) and WHO grade III tumours (8). The A3-C2-S2 and the A3-C2-S1 (corresponding to the subcortical insula/external capsule/basal ganglia and the frontoinsular region) were the most frequently infiltrated voxels, in 86% (18/21) and 66% (14/21) of the cases with left or bilateral infiltration. In patients with right-sided or bilateral infiltration, the A2-C2-S2 (89%, 17/19) and the A1-C2-S2 (63%, 12/19) were the most frequently involved voxels (Figure 6). The number and location of involved Brain-Grid voxels was consistent in all the cases re-analysed in the MNI space. The qualitative analysis of the grid voxels based on DTT atlas (Figure 3) showed that IFOF, UF, external capsule, and anterior thalamic radiation (ATR) were the WM structures most frequently associated with the tumours in the sub-insular/basal ganglia voxels (A2-C2-S2 and A3-C2-S2). The ATR, the genu of corpus callosum, Ci, and the anterior portion of IFOF were the most often identified tracts in tumours harboured in the fronto-medial voxels (A2-C2-S1 and A3-C2-S1). The AF, hSLF, and FAT were the second most associated with tumours of insular cortical /fronto-opercular region (A1-C2-S2) on the right side. In patients with serial MRI investigations, the Brain-Grid classification system enabled us to capture details about the direction of tumour progression even after oncological treatment (Figure 7).
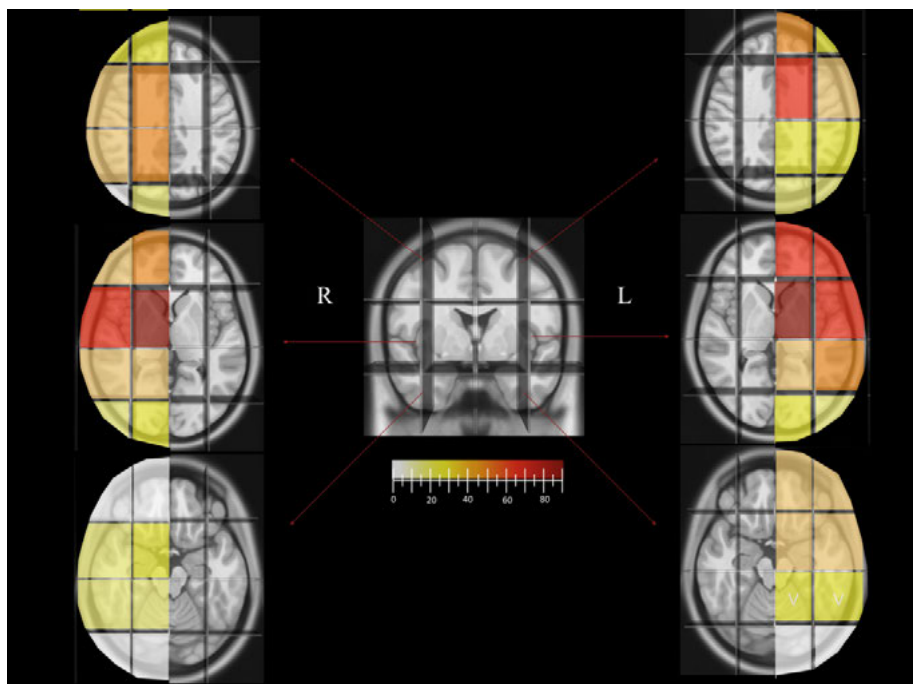
*Figure 6.* The picture shows the trend in the frequency of Brain-Grid voxels in pa-
tients with left- or right-sided tumours according to a colour gradient from white (0–
5%) to dark red (more than 80% of the cases). The cut-off for a high frequency (in-
tense orange) was set at 50% of the lesions. The A1C2S2 and A2C2S2 are most fre-
quently involved on the right side, while A3C1S2, A3C2S2, and A4C2S2 are most
frequently involved in patients with left-sided tumours, with the highest incidence
being displayed by the median and central voxels bilaterally (subcortical insular re-
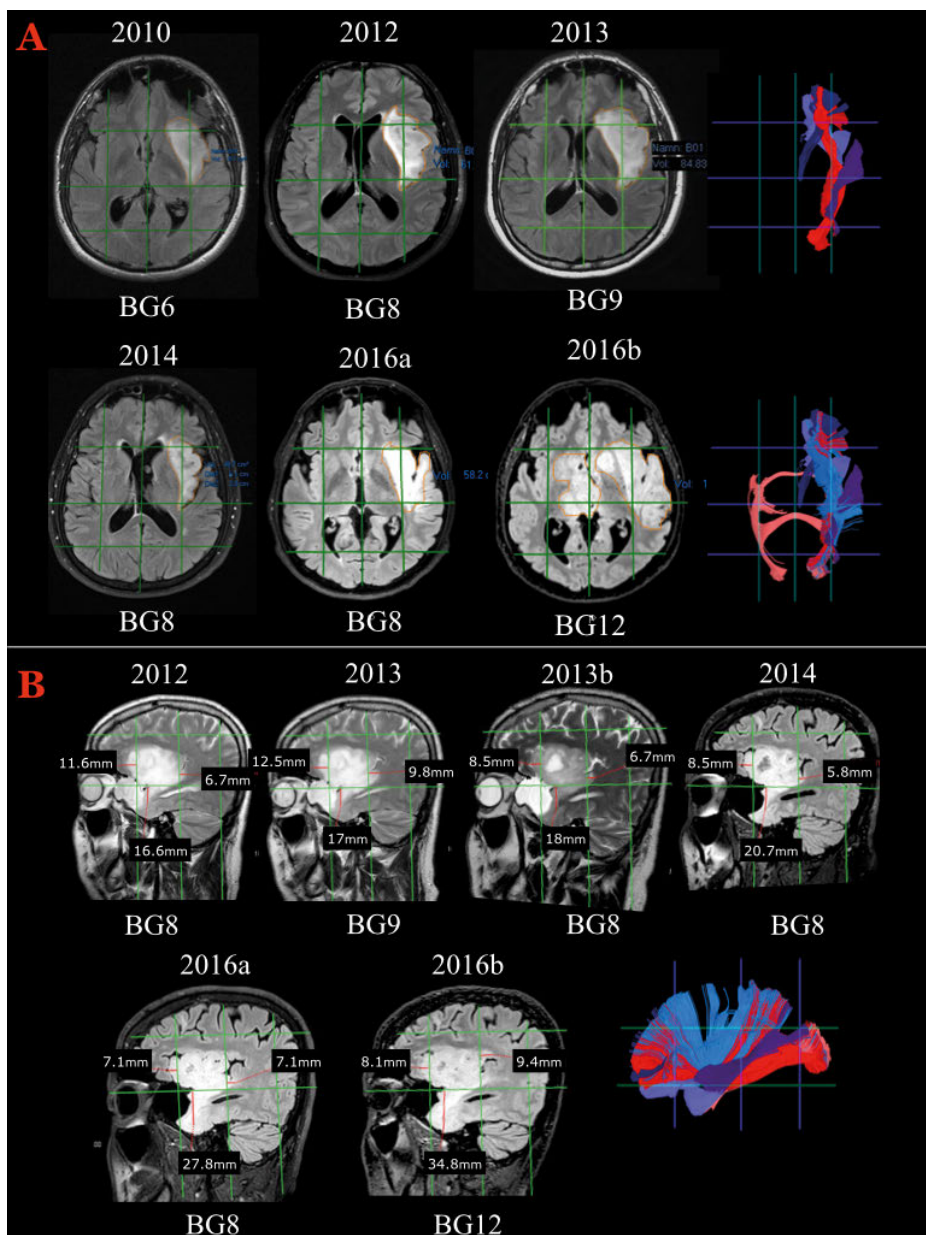gions' basal ganglia), both involved in over 80% of the cases (dark red).

*Figure 7.* **A)** Axial slices showing morphological FLAIR MR sequences during a longitudinal follow-up from 2010 and onwards. The signal hyperintensity evolved from 6 Brain-Grid units to 12 units, with a clear morphological transformation from a bulky shape to a diffuse and digitated shape infiltrating along the subcortical WM. On the right, tractographic reconstructions from the Brain-Grid atlas revealed the major WM involved during the progression. External capsule (light blue), UF (violet), IFOF (red), anterior thalamic radiation (dark blue), MdLF (purple), AC (salmon). Follow-up MRIs in 2012 and 2013 demonstrated increased tumour volume involving also a radial extension of hyperintensity from the insula through the extreme and external capsule. Eight grid voxels were infiltrated in 2012, 9 voxels in 2013, with involvement of the S3 areas on both the lateral side (A4) and medial side (A3) within the intermediate coronal area (C2). The invasion at this time point, as shown in **A–B**, is more prominent through the posterior portion of the insula and sub-insular WM. The potential pathways of infiltration are represented by the MdLF fibres on the lateral (A4) grid voxel and the IFOF fibres medially (A3), caudally through the periventricular WM (within the C3 area). After radiotherapy, the tumour volume and the infiltration along the longitudinal posterior pathways decreased significantly. The number of segments decreased to 8, due to a reduction of the hyperintensity in the A3C3S3 voxel. B) Details of the radiological follow-up between 2011 and 2016 that capture the switch from a bulky shape to a more diffuse and infiltrative appearance. On the right side, the Brain-Grid tractographic reconstructions summarizing the major WM bundles involved during tumour progression. External capsule (light blue), UF (violet), IFOF (red), anterior thalamic radiation (dark blue), MdLF (purple), AC (salmon). The sagittal projection shows that further infiltration along the antero-ventral pathways (UF) was not prevented by radiotherapy and that slow but continuous tumour growth occurred during the 3 years following radiotherapy. In 2016, when the entire anterior temporo-basal area was infiltrated, the number of infiltrated grid voxels was 12, showing also interhemispheric spread through the anterior commissure to the medial (A2) and intermediate coronal (C2) S2 and S3 grid voxels.

## 4.4. Study IV

A total of 102 patients were analysed to investigate differences in preferential cortical/subcortical locations of DG subtypes: 62 were diagnosed with WHO-II astrocytomas and 40 with WHO-II oligodendrogliomas. A molecular analysis confirming the histological diagnosis according to WHO-2016 classification [51] was performed in all the previously classified WHO-II oligo-astrocytomas (14 cases of which 6 were oligodendrogliomas and 8 were astrocytomas). In 41/62 astrocytomas the molecular analysis was available and revealed 25 IDHm profiles and 16 IDHwt. In the remaining 21 cases, the IDH status was unavailable, and they were therefore classified as astrocytomas NOS. In 26/40 oligodendrogliomas, the diagnosis was confirmed by molecular analysis (IDH mutation and LOH1p19q+). The patients without molecular confirmation were, however, included in the histological subgroups (matching radiological criteria, histological criteria, and proliferation index level <5%) but considered as diffuse astrocytomas NOS and diffuse oligodendrogliomas NOS [51]. The mean follow-up was 6.4 years (range 0.5–17 years).

No significative differences were detected in astrocytomas or oligodendrogliomas among molecular confirmed/NOS subgroups regarding age, survival from diagnosis, number of BG voxels, volume, EOR, radiological borders, and eloquent WM infiltration. No difference in the outcome of the different subgroups was detected with a log-rank Mantel–Cox analysis.

No difference between astrocytomas and oligodendrogliomas regarding the frequency of radiological and topographical features was detected. The quantitative analysis of the BG system analysis showed a median of 7 BG voxels infiltrated in the astrocytomas and 8 in the oligodendrogliomas. The qualitative analysis demonstrated that the A3-4C1S2 voxels (frontal cortical-subcortical SMA on the left side) and the A3-4C2-3 S2 (cortical-subcortical insular region on the left side) had the highest rate of invasion in patients with diffuse astrocytomas. In patients with oligodendrogliomas, the A2-3C2-S1-2 (fronto-mesial/fronto-striatal regions on both sides) were the most invaded BG voxels. The ROC curves for radiological variables applied to survival, displayed an optimal cut-off value for tumour volume at 47 ml for astrocytomas and 62 ml for oligodendrogliomas, while the number of BG voxels optimal for a cut-off analysis was 7 BG voxels for astrocytomas and 10 for oligodendrogliomas. Using the probabilistic gradient maps, the highest tumour index was identified for astrocytomas within the fronto-temporo-insular region on the left side, whereas the insula was involved both cortically and subcortically. For oligodendrogliomas, the gradient maps displayed a high tumour index in both the frontal lobes but more specifically within the deep WM of both sides, with symmetrical distribution (Figures 8–9).
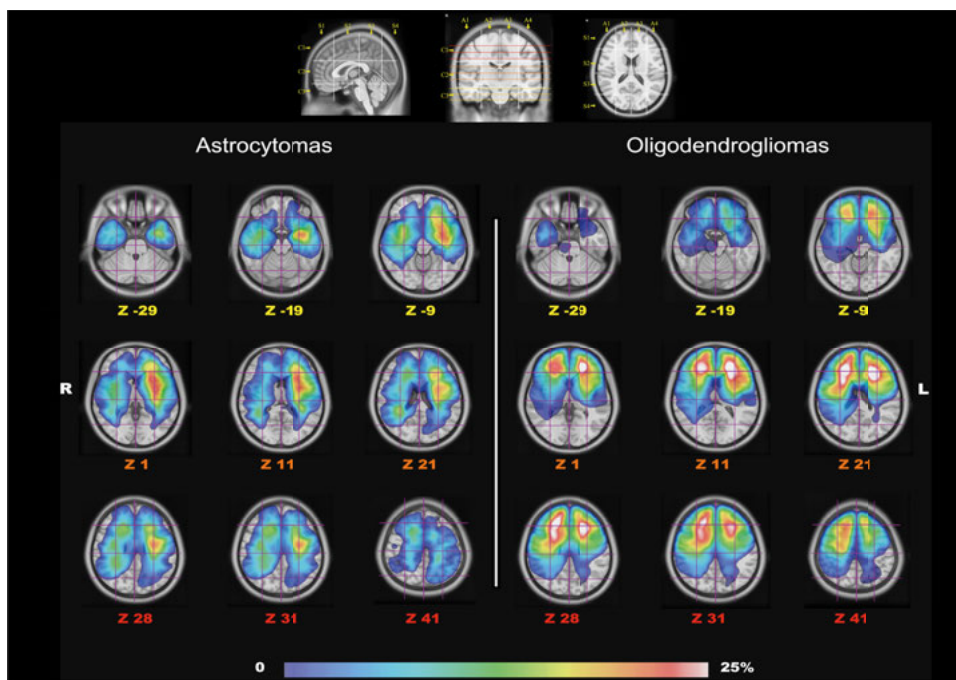
*Figure 8*. The image shows the gradient maps reconstructed from the fusion of each tumour region with Brain-Grid system for astrocytomas and oligodendrogliomas within the MNI space (*Z MNI* coordinates for each slice). In the upper part, the Brain-Grid system used as a reference for BG voxels count with sagittal, coronal, and axial projection of the BG lines. In the lower part, the frequency of tumour location for the two populations is colour graded (0%–25% in the gradient scale) according to the rate of voxel infiltration. R: right; L: left.
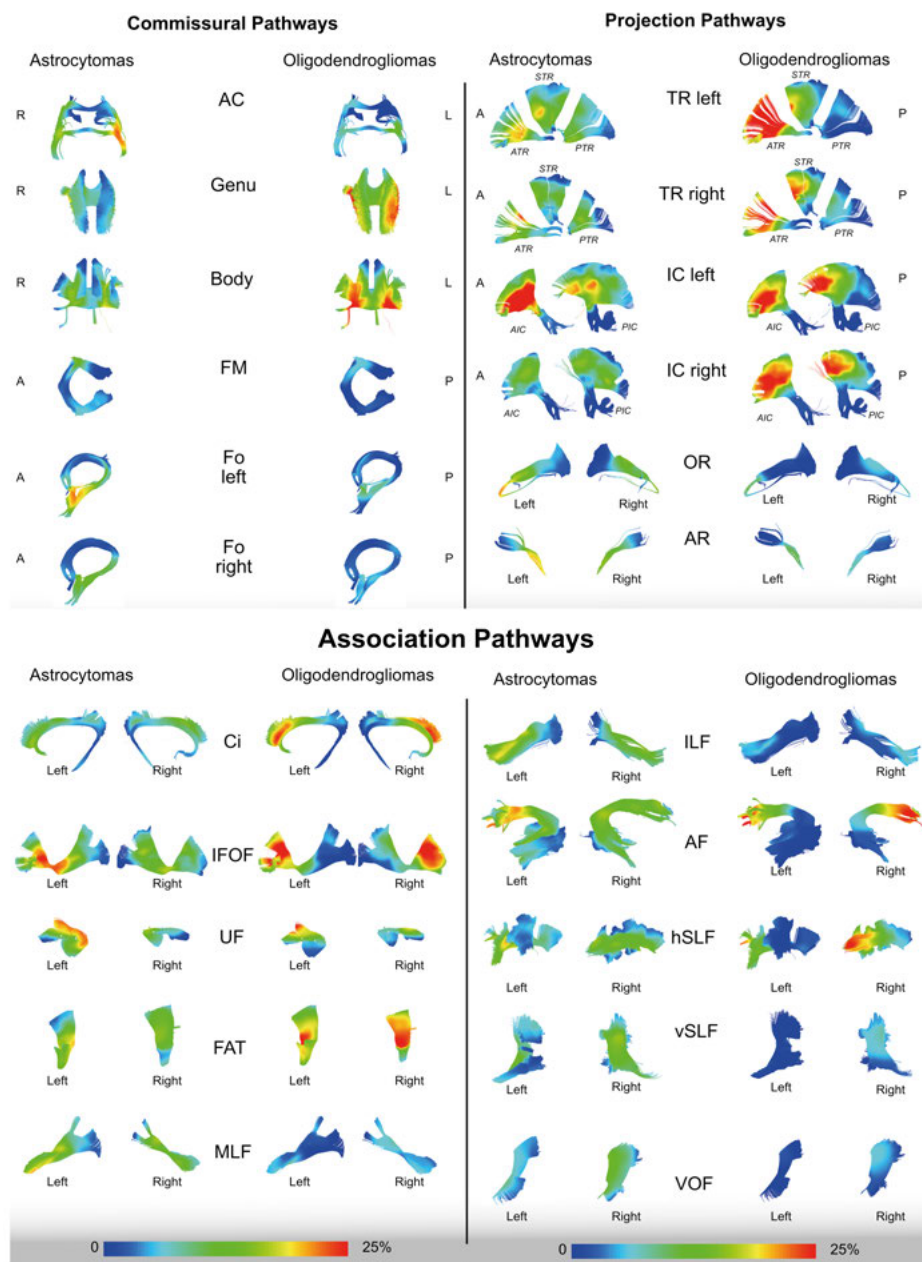
*Figure 9.* The image shows the frequency of invasion of commissural, projection and association pathways in astrocytomas and oligodendrogliomas using a gradient scale from the voxel-based analysis (0%–25% in the gradient scale) according to the rate of voxel infiltration. All the WM pathways are tracked in MNI space according to the Brain-Grid tractography Atlas [172].

AC, anterior commissure; Genu, anterior portion of corpus callosum; Body, middle portion of corpus callosum; FM, forceps major (posterior part of corpus callosum); Fo, fornix; R, right; L, left; A, anterior; P, posterior; TR, thalamic radiation; IC, fibres crossing the internal capsule; OR, optic radiation; AR, acoustic radiation; Ci, cingulum; IFOF, inferior fronto-occipital fasciculus; FAT, frontal aslant tract; MdLF, middle longitudinal fasciculus; ILF, inferior longitudinal fasciculus; AF, arcuate fasciculus; hSLF, horizontal indirect component of superior longitudinal fasciculus; vSLF, vertical indirect component of superior longitudinal fasciculus; VOF, vertical occipital fasciculus.

OS at 5 years was 85% for the astrocytoma group and 82% for the oligodendroglioma group. Overall survival at 10 years was 47% for the astrocytoma group and 60% for the oligodendroglioma group. At the univariate analysis, astrocytomas showed a shorter OS if bilateral invasion was detected ($p = 0.03$), if 7 or more BG voxels were invaded at the time of diagnosis ($p = 0.04$), and/or the anterior portion of the AF, IFOF, IC (considered eloquent WM) on the left side was invaded within the A3C2-S2 voxel ($p = 0.04$). In patients with oligodendrogliomas, a shorter OS was demonstrated if preoperative volume was larger than 62 ml ($p = 0.02$), and if the number of BG voxels was higher than 10 ($p = 0.002$) (Figure 10).
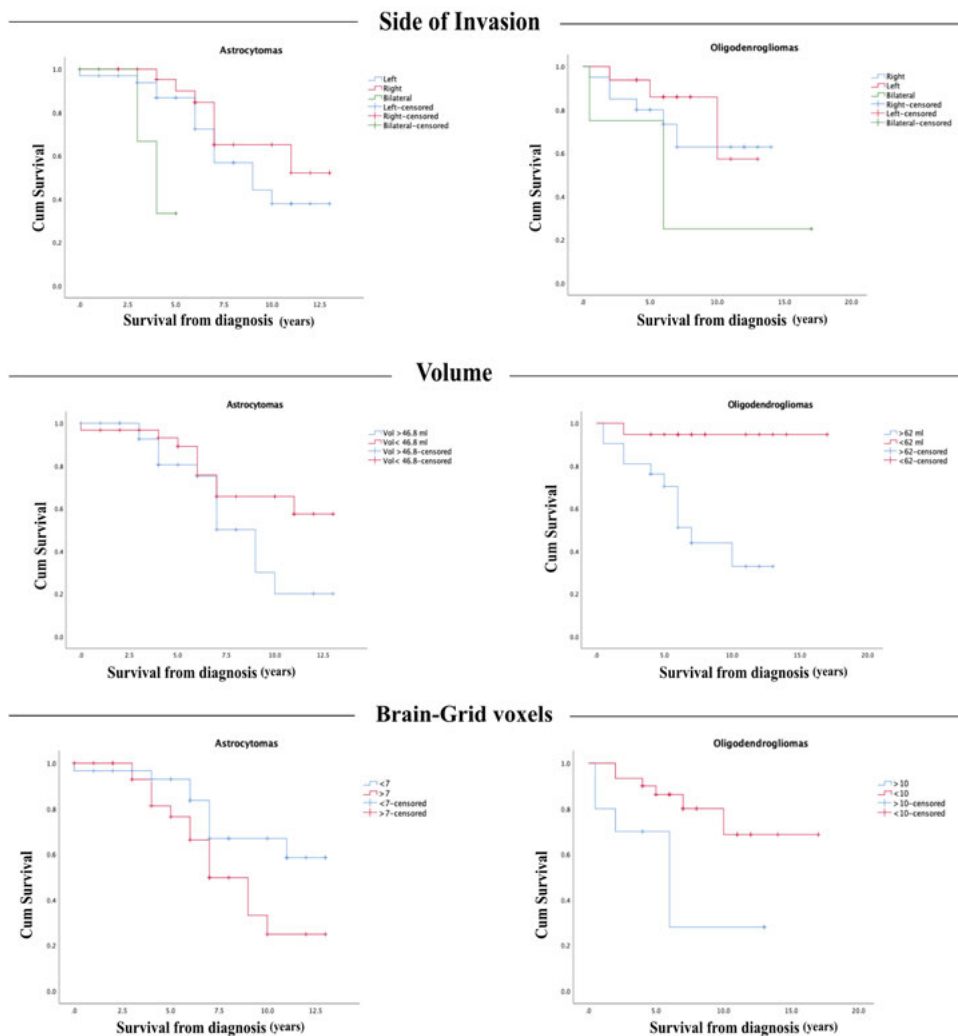
*Figure 10.* The image shows the result of survival probability using the Kaplan–Meier method [183], performing comparisons with the log-rank test to assess the effect of variables on overall survival (OS). The Kaplan–Meier graphs show the difference in OS in relation to side of invasion, tumour volume cut-off, Brain-Grid voxel cut-off.

In the logistic regression model, the univariate analysis of hazard ratio demonstrated that the side of invasion and the EOR were statistically significant predictors of OS (Table 2) in patients with diffuse astrocytomas. In patients with oligodendrogliomas, preoperative large tumour volume (>62 ml) and the number of BG voxels (>10) demonstrated a statistically significant predictor for shorter OS ($p < 0.05$).

In the multivariate model, bilateral tumour extension was the only independent predictor of shorter OS for patients with astrocytomas ($p = 0.018$, HR 2.997, 95% CI 1.204–7.458). Volume larger than 62 ml at diagnosis was the

only independent predictor of shorter OS in the patients with oligodendrogliomas ($p$ = 0.006, HR 1.012, 95% CI 1.003–1.021). The second level analysis between the variables demonstrated no significant interaction as indicating an increased risk for a shorter OS in either astrocytomas or in oligodendrogliomas (Table 3).

Table 3. The upper part of the table shows the univariate OS analyses. Proportional hazards models were used to assess the prognostic significance of multiple variables OS in the two different groups: astrocytomas and oligodendrogliomas. The IDH status (IDH mutant, IDHm or IDH wildtype, IDHwt) was tested in astrocytomas only. The comparison between the molecular confirmation against the not otherwise specified (NOS) groups was tested in both astrocytomas and oligodendrogliomas. The middle part of the table shows the forward step-wise proportional hazards modelling which was performed to assess the relative and independent prognostic capacity of each parameter. These two variables were selected by the equation as independent prognostic factors. The lower part of the table shows the interaction analysis as second block of the multivariate analysis for the most relevant variables: volume, EOR, Brain-Grid voxels, and eloquent WM. ([†]statistically significant for $p < 0.05$). OS: overall survival; HR: hazard risk; O c-off: optimal cut-off defined by ROC curves.

| Analyzed variables | | Astrocytomas | | | Oligodendrogliomas | | |
|---|---|---|---|---|---|---|---|
| **Univariate analysis** | | $p$ | HR | 95% CI | $p$ | HR | 95% CI |
| Side of invasion | -left/right/bilateral | .012[†] | .108 | .019–.611 | .614 | 1.709 | .212-13.748 |
| Radiological border | - bulky/diffuse | .319 | 1.613 | .629–4.137 | .172 | .355 | .080–1.570 |
| Volume | - >O c-off | .122 | .508 | .216–1.197 | .022[†] | .314 | .117–.848 |
| Brain-Grid Voxels | - >O c-off | .062 | .433 | .180–1.043 | .017[†] | 3.992 | 1.279–12.455 |
| Eloquent WM (BG) | -infiltrated | .063 | 2.327 | .956–5.668 | .904 | 1.064 | .386–2933 |
| Extent of Resection. | - GTR/ STR | .044[†] | .363 | .135–.972 | .619 | .772 | .279–2.141 |
| IDH status | - IDHm/IDHwt | .522 | 1.238 | .644- 2.337 | | | |
| Molecular status | -Confirmed / NOS | .756 | 1.171 | .432- 3.176 | .902 | 1.078 | .324- 3.589 |
| **Multivariate analysis** | | | | | | | |
| Side of invasion | - bilateral | .018[†] | 2.997 | 1.204-7.458 | | | |
| Volume | - > O c-off | | | | .006[†] | 1.012 | 1.003–1.021 |
| **Interaction analysis** | | | | | | | |
| Volume · EOR | | .780 | .995 | .964- 1.028 | .943 | 1.002 | .950-1.056 |
| Volume · Brain-Grid Voxels | | .668 | 1.692 | .153- 18.719 | .280 | 7.703 | .190-312.645 |
| Eloquent WM (BG) · EOR | | .629 | .994 | .972- 1.017 | .915 | .999 | .981-1.018 |
| Brain-Grid Voxels · EOR | | .629 | .994 | .991- 1.031 | .117 | .968 | .929-1.008 |

# 4.5. Study V

To investigate differences in WM preferential infiltration in DG, the tumour volume reconstructions of 102 patients analysed in Study IV were successfully merged into one probabilistic infiltration weighted gradient map into MNI space.

The statistics of each ROI displayed the mean infiltration based on the infiltration gradient index from 0 to 25%. The mean infiltration for the ROIs was 9% while the median infiltration was 8%. The median value was chosen as cut-off measure for further subgroup analysis. ROIs showing a mean infiltration >than 8% were considered HIF, while those with mean infiltration lower than 8% were considered LIF.

At the three-dimensional reconstruction of the five selected WM pathways, CaR, Genu, $Ci_F$, $AF_F$, and $IFOF_F$ were then considered regions showing HIF, and $Ci_T$, $AF_{TP}$, $IFOF_{SSS}$, $CST_F$, and $CST_{BS}$ were considered regions with LIF (Figure 11). HIF and LIF regions were compared using the frequency of infiltration from the gradient map as variable showing significative difference ($p$ = .003).

*Figure 11.* The figure shows the probabilistic infiltration map obtained merging 102 volumes of DLGG within MNI space. The genu of corpus callosum (Genu CC), the cingulum (Ci), the arcuate fasciculus (AF), the inferior fronto-occipital fasciculus (IFOF), and the cortico-spinal tract (CST) were reconstructed within the MNI space and merged with the gradient map. The left side of the WM bundles are displayed within a glass-brain three-dimensional reconstruction to show the position of the 20 region of interests (ROIs) analysed in the 20 subjects from the HCP database. Two ROIs were collected for each WM bundles for each side. The ROIs were collected based on the same anatomical criteria used for the TEM samples and based on the different infiltration rate according to the probabilistic map in HIF and LIF. The colour gradient in the red spectrum indicates the higher frequency of infiltration per voxels (25%).
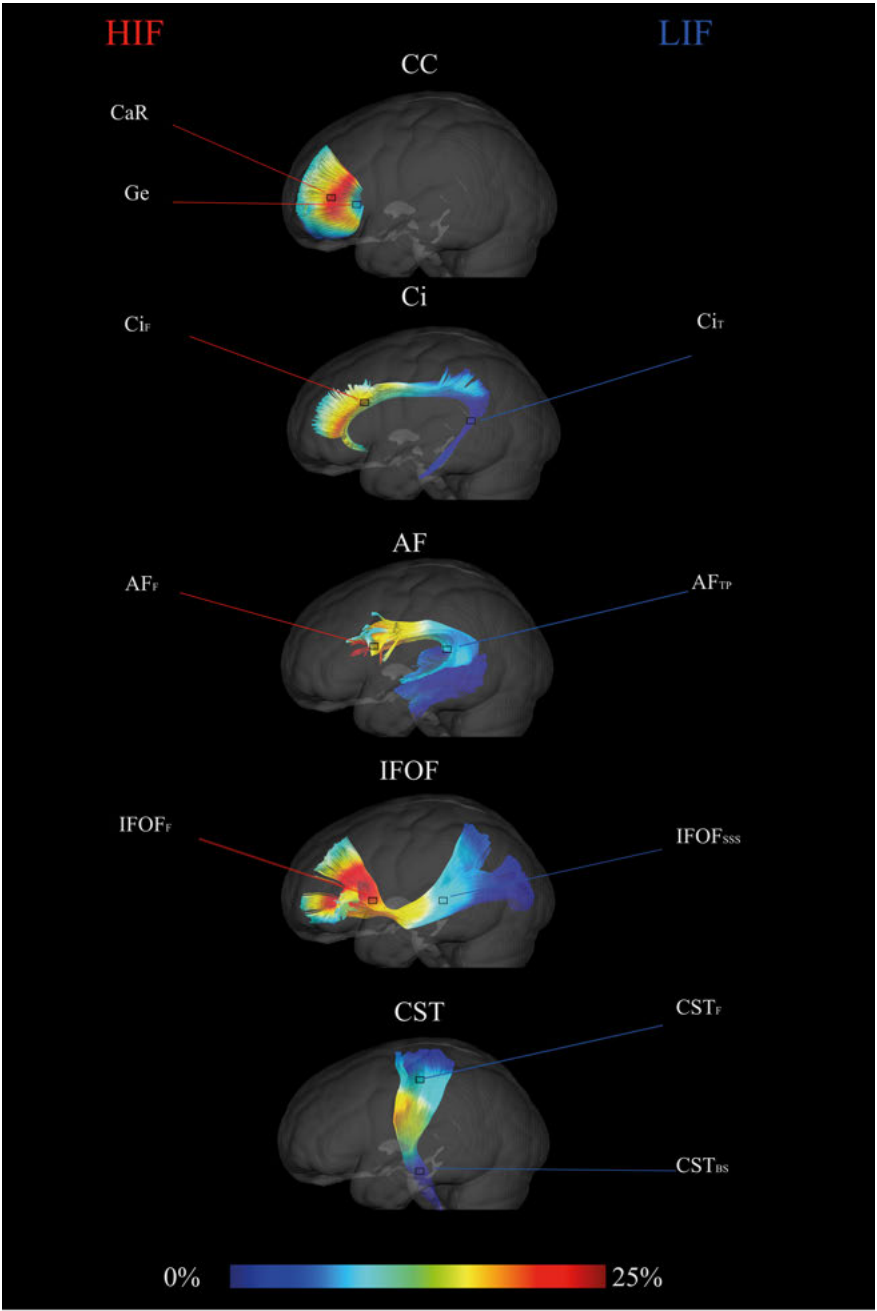
Using the TEM analysis, 5509 fibres were measured in 100 WM samples (mean $55.09 \pm 17.20$). The fibre density was significantly lower in the $IFOF_{SSS}$ compared with the $IFOF_F$ ($p < .001$). The fibre diameter (inner and/or outer) was significantly larger in the samples of the $Ci_F$, genu, $IFOF_{SSS}$ and $CST_{BS}$. The g-ratio was significantly lower in Ge, $IFOF_{SSS}$ and $CST_{BS}$ compared with the respective counterpart. The 100 sample regions were analysed according to the infiltration frequency with HIF regions, which displayed a significantly higher fibre density ($p = .02$), a smaller inner diameter ($p < .000$) and outer diameter ($p < .000$) but also a smaller g-ratio ($p < .013$). DTI was used for diffusion parameters analysis of the 400 selected ROIs, sampled with the anatomical criteria used for TEM. The mean volume for each ROI was $0.45 \pm 0.13$ cm3. Ge ROIs showed higher FA and lower MD-RD compared with callosal radiation. The $Ci_F$ displayed a lower AD compared with the temporal region ($p = .006$). The $AF_F$ showed a lower FA and AD compared with the $AF_{TP}$ region. The $IFOF_F$ presented lower FA, higher MD, and RD in respect to the $IFOF_{SSS}$. The $CST_F$ displayed a lower MD and AD compared with the $CST_{BS}$. No other differences were detected among the WM regions. A negative correlation ($r = -0.57$, $p = 0.008$) was found between infiltration frequency and AD. The HIF regions showed a significative lower AD compared with LIF regions ($p = 0.016$) (Table 4). No correlation between infiltration frequency and other diffusion parameters nor significant differences between HIF and LIF regions were found.

Table 4. Summary of the TEM results and DTI results for regions with high infiltration frequency (HIF) and region with low infiltration frequency (LIF). Mann Whitney U test was used for comparison between the two groups with significative results with p< 0.05 and 95 % Confidence interval.

| Infiltration Frequency | TEM | | | | | | | | | | | |
| --- | --- | --- | --- | --- | --- | --- | --- | --- | --- | --- | --- | --- |
| | Fiber density | SD | p | ID | SD | p | OD | SD | p | g-ratio | SD | p |
| LIF | .302 | .99 | .020* | .585 | .339 | .000* | 1.00 | .465 | .000* | .570 | .121 | .013* |
| HIF | .348 | .10 | | .530 | .299 | | .924 | .423 | | .560 | .125 | |
| | DTI | | | | | | | | | | | |
| | FA | SD | p | MD | SD | p | AD | SD | p | RD | SD | p |
| LIF | .730 | .087 | .210 | .210 | .036 | .091 | .420 | .03 | .016* | .11 | .045 | 540 |
| HIF | .670 | .014 | | .210 | .004 | | .390 | .04 | | .12 | .052 | |

N: number; SD: standard deviation; ID: inner diameter; OD: outer diameter; FA: fractional anisotropy; MD: mean diffusivity; AD: axial diffusivity; RD: radial diffusivity.

## 4.6. Study VI

Thirty-six patients were enrolled in this study to investigate the relationship between preoperative assessment, tumour-induced plasticity, and findings from intraoperative brain mapping (25 males; mean age $40 \pm 10$ years). In 23 cases the histological diagnosis revealed astrocytomas (12 WHO-II, 11 WHO-III), while 13 patients displayed oligodendrogliomas (4 WHO-II, and 9 WHO-III). In 34 patients the tumours were located on the left dominant hemisphere; in two patients the tumour was located on the right hemisphere, but the patients displayed preoperative bi-hemispheric dominance. The clinical onset included epileptic symptoms in 72% of the patients. The preoperative language examination revealed that 66% of the patients suffered some form of speech impairment (semantic 38%, phonology 13%, comprehension 8%, dysarthria 5%, verbal memory 2 %), while 84 % of the analysed patients displayed neuropsychological impairment (working memory 53%, attention 40%, learning 26%, executive functions 26%, memory 20%).

The radiological border was diffuse in the 61% of the cases. In 55% of the patients the tumour volume was larger than 56 ml (mean value/cut-off value according to ROC curves). The Brain-Grid classification system showed a median of 6 BG voxels infiltrated at the radiological diagnosis (BG voxels number > 6 in 55% of the patients). The qualitative analysis demonstrated that the A4C2S2 (left fronto-temporal opercula and insular cortex) had the highest rate of invasion (80%), followed by A3C2S2 (left subcortical insular and basal ganglia) (72%) and A4C1S2 (left dorsolateral prefrontal cortex) (50%).

We found intratumoral eloquent spots in 75% of the cases. The mean resection rate was $79\% \pm 15.8$. An overall number of 254 eloquent spots (156 cortical, 98 subcortical) were collected by using direct cortical or subcortical stimulation among 11 cortical and 13 subcortical functional domains (Tables 5–6).


Table 5. Summary of the descriptive results of demographic, radiological, histological, intraoperative and outcome variables. * NPS assessment was performed in only in 26 patients.

M: male; f: females; SD: standard deviation; IQR: inter quartile range; n°: number of cases; EP: epileptic onset; imp: impairment; NPS: neuropsychological.

| Type of variables | | Values |
|---|---|---|
| **Demographic variables** | | |
| Age | mean (SD) | 40.36 (10.8) |
| Gender | m (%)/ f (%) | 25 (69.4)/ 11(30.6) |
| **Radiological variables** | | |
| Tumour volume | mean (SD) | 57.30 (47.4) |
| Tumour border | sharp (%) /diffuse (%) | 14 (38.9)/ 22(61.1) |
| Brain-Grid voxels | median (IQR) | 6 (4-8) |
| **Clinical variables** | | |
| Onset symptoms | n° (%) | |
| EP focal | | 15(41.7) |
| Ep generalized | | 11(30.6) |
| Headache | | 1 (2.8) |
| Incidental | | 9 (25.0) |
| Preoperative language imp. | y(%) / n(%) | 24 (66.7) / 12 (33.3) |
| Preoperative NPS imp.* | y(%) / n(%) | 22 (84.6) / 4 (15.4) |
| **Histo-pathological variables** | | |
| Histology | n° (%) | |
| Astrocytomas | | 23 (63.9) |
| Oligodendrogliomas | | 13 (36.1) |
| Grade | | |
| A2 | | 12 (33.3) |
| A3 | | 11 (30.6) |
| O2 | | 4 (11.1) |
| O3 | | 9 (25.0) |
| IDH 1-2 status | (m/NOS) | |
| A2 | | 8/4 |
| A3 | | 9/2 |
| O2 | | 2/2 |
| O3 | | 7/2 |
| **Surgical variables** | | |
| Eloquent tumour | y(%)/ n(%) | 27(75)/ 9(25) |
| Intra-tumoral spots cortical. | mean (SD) | .36 (.93) |
| Intra-tumoral spots Subcortical  mean (SD) | | 1.33 (1.37) |
| Peritumoral spots cortical | mean (SD) | 1.39 (1.47) |
| Peritumoral subcortical | mean (SD) | 1.00 (1.37) |
| Intra-tumoral spots | mean (SD) | 1.61 (1.69) |
| Peritumoral spots | mean (SD) | 2.36 (2.1) |
| Cortical spots total | mean (SD) | 4.33 (2.7) |
| Subcortical spots total | mean (SD) | 2.72 (2.17) |
| Resection grade | mean (SD) | 79.07 (15.8) |
| **Outcome variables** | | |
| Survival | years (SD) | 3.36 (1.8) |

Table 6. A summary of the intraoperative eloquent spots displayed for each patient and organized according to the proximity to the FLAIR signal. Spots acquired within the FLAIR tumour signal were considered intratumoral (red colour shading, cortical or subcortical). Spots acquired between 1 and 10 mm from the tumour border were included as peritumoral (orange colour shading, cortical or subcortical). Those spots acquired with a distance superior than 10 mm were considered outside the tumour border (green colour shading, cortical or subcortical).

| Pat n | Localization | Intratumoral | | Peritumoral | | Outside tumor border | | Total number | |
|---|---|---|---|---|---|---|---|---|---|
| | | C | SC | C | SC | C | SC | C | SC |
| 1 | F-o L | SO | | | SO | | | 1 | 1 |
| 2 | F L | SO | SA | | SO | | | 1 | 2 |
| 3 | F-T-I L | | Hand(M) | | | SO Face(M) | | 2 | 1 |
| 4 | F-T-I L | | | | Arm(M) | SOx2 | | 2 | 1 |
| 5 | F-I L | | SP SP | SO SA | | SO | | 3 | 2 |
| 6 | T-I L | | | SA SO | | SO x3 Mouth(M) | | 6 | 0 |
| 7 | F-T-I L | | An | SO SA | | SO Mouth(M) | | 4 | 1 |
| 8 | F-T-I L | | | | | SA, Mouth(M) | | 2 | 0 |
| 9 | F-I L | | SP | | | SO, Mouth (M) | | 2 | 1 |
| 10 | F L | | | SOx2 Mouth(M) | SAx2 | Hand (M) Face (M) Mouth (M)x2 Tongue (M) An x2 SA | | 11 | 2 |
| 11 | T-I L | | | SO | | SOx2 Hand(M) SA | | 5 | 0 |
| 12 | DLPFC L | | | SA | SA Mc | Hand (M)x3 PP SA | | 6 | 2 |
| 13 | F-T-I L | SO | SP SA Mouth (M) | Mouth (M) Tongue(M) | | SP SAx2 An | | 6 | 3 |
| 14 | F-T-I L | An | SP SA | | | SOx2 Face(M) An | | 5 | 2 |
| 15 | F-I L | | SA | SAx2 | | SO Mouth(M) SAx2 | | 6 | 1 |
| 16 | DLPFC R | | Mc | Hand(M) | | Hand(M) Arm(M) Tongue(M) | | 4 | 1 |
| 17 | F o L | | | SOx3 SAx3 | SA Sox2 | Face (M) Mouth(M)x2 SO SA | | 11 | 3 |
| 18 | P L | | WMx3 | Hand(S) Arm(S) | Arm (S) | Leg(M) Arm(M) | | 4 | 4 |
| 19 | T-P-O L | | Anx3 Vifx2 Mouth (M) | Anx2 | | Tongue(S) | | 3 | 6 |
| 20 | F-I L | | An Mouth(M) SO | Tongue(M) Mouth (M) SOx2 | | Tongue(M)x2 Mouth (M) | | 7 | 3 |

66

| # | Location | | | | | | | | |
|---|---|---|---|---|---|---|---|---|---|
| 21 | P L | | SAx2 Mouth(S) | SO Mouth(M) Tongue(S) | | | Mouth(M) Hand(M) | 3 | 5 |
| 22 | F-T-I L | SO SP | SP | | | Mouth(M)x2 Face(M) Tongue(M)x2 SAx2 PPx2 | | 11 | 1 |
| 23 | T-P-I L | SAX2 SO Aux2 | SP | | SP | Mouth(M) SA PP | SP | 8 | 3 |
| 24 | T-O L | | R | Anx2 SA | SPx2 | SA | VifX2 | 4 | 5 |
| 25 | F L | | | An | WM SA | Ha(M) SA | | 3 | 2 |
| 26 | F-I L | | SAx2 SP | SA Tongue(M) SO SA | VA SA | SOx2 | Arm (M) Hand(M) Face(M) | 6 | 8 |
| 27 | F L | | SP | | Anx3 SA SP | SO | | 1 | 6 |
| 28 | T-I-O R | | | | | SO Face(M) | | 2 | 0 |
| 29 | T-I L | | PPx2 | | Vis PPx2 | SO Face(M) | | 2 | 5 |
| 30 | T-I L | | SP | | SP Vis | SO | | 1 | 3 |
| 31 | T-I L | | SP | SP | | SOx3 | Arm (M) SO | 4 | 3 |
| 32 | P L | | SA | Hand(M) SPP | An x2 | Face(M) | | 3 | 3 |
| 33 | F-T-I L | | PPx2 An Mc | PPx2 Mc | | SOx2 | | 5 | 4 |
| 34 | P L | Mouth(S) | | SA Mouth(M) | PP SAx4 | SOx2 Mouth(M) | SAx2 SO Vis | 6 | 9 |
| 35 | P L | | SPPx2 | SPP | SP | SO SA | | 3 | 3 |
| 36 | SMA L | Mc | Mc, AN | | | SO | Hand(M) | 2 | 3 |

Locations: F: frontal; P: parietal; T: temporal; I: insular; O: occipital; o: opercular; SMA: supplementary motor area; DLPFC: dorso-lateral prefrontal cortex; L: left side; R: right side.

M: motor; S: sensory; SP: semantic paraphasia; Mc: motor control (including negative motor mapping); SPP: spatial perception; An: anomia; SA: speech articulation domain (including verbal apraxia, latency, dysarthria); SO: speech output domain (including speech arrest); VIS: visceral sensation; Au: auditory phenomena; R: reading; Vif: visual field; Wm: working memory.

A total of 61 intratumoral and 85 peritumoral eloquent spots were acquired. One hundred and eight eloquent spots were detected outside the peritumoral area. A proximity of eloquent spots with the reconstructed WM bundles (< 5 mm) was detected in 40% of the cortical and 50% of the subcortical points.

At the comparison between eloquent/non-eloquent tumours, no difference was detected for age, gender, tumour grade, histology, tumour volume, number of BG voxels, radiological border, epileptic onset, preoperative language, or neuropsychological impairment.

At the correlation analysis, older age negatively correlated with the number of peritumoral cortical eloquent spots ($p < .05$) and directly correlated with the intratumoral cortical eloquent spots ($p < .05$). Preoperative tumour volume was directly correlated with the number of BG voxels ($p < .001$) with epileptic onset ($p < .05$) and negatively correlated with the number peritumoral subcortical eloquent spots ($p < .05$) and with the resection grade ($p < .05$). The EOR was positively correlated with the number of peritumoral eloquent spots subcortical ($p < .05$) and negatively correlated with the number of intratumoral eloquent spots cortical ($p < .05$). The number of intratumoral cortical eloquent spots was negatively correlated with the number of peritumoral cortical eloquent spots ($p < .05$).

Epileptic onset was correlated with tumour volume ($p < .05$), and A3C2S2/A4C2S2 voxels infiltration ($p < .05$). Preoperative NPS impairment was correlated with the number of BG voxels (>6) ($p < .05$).

Group comparison between younger and older patients (cut-off at 38 years old based on ROC curves) showed no significative difference for gender, histology, tumour grade, radiological borders, tumour volume, number of BG voxels, clinical variables, or location ($p >. 05$). The two groups displayed a significative difference in the number of intratumoral cortical eloquent spots ($p < .05$) and the number of peritumoral cortical eloquent spots ($p < .001$).

At the univariate logistic regression analysis, the presence of intratumoral eloquent spots at the subcortical level was correlated with a higher risk for NPS impairment ($p < .05$) and epilepsy ($p < .05$). A slightly higher risk of epileptic onset was also correlated with the presence of peritumoral eloquent spots at the cortical level ($p < .05$). The infiltration of the BG voxel A3C2S2 (left subcortical insular and basal ganglia) was correlated with a significant high risk of NPS impairment ($p < .05$, HR 7.5), epilepsy ($p < .01$, HR 5.5), and language impairment ($p < .05$, HR 1.2). The infiltration of the BG voxel A4C2S2 (left fronto-temporal opercula and insular cortex) was correlated with a significant higher risk of NPS impairment ($p < .05$, HR 3.7), and epileptic onset ($p < .01$, HR 6.2). At the multivariate logistic regression analysis, preoperative NPS impairment was the only independent variable able to predict the intraoperative finding of eloquent tumours ($p < .01$, HR 6.3) (Table 7).

Table 7. Summary of the logistic regression analysis. Univariate model with NPS impairment, epilepsy and language impairment as dependent variables correlated with the number of intraoperative eloquent spots and the different infiltrated BG voxels. In the lower part the result from the multivariate analysis with eloquent tumours as dependent variable and all the demographic, radiological, and clinical variables analysed as predictor factors. *. Correlation is significant with $p$ value < 0.05. HR: hazard risk; CI: confidence interval.

| Univariate | Binary Logistic regression | | |
| | p | HR | CI (95%) |
| --- | --- | --- | --- |
| NPS impairment / intratumoral spots cortical | .201 | 3.679 | .501- 27.036 |
| NPS impairment / intratumoral spots subcortical | .019* | 2.200 | 1.140-4.244 |
| NPS impairment / peritumoral spots cortical | .096 | 1.464 | .935- 2.294 |
| NPS impairment / peritumoral spots subcortical | .112 | 1.548 | .903- 2.651 |
| Epilepsy /intratumoral spots cortical | .105 | 5.429 | .704- 41.875 |
| Epilepsy /intratumoral spots subcortical | .028* | 1.766 | 1.064-2.929 |
| Epilepsy /peritumoral spots cortical | .047* | 1.533 | 1.069-2.337 |
| Epilepsy /peritumoral spots subcortical | .251 | 1.288 | .836- 1.985 |
| Language impairment /Intratumoral spots cortical | .196 | 2.554 | .616-10.583 |
| Language impairment /Intratumoral spots subcortical | .098 | 1.421 | .937-2.153 |
| Language impairment /Peritumoral spots cortical | .511 | 1.118 | .802-1.558 |
| Language impairment /Peritumoral spots subcortical | .693 | .924 | .624- 1.368 |
| NPS impairment /A3C2S2 infiltration | .007* | 7.500 | 1.715-32.796 |
| NPS impairment /A4C1S2 infiltration | .121 | 2.500 | .784- 7.971 |
| NPS impairment /A4C2S2 infiltration | .019* | 3.750 | 1.245-11.299 |
| Epilepsy /A3C2S2 infiltration | .002* | 5.500 | 1.895-15.960 |
| Epilepsy /A4C1S2 infiltration | .127 | 3.500 | 1.152-10.633 |
| Epilepsy /A4C2S2 infiltration | .001* | 6.250 | 2.175-17.958 |
| Language impairment / A3C2S2 infiltration | .024* | 2.714 | 1.141-6.457 |
| Language impairment / A4C1S2 infiltration | .638 | 1.250 | .493-3.167 |
| Language impairment / A4C2S2 infiltration | .100 | 1.900 | .883-4.086 |
| **Multivariate** | | | |
| Eloquent tumours / Preoperative NPS impairment | .003* | 6.333 | 1.874-21.402 |

# 5. General Discussion

The six studies herein presented in this thesis describe a new way to investigate the complex and not fully understood WM-glioma interaction.

There are several limiting factors influencing our comprehension of this interaction. First, the description of the human connectome is far from being complete. Methodological advances in the anatomic subcortical characterization have demonstrated the important role of the WM in clarifying how cortical skills are combined in the short and long term [30,36–40]. Consequently, it has become clear that the functional contribution of a given area depends on its integration with the activity of anatomically interconnected regions. Using a systematic validation between WM dissection and DT tractography, new networks/connections have been described that have improved the general comprehension of the brain connectome [1,10,21,35,96,142]. On the other hand, many of the structural connections and functional correlates are still unclear [31,34,35], and already described fibre bundles have only recently been decoded in functional terms [26,46,48]. Moreover, even though new connections have been extensively described on the macroscale level, in biological terms, structural connectivity is encountered at many levels, from molecules to the morphology of cells [39,186,187]. In fact, while a larger number of anatomical studies of the human brain have been carried out at the macroscopic (cerebral lobes, surface landmarks, and WM tracts) or microscopic (cytoarchitectonic, myeloarchitectonic, chemoarchitectonic, etc.) anatomical level, there is virtually no information on the finer connectivity patterns, including neuronal connection densities or laminar projection patterns in relation to anatomically segregated cortical areas or intraregional differentiation [39,186,187]. Structure enables function, defining the set of possible actions and interactions of a biological system. The connectivity structure of a neural system defines its internal dynamic states, and its range of responses to external perturbation at the individual level is therefore still poorly understood.

The second limiting factor is the complex nature of pathological/lesion models to study the individual connectome. A pathological process such as a glioma concerns not only the anatomic region directly affected by the tumour but also affects the global and regional nature of the structural and functional architecture of the brain at the individual level [6,32,43–46]. Biomathematical models also demonstrated that glioma cells take advantage of WM fibres to disseminate, making the management of these lesions challenging because of

their high sub-cortical infiltrative potential [32,109,132,135,139,188,189]. In addition, DLGGs show preferential location into areas of the brain that are not resectable without inflicting functional neurological impairment in the patient [109,147]. The result is that not only the individual mechanisms behind the clinical heterogeneity in glioma phases and clinical onset are still not clear, but also gliomas' tendency to infiltrate eloquent areas [57,68–70] is still poorly understood.

The third limiting factor regards the underestimated role of WM anatomy in modern radiological classification systems. WM bundles are the main eloquent component of the so-called "minimal common brain" [109,147,190]. They are central from the surgical perspective and thus for functional outcome, but still neglected by standard classification systems. In fact, gliomas are still named according to the nomenclature of major lobes invaded despite their subcortical extension [57,70,83], which may limit our comprehension of infiltration patterns and possibly the common origin of some histological subtypes.

A better understanding of the WM/glioma interplay would need to address these limitations with more attention to the role of WM anatomy in each patient with a DG. This would improve our comprehension of the individual connectome [32,41,66] and would advance our understanding of the biological origin and kinetics of gliomas, the tumour-induced neuroplasticity/reorganization, and the resectability of these lesions.

The work presented in this thesis represents an effort to merge structural WM information (the brain connectome at macroscale level), topographical/radiological features (tumour invasiveness), clinical/cognitive assessment (NPS and language), and intraoperative findings. These methods can be applied in clinical practice for all possible tumour locations on an individual level but with use of a standardized model.


## 5.1. Study I

Two different techniques were used in Study I to explore the unclear connectivity of the ILF. Our results from post-mortem WM dissection and subject-by-subject in vivo DTT revealed a clear, constant, and detailed organization of the ILF fibres in the occipito-temporal region. The connectomic organization of the ILF is formed by fusiform, lingual, dorsolateral occipital, and cuneal sub-components with different and specific connectivity between temporal and occipital lobes. Both post-mortem and in vivo analyses of the anatomical pattern of connectivity revealed that the Fu branch and the DLOC branches had the richest pattern of connectivity among the ILF subcomponents (Figure 4). These bundles seem to support a parallel and bidirectional network between extrastriate visual cortices and the anterior temporal region, with a very wide distribution of cortical terminations. The Li branch showed a quite constant cortical occipital endpoint, with a trajectory from the caudal

portion of occipital early visual areas (visual area 3/lingual gyrus) to the anterior temporal lobe and with a minor number of cortical end points but with a distribution similar to the other branches (T2–T4). The cuneal branch displayed a higher individual variability and showed the lowest amount of connectivity (average of 1.2 of 5 potential cortical endpoints).

Methodologically, we can confirm the concordance between WM dissection and diffusion tensor imaging that has already been demonstrated by other studies [21,26–29]. The use of both techniques (WM dissection and diffusion tensor imaging) was important for the study of this poorly understood bundle to increase the accuracy of the results, minimizing the risk for artefacts resulting from each technique's limitations.

Merging our detailed anatomical results with functional non-invasive studies and using information from direct cortical/subcortical stimulation studies [46,147,191–193], we were able to confirm a pivotal role of the ILF in connecting highly specialized visual areas to anterior temporal areas important for emotional, semantic, and visual memory processes. We believe that the combination of these two techniques should be considered the gold standard anatomical investigation to reveal the connectomic organization of WM.

# 5.2. Study II

Anatomy, connectivity, and clinical implications of the MdLF were investigated with a combination of WM dissection, DTT and clinical cases. In 100% of the examined hemispheres (with both dissection and DTT) a clear, constant, and detailed organization of the MdLF fibres in the temporo-parieto-occipital region was identified. Three major controversies regarding the MdLF were discussed in relation to our results: its posterior cortical terminations, its subdivisions, and its functional role.

First, posterior terminations covered a broad area going from the SPL and PreCu to the Cu and LOC. The absence of cortical terminations of the IPL (AG and/or SG) was probably the most striking dissonance between pure virtual dissection studies [194–199] and WM dissection studies. This was consistent with previous anatomic studies showing that the MdLF connects the entire STG with the SPL and the occipital lobe [200–202]. This result is probably due to the superior spatial resolution of WM dissection compared with tractography analysis [27,203,204], which allows a clear documentation of the spatial relationship of the two branches of the MdLF and of their cortical terminations.

The second controversy regarded the MdLF subdivision. Our main finding was that the MdLF is consistently organized into two layers: an antero-ventral segment (aMdLF) connecting the anterior STG (including TP and PP) and the extrastriate lateral occipital cortex, and a posterior-dorsal segment (pMdLF)

connecting the posterior STG (including aTTG and PT) and the superior parietal lobule and lateral occipital cortex. These findings are in line with the description by Wang et al. [202] and in disagreement with the results reported by Kalyvas and colleagues [200], who described three subcomponents with different connection patterns. Our findings seem consistent and based on congruent data derived by high quality anatomical specimens and DTI imaging with high angular resolution of imaging, as described by other authors [165,166].

Third, no conclusive data have been provided by electrical stimulation during awake surgery [205] nor by lesion models, such as after post-operative resection of the bundle. To better understand the functional implications of the MdLF connectivity, anatomical results and two clinical cases of DLGGs impinging on MdLF territories were used in our study. The patients underwent an extensive cognitive and language assessment pre-and postoperatively. Due to the anatomical substrate (involving cortical region and surrounding WM pathways), the pMdLF, especially on left side, may be involved in learning process for verbal-auditory stimuli. The aMdLF may, on the other hand, be involved in processing and retrieving auditory information already consolidated within the temporal lobe after passing sematic and emotional filters. In our patients, the tumours have interfered with normal brain function by disrupting the functional connectivity of the auditory brain networks within peritumoral and distant brain areas, thereby promoting hallucinatory activity [63,64]. According to the connectomic organization of the areas close to the tumours, peritumoral loco-regional connectivity, subcortical connectivity (MdLF, AF), and interhemispheric connectivity (via thalamus) may have been unbalanced by DLGG infiltration of the STG, with both negative and positive symptoms.

We suggest that the damage to MdLF sub-segments may create a loss of balance within the auditory networks, contributing to impaired verbal learning and memory, auditory hallucinations, and even psychiatric disorders [206–211]. The application of new anatomical details to the clinical cases, within a common radiological space (MNI) created a more advanced model to explore the interaction between gliomas and WM connectivity at the individual level.

## 5.3. Study III

In this study, local radiological anatomy (MRI sequences), WM architecture (a tractography atlas), morphology, and kinetics of gliomas (longitudinal investigations) were merged into one classification system. A standardized grid system (the Brain-Grid) was created, providing an accurate and reliable radiological classification in a cohort of patients with suspected DGs. The system was applied in 105 MRI investigations and was consistent regarding the comparison between the MNI space and the patient-specific space and displayed several advantages compared with other methods.

The Brain-Grid voxels analysis on serial MRIs highlighted the direction and speed of tumour invasion through WM pathways, otherwise neglected by standard volume computation and the lobar classification system. In addition, we were also able to detect changes in the direction of WM infiltration after radiotherapy that were easily missed with use of standard techniques.

We collected both quantitative and qualitative information about the kinetics of gliomas. The system emphasized the differences between diffuse and bulky tumours (sharp tumour borders) in terms of number of voxels involved and their preferential locations, possibly reflecting different stages of glioma proliferation. As a complement to information regarding the localization and extension of gliomas, the real value of this system was the possibility to predict which WM bundles are associated with the invaded voxels. For instance, the ATR was found to be a different potential direction of tumour spread besides the IFOF, UF, and external capsule in right- and left-sided tumours harboured in insular and basal ganglia grid voxels.

Our results support the use of this radiological-anatomical system in the field of neurosurgical oncology, where a more precise classification and a better orientation among the deep located pathways is mandatory. From the neurosurgical perspective, considering the limited plastic capacity of WM [109,147], qualitative and quantitative information provided by this technique could provide new insights into the surgical resectability of DGs for each Brain-Grid voxel. A tailored surgical approach and the optimal timing for combined surgical and adjuvant therapies may be based on this map of resectability and preferential direction of the WM fibre bundles invaded by gliomas [212].

# 5.4. Study IV

Applying more extensive knowledge of WM anatomy to glioma patients, this study described the invasiveness of 102 DLGGs (using the Brain-Grid system), their preferential locations (with a frequency probabilistic map), and the involved WM networks (BG tractography atlas).

The most important result provided by this study is the clear difference in preferential location between histological types of diffuse gliomas.

Astrocytomas were preferentially located in the fronto-temporo-insular region on the left side, while oligodendrogliomas infiltrate the deep WM of the frontal lobes bilaterally. Previous articles investigating preferential locations of diffuse gliomas, where different histological subtypes and grades were considered as one single entity, did not show similar distributions [68,71,83,109,213]. When the WM was analysed, diffuse astrocytomas tended to significantly invade association and projection WM pathways between the insula and ventricles within the fronto-temporo-insular region (A3C2S2). Diffuse oligodendro-

gliomas on the other hand, infiltrate larger and more heterogeneous WM networks (association-commissural-projection WM pathways), preferentially between basal ganglia and the deep and mesial regions of the frontal lobe bilaterally.

These topographical differences in the regions involved bear some similarities to the mechanisms of cell migration during brain development [214–216]. The insula is among the first cortical regions to appear, and its development is linked to radial glial migration, which establishes the general cyto-architectonical framework of the different forebrain subdivisions from the ventricular zone to pia [214,215,217]. After neuronal production ceases, radial glial cells retract their ventricular and pial attachments and differentiate into astrocytes [214,218–220]. On the other hand, the process of oligodendrocytes migration is regulated by a more prominent tangential migration, which increases the cellular complexity of forebrain circuits following preferential WM tracts from the globus pallidus internus (in human, anterior entopeduncular nucleus in rodents and birds) to anterior and dorsal cortical regions [214,216,221–223]. The differences in preferential location and WM pathways invaded by tumours may reflect the different biological behaviours of the two groups of glia cells, suggesting abnormalities in cell migration at some point in the developmental or the adult stage [214,215]. The link between the type of WM invasion and outcome was evident in diffuse astrocytomas that preferentially invaded association and projection WM networks on the left side within the fronto-temporo-insular BG voxel (A3C2S2) because these tumours were associated with a significantly reduced OS ($p = 0.02$).

Oligodendrogliomas showed a larger volume at diagnosis (62 ml vs 46 ml for astrocytomas) but without significative difference between the two groups. Analysed in relation to its impact on OS, only in oligodendrogliomas was there a strong association between preoperative volume and a shorter OS. On the other hand, tumours with the same volume can behave differently based on their location and radiological borders (sharp or diffuse), and when only these two parameters were considered, we were unable to detect tumour invasiveness. The BG system allowed us to identify a new quantitative difference between the two groups in terms of invasiveness. The critical number of 7 BG voxels for astrocytomas and 10 BG voxels infiltrated in oligodendrogliomas significantly predicted the probability of a shorter OS in both groups ($p < 0.05$) and more consistently in oligodendrogliomas, where the number of BG voxels can be considered a risk factor for the prognosis (Table 3). The number of BG voxels can represent a new prognostic variable able to predict tumour invasiveness and its impact on OS and thereby suggest an advanced stage of tumour infiltration at the time of radiological diagnosis.

## 5.5. Study V

To further investigate differences in gliomas' preferential locations, we focused on possible morphological WM factors facilitating glioma invasion. Infiltration analysis of 102 patients with DLGGs was used to detect HIF and LIF regions within major white matter pathways. Then, transmission electronic microscopy (TEM) of different WM regions (in cadaver specimens) and diffusion parameters analysis (in healthy individuals) were used to detect morphological and diffusion differences between the two groups. Our study provided four main results.

First, the infiltration analysis demonstrated clear regional differences in the infiltration frequency of five major WM bundles. In our population, anterior frontal regions were significantly involved in DLGG preferential locations, with hot spots for locations which were mostly subcortical. These topographical differences in pathways of infiltration recall some similarities with the mechanisms of cell migration during brain development [214–216]. Glioma cells actively migrate through extracellular spaces of the brain, and especially along WM fibres, acting like non-malignant brain cells during embryonic development or adult stem cells in the mature brain [224]. Once the tumour front cells reach the deep subcortical WM, these tumours share similar pathways according to the original locations [225]. These major pathways seem to show a common pattern of infiltration which is centripetal towards the central core and basal ganglia [132,139,226]. This tendency to infiltrate anterior regions close to basal ganglia was identified in our population, enhancing regional differences within the same WM bundles.

Second, regional differences within the same WM bundles were detected by morphological analysis and diffusion parameter analysis. The frontal portion of IFOF displayed higher fibre density, a smaller fibre diameter, and a higher myelin concentration. These differences may also match the lower FA and higher MD and RD presented by the frontal portion of the IFOF. Even for the CST, the frontal (dorsal) region displayed a smaller diameter (both inner and outer) but higher myelin thickness compared with the BS. The diffusion analysis demonstrated a significantly lower MD and AD in the frontal portion. These results may be linked to a different organization of the fibres within the two regions, with more organized and packed WM fibres at the level of the brainstem reflecting higher MD and AD. Altogether, morphological features and diffusion proprieties seem to indicate that regional differences within the same pathways are associated with different topographical variables, such as coherent fibre orientation or packing of myelinated fibres. Differences within the same bundles may therefore be expected, as suggested by other authors [227,228]. These differences seem also to indicate a consistent topographical variability. In fact, regions within the limbic system (frontal-fronto/mesial, subinsular/insular) or the frontal lobe, which synchronizes large scale networks,

displayed differences in extracellular space, higher myelin contents, and high connectivity [34,229–231].

Third, regions with HIF displayed a clear difference in fibre density, fibre diameter, and myelin thickness compared with LIF regions. Fourth, DTI analysis indicated that HIF regions present a lower AD in respect to LIF regions.

All together, these results may suggest that the fibre diameter and the organization of the fibres within the HIF regions may be consistently linked to the tumour preferential location in DLGGs compared with LIF regions. The smaller diameter with high myelin concentration may be linked to two different considerations. First, the invasion of glioma cells into the adjacent brain tissue is guided by a combination of multiple molecular and physical mechanisms along pre-existing tracks of least resistance [224]. The major invasion routes are basement membranes and intercellular tracks provided by myelinated axons and astrocyte processes [232,233]. Larger extracellular space between fibres may be therefore facilitate tumour cells becoming a pathway of least resistance for dissemination. The second consideration is that the lower AD detected in HIF regions may also represent a measure of a less coherent organization of WM tracts. This seems to be related to regions with a higher number of crossing fibres (i.e., fronto-orbital region, deep frontal regions) rather than those with packed myelinated fibres (such as SSS or BS)[229,230]. On the other hand, reduced AD with age may result from increased numbers of brain fibres or increased axonal calibre in those areas, allowing fibres to become less straight due to reduced inter-axonal space[234–237].

Merging our results with the theories on glioma cells migration, we may hypothesize that the less organized WM (higher fibre density with lower AD) and larger extracellular space (smaller diameter) but high functional demand (higher myelin thickness) may represent permissive environmental factors that promote/facilitate the growth of gliomas cells [132,139,238].

# 5.6. Study VI

WM connectivity and the possible rate of tumour-induced neuroplasticity were investigated in 36 patients with DGs, merging clinical information, preoperative assessment (including neuropsychological [NPS] and language evaluation), and demographic information and comparing these factors with intraoperative findings from awake surgery. Our study showed three main results.

First, the preoperative evidence of neuropsychological impairment was linked to a high risk of finding an eloquent tumour at brain mapping. In our population, 84.6% of the patients displayed neuropsychological symptoms in the preoperative assessment. In 75% of patients there were intraoperative findings of eloquent spots. The presence of preoperative neuropsychological

symptoms was the only independent factor linked to a high risk (HR 6.3) of finding an eloquent tumour intraoperatively. A careful preoperative assessment seems of paramount importance to identify good candidates for surgery and tailor brain mapping at the individual level [61,66,67]. Several studies suggest that the local growth of gliomas affect the global brain functional organization by causing impaired communication of large-scale networks for cognition and behaviour [188,239]. The insult to the subcortical WM structural connectivity is correlated with a decline in cognitive functions, confirming that axonal bundles represent a major limitation in neuroplasticity [239,240]. Moreover, the link between global network disturbance and a higher risk of finding eloquent spots within the tumour area may suggest that an exhaustion of local adaptation and the insult to global redistribution of the neural activity may be closely linked in time, at radiological diagnosis. Neuropsychological impairment may emerge when the global networks are no longer able to recruit and compensate for the local invasion of large-scale networks.

Second, we found correlations between radiological/topographical features and clinical variables, NPS impairment, epileptic onset, and language impairment. The number of BG voxels (>6) was correlated with a preoperative cognitive or NPS problem. Based on the intrinsic advantage of BG voxel analysis in quantifying invasiveness of DGs [172,241], this result may suggest a predominant invasion to the subcortical networks as a constant finding in NPS impairment, as reported by other authors [148,188,239]. A higher number of BG voxels usually indicate a possible invasion of interhemispheric and periventricular WM networks with secondary insult to large-scale networks characterized by less plastic potential [188,239]. At the qualitative analysis of BG voxels, the infiltration of the A3C2S2 voxel was linked to a five times higher risk that the patient will demonstrate preoperative NPS impairment. This region (sub-insular/basal ganglia on the left side) has been often associated with cognitive or psychiatric disturbances [242–245]. In our population, DGs associated with impaired neuropsychological performance at the moment of diagnosis displayed more invasive tumours (>6 BG voxels), a crucial preferential location (A3C2S2 voxel), and a higher risk of intraoperative findings of eloquent tumours. All together, these results support two main considerations. First, NPS assessment may be able to detect differences in the invasiveness of brain tumours, clinically detecting damage to large scale networks. Second, since the evidence of NPS impairment suggests the exhaustion of adaptive mechanisms and the insult of large-scale networks, an early diagnosis and surgical approach may be advocated [56,246,247], perhaps making it possible to increase the resection before the tumours reach a not compensable level of invasion.

Epileptic onset was the second most frequent clinical variable, displayed in 77.3% of the patients. Epilepsy as onset symptom was correlated with a larger tumour volume (>56 ml). This correlation has not been found in other studies [148,248], and for this reason should be carefully interpreted. Some authors suggested that larger tumours are linked to less functional reorganization [175,188],

implying that larger gliomas trigger compensatory neuroplasticity before the surgery. There is, however, evidence that the combination between volume and special locations may induce epileptic onset as a multifactorial result [148]. In our population, the epileptic onset was correlated with volumes larger than 56 ml but not with the number of BG voxels. Our results suggest that the epileptic onset may reflect a local/focal phenomenon. This may be due to the higher volume expansion at the cortical level rather than infiltrative features of the tumour in subcortical areas, as also supported by other authors [61,148]. In fact, slow-growing tumours could produce an epileptogenic environment by partial deafferentation of the cortical regions, thus causing denervation hypersensitivity [249]. Studies using magnetoencephalographic recordings have shown that functional connectivity and network topology are significantly altered in DG cases. Low-frequency connectivity seems pathologically increased, probably due to adaptive recruitment, and the normal "small-world network" configuration is altered, leading to a lower threshold for seizures [249–253] in the peritumoral cortical areas [148]. The infiltration of A4C2S2 and the A3C2S2 voxels increased the risk of epileptic onset almost six times. Hence, the left fronto-temporal opercula and the insular/sub-insular/basal ganglia regions seem to represent a crucial location for the epileptic onset in DG patients. These regions are also among the most often preferentially infiltrated in patients with DGs [68,172,241], and infiltration of these regions is often correlated with neurological impairment and epilepsy [148,248,249].

Language impairment was found at the preoperative evaluation in 66.7% of our patients. The possible risk of language problems was linked to the topographical variables. The infiltration of A3C2S2 BG voxel was linked to a higher risk of language impairment. This voxel includes the sub-insular/basal ganglia region on the left side, and it is considered highly functional as a part of the minimal common brain [109,147]. This region is among the less plastic ones due to the presence of basal ganglia, fibres from the external and internal capsules, and fronto-striatal circuits [109,147,172]. An infiltrative tumour reaching this region would probably affect WM fibres, thereby exerting an effect on large networks through their connecting hubs rather than peripheral cortical terminations with a lower possibility for early adaptive mechanisms due to the limited WM plasticity [62,188,239,254].

The third main result showed that intraoperative mapping reflected a pattern of tumour-induced changes in the peritumoral functional environment. The presence of eloquent spots inside the tumour area was linked to NPS impairment. This suggests that the insult to large scale networks may decrease the possibility for the peritumoral environment to compensate at the local level. What we know about the peritumoral milieu is that it is from there that the epileptic onset is triggered; it starts from the peritumoral cortical areas and not from the tumour core [148,188,249]. In support of this theory, the epileptic onset was correlated with the presence of peritumoral eloquent spots at the cortical level and at the same time the intratumoral eloquent spots subcortically. This

implies that when the epileptic activity emerges, the tumour has 1) already invaded subcortical larger networks, limiting the possible large-scale reorganization/adaptation of the neural activity; 2) the peritumoral cortices have been recruited within the same functional hub through short intermediate fibres as the first mechanism of local reorganization; 3) the subcortical networks (intermediate/long fibres) newly invaded by the tumours (intratumoral subcortical eloquent spots) are a constant correlation in both epilepsy and NPS impairment. We identified a negative correlation between peritumoral cortical eloquent spots and intratumoral cortical eloquent spots. This suggests that the two findings are signs of different stages of the adaptive process during glioma formation and proliferation that are not often present at the same time [32,188,239]. Interestingly, we found that age was a possible factor affecting this adaptive potential. The two groups (with age cut-off at 38 years old) displayed a difference in the number of intratumoral cortical and peritumoral cortical eloquent spots. Older age was negatively correlated with the number of peritumoral cortical eloquent spots and directly correlated with the number of intratumoral cortical eloquent spots. This seems in agreement with other authors, suggesting a decrease rate of myelin/WM plasticity with age [255,256]. We may hypothesize that small cortical DGs may activate an early cortical adaptive mechanism in younger people, who are able to compensate for the glioma's expansion, recruiting adjacent cortices. An increase in tumour volume leads to epilepsy due to the insult on large-scale networks that are unable to modulate the peritumoral environment. At this point, the invasion of large-scale networks may reflect patients' NPS preoperative impairment and the possible exhaustion of adaptive mechanisms at the peritumoral level due to a lower WM plasticity.

Finally, no correlation was detected between the number or distribution of cortical spots and the subcortical eloquent spots. In other words, the risk of finding intratumoral eloquent spots at the subcortical level cannot be predicted by the cortical mapping.

# 5.7. Methodological considerations and constraints

## 5.7.1. Deterministic diffusion tensor tractography

In the work presented in this thesis, we used two different types of algorithms to process deterministic tractography. In the Studies I and VI the fiber assignment by the continuous tracking (FACT) algorithm was used to detect the organization of the ILF and the preoperative assessment of patients with DG. It is mandatory to consider that using deterministic tractography (and especially with the FACT algorithm) artefacts can arise due to crossing and kissing fibres in the voxel-averaged tensor data [102,104,257,258]. Variability across subjects may

increase in regions containing crossing fibres where FA values tend to decrease [258], which can lead to interrupted fibres. Furthermore, errors can occur when attempts to follow incoherently organized tracts are made [259]. False connections that do not exist anatomically can appear to be present between brain regions, even though the deterministic tensor-based tractography algorithm was chosen in order to obtain sufficient quality without increasing the risk of obtaining false positives, which might have been the case if probabilistic tractography had been used. [260]. A high level of anatomic knowledge and great care must therefore be exercised in obtaining and interpreting all tractography data, for example, when analyzing results like those obtained regarding the ILF, where no streamlines were detected. User dependency may also be a factor when the tracts are extracted by drawing ROIs manually [261].

Another source of bias may be partial volume effects, which can arise due to contributions to parameter values within voxels from neighbouring structures [262]. To overcome these potential limitations, we used diffusion data acquired from the HCP database that included high angular resolution diffusion imaging (dMRI) in Studies II, III, IV, and V. All diffusion datasets were preprocessed using the HCP MR Diffusion Pipeline (v3.19.0), which includes the EPI distortion correction algorithm, eddy current and motion correction algorithm, gradient nonlinearity correction, and calculation of b-value/b-vector deviation [162–164]. HCP diffusion data were reconstructed using the more advanced generalized q-sampling imaging approach [165]. Moreover, prior to reconstruction, all included datasets were thoroughly examined to ensure the quality and integrity of diffusion data using the built-in quality control in DSI studio and by visual examination [173]. Tracking results were then based on changes in the quantitative anisotropy (QA) [166], increasing the high resolution of tractographic results. This more advanced approach allowed us a more realistic direct investigation of the cortical termination of long-range fibre tracts and improved the connectomic analysis of WM [165,166,202,263]. Moreover, since individual brains may show structural differences in relation to, for example, age [264], we tried to enrol only a population with a narrow age range to reduce this source of variability in all the anatomical studies.

Another limitation is represented by the lack of universal consensus regarding the interpretation of DTI results [265–269]. For this reason, results based only on DTI should be carefully interpreted. Our effort in adopting new software, new algorithms, and complementary techniques was driven by the necessity to validate DTI results. We merged DTI with morphological/anatomical results from WM dissection that have higher spatial resolution (Studies I and II); we used TEM to correlate diffusion parameters with histological features (Study V), and we also evaluated DTI results with brain mapping and navigation system (Study VI). Our conclusion is that with complementary techniques able to increase reliability of the results, DTI represents an important pedagogic and research tool, but too many limitations may influence its use in daily

clinical practice as stand-alone tool for decision-making in patients with gliomas [102,104,270,271], as demonstrated in Study VI.

In fact, despite tractography being present in all the cases as an integral part of the preoperative assessment, we detected inconsistent results. A close proximity of eloquent spots with the reconstructed WM bundles (< 5 mm) was detected in 40% of the cortical and 50% of the subcortical points. Hence, we decided not to use the results for further anatomical/functional connectivity analysis.

## 5.7.2. The Brain-Grid system

The Brain-Grid classification system was firstly defined in the MNI space; then its application in the patient-specific space and its reproducibility in longitudinal studies were tested in 105 MRI investigations (Study III). Despite the Brain-Grid classification system and subsequent analysis showing consistent results using a different software in patients normalized to the MNI space, we decided to further analyse this method in the MNI space only (Studies IV, VI). This was based on the necessity of creating probabilistic gradient maps (for infiltration analysis) and to better validate tumour invasiveness, minimizing the risk for inconsistencies in metric measurement. However, this tool displayed the potential to detect differences in millimetric infiltrations of gliomas in serial MRI in the patient-specific space (Study III, Figure 7). Only further studies with larger cohorts and longitudinal MRI investigations may be able to validate the use of BG system in detecting/predicting tumour kinetics.

## 5.7.3. Patient cohorts: sample size and characteristics

Different cohorts of patients with DGs and or DLGGs were analysed in work presented in this thesis during the period 2005–2020. The population which recruited until 2015/2016 presented different limitations that need to be addressed.

First, the histological diagnosis of the included patients was incomplete with regard to the WHO-2016 classification criteria for brain tumours. The IDH mutation analysis and the 1p19q codeletion are the gold standard nowadays for the diagnosis and classification of gliomas [51]. Because of the retrospective nature of this study, not all the patients had a molecular analysis available at the time of treatment, and the methods and the histo-immunological criteria have changed dramatically in the last 15 years. However, all the previously mixed oligo-astrocytomas were reviewed in light of the new classification criteria. Moreover, the proliferation index was taken into consideration, and WHO-III gliomas were not included in Studies IV and V, showing our effort to analyse a more homogeneous population. Hence, all the NOS patients

were included into the respective subgroups of histological diagnoses. Although this may have brought some diagnostic faults into the main groups, as the subgroup of tumours without the molecular classifications (LOH 1p19q and IDH, i.e., NOS) will somewhat obscure the results, the differences we observed in Study IV would most likely be larger rather than those presented, had all the tumours been molecularly classified. In addition, since no differences were detected in clinical or radiological variables among the subgroups (not even between IDHm and IDHwt), the topographical analysis was performed using gradient/probabilistic maps in the two main groups (astrocytomas and oligodendrogliomas). Despite the already discussed differences in molecular profiles, we believed that this was the best choice to detect differences/similarities in tumour topography based on the histological origin of the tumours.

Second, it is also important to consider that during the decade 2005–2015, the use of MRI tractography, awake surgery, and neuropsychological testing was not fully established at our centre. The favourable impact on overall survival of surgical resection compared to biopsy is nowadays commonly accepted and cannot be neglected [83,115,272]. The paradigm for treatment choice in these patients is now different, and many more patients benefited from a surgical cytoreduction of DLGGs despite the procedure taking place even several years after an initial diagnostic biopsy. We agreed with the paradigmatic shift that has taken place in the last decade, advocating a more prominent role of surgical resection according to functional boundaries to increase the resection rate while respecting the WM within the minimal common brain [109,119,147,273–275]. However, despite the improvement in our perioperative planning (including DTI tractography) and our surgical strategy with use of direct cortical-subcortical mapping and monitoring of high cognitive functions, we cannot exclude that a part of our results regarding OS and general outcome were due to a different management algorithm that reflected our learning curve and previous international consensus on the treatment of DGs.

Even for the patients enrolled prospectively from 2015 (Studies II and VI) some limitations need to be discussed. The first one regards the size and type of our population. In Study II, only two patients were analysed to support anatomical-functional results, raising possible criticism because of the inter-individual variability in patients with DLGGs. Even though the lesions (normalized within the MNI space) may have resulted in minimal anatomical differences compared to the patient-specific space, we believe that these two cases supported complement anatomical information regarding MdLF anatomy and that they have functional/clinical implications (such as the type and origin of auditory hallucinations) owing to the language/neuropsychological examinations. Aware of the low level of evidence provided by only two neurosurgical cases without direct cortical subcortical mapping, we have invited the reader to carefully interpret our inferences regarding the functional implications of

the MdLF. However, we believe that the results from the very extensive pre-operative and postoperative assessment support the role of the MdLF in auditory networks in the presented cases. Moreover, since the scientific community is still lacking a validated intraoperative test to demonstrate the on-line inhibition of the MdLF, we believe that our results may encourage further studies to develop one or more dedicated tests for intraoperative mapping of auditory functions.

In Study VI, only 36 patients had a diagnosis of DG (WHO-II/III) no previous resection, no previous radio-chemotherapy, and at the same time a cognitive and/or linguistic performance suitable for awake surgery and brain mapping. This reduced the potential number of analyses. For instance, no difference was detected among the four histological groups, and most of the patients displayed a mutated status of IDH1, while in 10 patients this status was not available. Therefore, we considered further analysis based on histology/molecular status beyond the aim of this study and to be rather speculative considering this population. Moreover, since the original indication for awake surgery in our centre was the language mapping, only patients with gliomas harbouring dominant hemispheres (2 bi-hemispheric dominant) were enrolled in this study, influencing the interpretation of the results. Despite these limitations, our study describes a homogeneous population of DG (dominant hemisphere at the first surgical brain mapping), with a consistent preoperative assessment (extensive preoperative cognitive and language assessment, qualitative and quantitative radiological features) and a consistent method of intraoperative registration of eloquent spots.

# 6. Conclusions

## 6.1. General conclusions

The study of WM is of paramount importance for the comprehension of brain organization and for the treatment of cerebral gliomas. Anatomical details provided by dissection and tractography studies are consistent and helpful in decoding the human brain connectome at a macroscale level. A standardized and systematic classification of gliomas based on their WM invasion seems pivotal to defining differences in tumour invasiveness and thus to better understanding gliomas' behaviour and their response to individual treatments. The combined use of these advanced radiological techniques revealed new insights into tumour-induced plasticity and possible factors influencing brain-adaptive mechanisms. The results provided in this thesis describe a new way to design the multidisciplinary perioperative management of these patients. The key to unravel the WM/glioma interactions relies on a systematic combination of: better knowledge of the structural connectome; better classification system for gliomas; extensive NPS and language assessment, and intraoperative monitoring of brain functional organization at the individual level. The systematic use of this new information would hopefully improve the functional outcome at the individual level, resulting in a prolonged survival for adults with diffuse gliomas.

## 6.2. Specific conclusions (Studies I-VI)

Study I
The WM architecture and connectivity of the ILF and its sub-segments were described. The main body of the ILF is formed by a fusiform, lingual, and dorsolateral occipital branch. The anatomical connectivity pattern and quantitative differences between the ILF subcomponents indicate a central role of the ILF in connecting highly specialized visual areas to anterior temporal areas important for emotional, semantic, and visual memory processes.

Study II
Anatomy and connectivity of the MdLF and its sub-segments was described. The main body of the MdLF is formed by an anterior-ventral segment

(aMdLF) and a posterior-dorsal segment (pMdLF). The anatomical connectivity pattern and quantitative differences between the MdLF subcomponents suggest a pivotal role of the MdLF in supporting high order functions related to acoustic information such as learning process for verbal-auditory cross-modal integration and processing/retrieving auditory information already consolidated. Damage to the MdLF sub-segments may contribute to impaired verbal learning and memory, auditory hallucinations, and even psychiatric disorders.

Study III
A novel radiological observational tool to classify cerebral gliomas was created. The Brain-Grid classification system provided an accurate, rapid, and reliable evaluation of tumour invasiveness, merging local radiological anatomy and the cortical and subcortical extensions of WM architecture. Important information about tumour kinetics. including extension and preferential direction of tumour invasion. can be observed and predicted by a comparative analysis of voxels on morphological MRI and a WM architecture atlas. This new integrated classification of gliomas can potentially help clinicians to plan tailored tumour resection and target the volume for radiotherapy based on a prediction of WM invasion.

Study IV
Differences in preferential topographical location between diffuse astrocytomas and oligodendrogliomas were identified. These differences reflected the type and the amount of WM structures involved at the time of radiologic diagnosis and affected the whole course of this disease. Tumour invasiveness analysed with the Brain-Grid system predicted shorter OS in both groups of tumours. This new information seemed to be valuable in neurosurgical oncology to classify and, possibly, to plan the best treatment strategy in patients with DGs.

Study V
Common WM regions for the preferential infiltration of DLGGs and differences in the infiltration frequency of five major WM bundles were identified. Regions with HIF displayed a higher density of fibres, smaller fibre diameter, but higher myelin thickness compared with LIF regions. HIF regions showed lower axial diffusivity compared with LIF regions, suggesting less coherent fibre organization. Fibre diameter, myelin thickness, and the organization of the fibres are different in HIF compared to LIF regions and, thus, may be linked to the preferential location of DLGGs.

Study VI
DGs displayed a pattern of early cortical neuroplasticity that shifted functions to adjacent cortices. This adaptive mechanism often seemed exhausted at the

time of diagnosis, with high risk of finding intratumoral subcortical eloquent spots. Age may represent an important factor to predict the adaptive mechanisms of neuroplasticity, but at the individual level the prediction of resection grade and eloquent spots was not possible. Preoperative neuropsychological and language assessment may reveal the involvement of large-scale networks for cognitive functions and detect signs of tumour-induced neuroplasticity. A systematic use of advanced neuroimaging techniques including topography and WM infiltration analysis is necessary to identify less compensable areas and their link with epileptic onset, NPS, and language impairment. A more systematic integration of functional and radiological assessment before awake surgery may lead to a better comprehension of the connectomic brain organization at the individual level and therefore to a better oncological/functional balance.

# Summary in Swedish

Diffusa gliom är heterogena tumörer som karakteriseras av långsam tillväxt men omfattande infiltration. De kinetiska egenskaperna hos diffusa gliom återspeglar en komplex interaktion över tid med den omgivande hjärnvävnaden, vilket kan påverka behandlingsplaneringen och slutligen kliniskt resultat efter operation. Diffusa gliom är utmanande tumörer att operera bort på grund av deras invasivitet och föredragna lokalisationer till elokventa områden (områden som vid skada kan ge funktionsnedsättning). Vitsubstans-banor är den huvudsakliga elokventa gränsen för kirurgisk resektion, men idag saknas robusta metoder för att förutsäga placering av den elokventa gränsen i förhållande till preoperativ anatomisk- och funktionell information på individuell nivå. Förståelsen för diffusa gliom-vitsubstans interaktion är idag begränsad; kartläggningen av hjärnans konnektom är inkomplett, tillämpningen av patologisk/lesionsmodell är komplex och rollen av vitsubstans anatomi i radiologiska klassificeringssystem är underskattad. Syftet med denna avhandling var att utforska nya metoder och tekniker för att studera och bättre förstå diffusa gliom-vitsubstans interaktion.

En kombination av vitsubstans-dissektion av hjärnpreparat donerade från avlidna personer och magnetresonanstomografi (MRT)-baserad diffusions tensor traktografi (DTT) på friska frivilliga användes för att beskriva den konnektomiska organisationen av två stora men fortfarande omdebatterade temporo-occipitala banor; fasciculus longitudinalis inferior och medio. Resultatet från studierna applicerades på patienter med diffusa gliom som visade hur vitsubstans-analys var viktigt för att förklara patientspecifik kognitiv och språkstörning. Därför skapades ett nytt klassificeringssystem för diffusa gliom, Brain-Grid, som förenar radiologisk anatomi med en DTT-atlas för infiltrationsanalys. Detta standardiserade radiologiska verktyg gav oss information om subkortikal extension (tumörernas invasivitet), hastighet och preferensriktning för tumörernas tillväxt. När vi tillämpade Brain-Grid på en större kohort av patienter, upptäcktes viktiga skillnader mellan diffusa gliom undertyper (astrocytom och oligodendrogliom). Föredragna lokalisationer, typ och omfattning av vitsubstans-involvering och antalet infiltrerade Brain-Grid -voxlar (tumörinvasivitet) skilde sig mellan undertyperna med en inverkan på överlevnad. Regionala skillnader i vitsubstans-infiltration upptäcktes bland 5 stora vitsubstans-banor och därför analyserade vi skillnader mellan dessa banor med transmissionselektronmikroskopi (på hjärnpreparat från avlidna) och

DTT (på friska individer). Fiberdiameter, myelintjocklek och organisationen av vitsubstans-fibrerna visade skillnader i regioner med hög infiltrationsfrekvens som ett möjligt samband till diffusa glioms föredragna lokalisationer.

Slutligen, jämfördes vitsubstans-konnektivitet, tumörinducerad neuroplasticitet, klinisk och demografisk information, och preoperativ bedömning (neuropsykologisk och språkutvärdering) med intraoperativa resultat under vakenkirurgi. Försämring i neuropsykologin kopplades till mer invasiva tumörer och till en högre risk för intraoperativ upptäckt av elokventa tumörer. Tidig kortikal neuroplasticitet verkade uttömd vid radiologiskt diagnosbesked med ålder som en möjlig faktor vilket förutsäger neuroplasticitetspotentialen.

Den kombinerade användningen av dessa nya metoder avslöjade ny kunskap i diffusa gliom/vitsubstans interaktionen. Avhandlingens ingående delarbeten beskriver nya sätt att strukturera multidisciplinär peri-operativ hantering av patienter med diffusa gliom, vilket kan förbättra det funktionella resultatet på individuell nivå samt leda till en förlängd överlevnad för patienter som opereras för diffusa gliom.

# Summary in Italian

I gliomi diffusi rappresentano un gruppo di tumori cerebrali estremamente eterogeneo caratterizzati da una crescita relativamente lenta ma da un'estesa infiltrazione. Le loro caratteristiche cinetiche riflettono la complessa interazione nel tempo con il tessuto cerebrale circostante, influenzando la scelta del trattamento e il conseguente risultato. Infatti, i gliomi diffusi sono delle lesioni molto difficili da operare a causa della loro invasività e della posizione preferenziale in aree eloquenti (aree che se danneggiate comportano un danno neurologico potenzialmente permanente). I fasci di sostanza bianca sono il principale limite anatomico-funzionale alla resezione chirurgica, ma questa informazione non può essere prevista in fase preoperatoria a livello individuale. Tra i principali limiti alla comprensione dell'interazione gliomi /sostanza bianca troviamo: l'incompleta descrizione del connettoma cerebrale (l'insieme di connessioni cerebrali anatomico-funzionali fin ora conosciute); la complessa applicazione del modello patologico / lesionale all'organizzazione connettomica del cervello; ed il ruolo sottovalutato dell'anatomia della sostanza bianca nei sistemi di classificazione radiologica.

L'obiettivo generale di questa tesi è stato esplorare un nuovo approccio e nuove tecniche per studiare l'interazione gliomi /sostanza bianca.

Una combinazione di dissezione di sostanza bianca e ricostruzione tramite trattografia (tecnica basata su risonanza magnetica che utilizza un tensore di diffusione per ricostruire immagini biomediche) è stata utilizzata per descrivere l'organizzazione connettomica di due importanti, ma ancora dibattute, connessioni temporo-occipitali, il fascicolo longitudinale inferiore ed il medio. Queste nuove informazioni sono state applicate ai pazienti con gliomi diffusi dimostrando quanto l'analisi della sostanza bianca fosse importante per decodificare il deterioramento cognitivo e del linguaggio identificato nei nostri pazienti. Quindi, è stato creato un nuovo sistema di classificazione per i gliomi diffusi, il Brain-Grid, che unisce anatomia radiologica topografica con un atlante trattografico per permettere un'analisi di infiltrazione del tumore. Questo strumento radiologico standardizzato ha inizialmente fornito informazioni sull'estensione sottocorticale (invasività del tumore), sulla velocità e sulla direzione preferenziale della progressione dei gliomi attraverso la sostanza bianca. Applicato ad una più ampia coorte di pazienti sono state rilevate differenze tra i sottotipi di gliomi diffusi. La posizione preferenziale, il tipo e l'entità del coinvolgimento della sostanza bianca e il numero di Brain-Grid-

90

voxels infiltrati (considerati indice di invasività del tumore), sono risultati diversi con un conseguente impatto sulla sopravvivenza. Sono state rilevate, inoltre, differenze regionali nell'infiltrazione di sostanza bianca fra 5 principali fasci e le possibili caratteristiche morfologiche e di diffusione potenzialmente responsabili di queste differenze, sono state studiate con microscopia elettronica (su preparati cadaverici) e trattografia (in soggetti sani). Il diametro delle fibre mielinizzate, lo spessore della mielina e l'organizzazione delle fibre di sostanza bianca sono risultati diversi nelle regioni con alta frequenza di infiltrazione come possibile collegamento con la posizione preferenziale dei gliomi diffusi.

Infine, la connettività di sostanza bianca, la neuroplasticità (la capacità del cervello di adattarsi dinamicamente ad un danno o cambiamento) indotta dal tumore, le informazioni cliniche e demografiche, e la valutazione preoperatoria (neuropsicologica e del linguaggio) sono state confrontate con i risultati intraoperatori durante la chirurgia da sveglio. Un danno alle funzioni cognitive/neuropsicologiche è risultato collegato a tumori più invasivi e ad un rischio più elevato di riscontro intraoperatorio di tumori eloquenti (funzioni cognitive e di linguaggio localizzate nei tumori). Il pattern di neuroplasticità corticale precoce è risultato esaurito al momento della diagnosi con l'età (sotto i 38 anni) come fattore predittivo positivo del potenziale di neuroplasticità.

L'uso combinato di queste nuove tecniche ha rivelato nuove informazioni sull'interazione gliomi /sostanza bianca. I risultati qui forniti descrivono un nuovo modo di strutturare la gestione perioperatoria multidisciplinare di questi pazienti. Si spera che queste nuove informazioni migliorino il risultato funzionale per i pazienti a livello individuale, prolungando la sopravvivenza negli gli adulti con gliomi cerebrali diffusi.

# Acknowledgments

I want to express my sincere gratitude to:

**Mats Ryttlefors**, my supervisor, my mentor, my role model, and my friend, for inviting me to Sweden, for believing in me and for giving me the opportunity to do research in the way I had only dreamed of. Thank you for the excellent guidance and for encouraging me to become better and wiser every day with passion and never-ending support.

**Per Enblad**, my co-supervisor, for his continuous and optimistic support, encouraging me to express my passion for neuroscience and for his excellent guidance into the field of neuro-intensive care.

**Michele Alessandro Cavallo**, director of the Neurosurgical Unit, Ferrara University Hospital, Italy, for being my mentor, for helping me to become a neurosurgeon, for the infinite support and encouragement in both professional and personal life, and for introducing me to the world of brain mapping and functional neurosurgery.

**Ali Krisht**, director of the Arkansas Neuroscience Institute, Little Rock, AR, USA, for accepting me as ANI fellow, for the advices and inspiration through one of my life-changing moments, and for teaching me how to look at my limits, every day, as the most important drive for improvement.

**Mats Hjortberg (1961-2016)**, for believing in me as neuroanatomist, for helping me with everything I have ever needed to start the first white matter dissection lab in Sweden. I feel honoured and proud of our unforgettable conversations on anatomy and life.

**The donors of brain specimens**, for your priceless gift to me, and for giving me the possibility to better understand the complex organization of the brain and possibly to better operate my patients.

**Markus Fahlström,** for your precious contribution to this thesis, for your hard work day and night on our projects, and for our infinite and diverse discussions, from diffeomorphic registration of MRI images to squash.

To all **NIMA personnel**, for taking good care of our patients, for your continuous and positive support in these times of changes, and for your constant will to improve by telling me every day what can be done better.

To the staff of **NIVA, Neuro-Op and 85E**, for keeping always the patient as a priority and for your help and support in all the possible situations.

To my friends around the world**, Piergiorgio, Ema, Francesco, Giorgio, and Giulio**, for being always my brothers despite the distance, the pandemic, children, and life-changing events. You are an important part of my inspiration with your kaleidoscopic knowledge and our shared experiences around the world. Thanks for reminding me how to "take it easy" and how to look at the world with different eyes.

To my sister **Chiara**, for all our shared moments and for showing me how a strong will, persistence and patience can lead you to your aims despite the difficulties.

To my parents **Enrico (1952-2019) and Rita**, to whom this thesis is dedicated, for providing me everything I have ever needed in life to become myself and to follow my path. Thank you for your never-ending support to my choices and decisions and for being exceptional loving parents.

To **Serena**, my love, for being the best person I have ever met and without whom this thesis would not have been the same. Thank you for your immense support and love and for showing me how to follow my dreams, with commitment, passion, and aiming to perfection. You are at the same time my solid point and my happy place. Life is wonderful with you by my side.

# References

1. Agrawal A, Kapfhammer JP, Kress A, et al. Josef Klingler's models of white matter tracts: influences on neuroanatomy, neurosurgery, and neuroimaging. *Neurosurgery*. 2011;69(2):238-252; discussion 252-254. doi:10.1227/NEU.0b013e318214ab79

2. Clarke E, O'Malley CD. *The Human Brain and Spinal Cord: A Historical Study Illustrated by Writings from Antiquity to the Twentieth Century*. Norman Publishing; 1996.

3. Latini F, Hjortberg M, Aldskogius H, Ryttlefors M. The use of a cerebral perfusion and immersion-fixation process for subsequent white matter dissection. *J Neurosci Methods*. 2015;253:161-169. doi:10.1016/j.jneumeth.2015.06.019

4. Türe U, Yaşargil MG, Friedman AH, Al-Mefty O. Fiber dissection technique: lateral aspect of the brain. *Neurosurgery*. 2000;47(2):417-426; discussion 426-427. doi:10.1097/00006123-200008000-00028

5. Catani M, ffytche DH. The rises and falls of disconnection syndromes. *Brain*. 2005;128(Pt 10):2224-2239. doi:10.1093/brain/awh622

6. Catani M, Dell'Acqua F, Bizzi A, et al. Beyond cortical localization in clinico-anatomical correlation. *Cortex*. 2012;48(10):1262-1287. doi:10.1016/j.cortex.2012.07.001

7. Ludwig E,. *Atlas Cerebri Humani*. S. Karger; 1956.

8. Klingler J. LE. *Noyaux et Faisceaux Du Cerveau Humain*. George Thomas; 1938.

9. Fernández-Miranda JC, Rhoton AL, Alvarez-Linera J, Kakizawa Y, Choi C, de Oliveira EP. Three-dimensional microsurgical and tractographic anatomy of the white matter of the human brain. *Neurosurgery*. 2008;62(6 Suppl 3):989-1026; discussion 1026-1028. doi:10.1227/01.neu.0000333767.05328.49

10. Catani M, Thiebaut de Schotten M. A diffusion tensor imaging tractography atlas for virtual in vivo dissections. *Cortex*. 2008;44(8):1105-1132. doi:10.1016/j.cortex.2008.05.004

11. Catani M, Howard RJ, Pajevic S, Jones DK. Virtual in vivo interactive dissection of white matter fasciculi in the human brain. *Neuroimage*. 2002;17(1):77-94.

12. Basser PJ, Mattiello J, LeBihan D. MR diffusion tensor spectroscopy and imaging. *Biophys J*. 1994;66(1):259-267. doi:10.1016/S0006-3495(94)80775-1

13. Basser PJ, Pajevic S, Pierpaoli C, Duda J, Aldroubi A. In vivo fiber tractography using DT-MRI data. *Magn Reson Med*. 2000;44(4):625-632. doi:10.1002/1522-2594(200010)44:4<625::aid-mrm17>3.0.co;2-o

14. Basser PJ. Inferring microstructural features and the physiological state of tissues from diffusion-weighted images. *NMR Biomed*. 1995;8(7-8):333-344.

15. Basser PJ, Pierpaoli C. Microstructural and physiological features of tissues elucidated by quantitative-diffusion-tensor MRI. *J Magn Reson B*. 1996;111(3):209-219.

16. Makris N, Worth AJ, Sorensen AG, et al. Morphometry of in vivo human white matter association pathways with diffusion-weighted magnetic resonance imaging. *Ann Neurol*. 1997;42(6):951-962. doi:10.1002/ana.410420617

17. Jones DK, Simmons A, Williams SC, Horsfield MA. Non-invasive assessment of axonal fiber connectivity in the human brain via diffusion tensor MRI. *Magn Reson Med*. 1999;42(1):37-41. doi:10.1002/(sici)1522-2594(199907)42:1<37::aid-mrm7>3.0.co;2-o

18. Mori S, Crain BJ, Chacko VP, van Zijl PC. Three-dimensional tracking of axonal projections in the brain by magnetic resonance imaging. *Ann Neurol*. 1999;45(2):265-269.

19. Poupon C, Clark CA, Frouin V, et al. Regularization of diffusion-based direction maps for the tracking of brain white matter fascicles. *Neuroimage*. 2000;12(2):184-195. doi:10.1006/nimg.2000.0607

20. Mori S, Kaufmann WE, Davatzikos C, et al. Imaging cortical association tracts in the human brain using diffusion-tensor-based axonal tracking. *Magn Reson Med*. 2002;47(2):215-223. doi:10.1002/mrm.10074

21. Zemmoura I, Serres B, Andersson F, et al. FIBRASCAN: a novel method for 3D white matter tract reconstruction in MR space from cadaveric dissection. *Neuroimage*. 2014;103:106-118. doi:10.1016/j.neuroimage.2014.09.016

22. Yu CS, Li KC, Xuan Y, Ji XM, Qin W. Diffusion tensor tractography in patients with cerebral tumors: a helpful technique for neurosurgical planning and post-operative assessment. *Eur J Radiol*. 2005;56(2):197-204. doi:10.1016/j.ejrad.2005.04.010

23. Nimsky C, Ganslandt O, Merhof D, Sorensen AG, Fahlbusch R. Intraoperative visualization of the pyramidal tract by diffusion-tensor-imaging-based fiber tracking. *Neuroimage*. 2006;30(4):1219-1229. doi:10.1016/j.neuroimage.2005.11.001

24. Kinoshita M, Yamada K, Hashimoto N, et al. Fiber-tracking does not accurately estimate size of fiber bundle in pathological condition: initial neurosurgical experience using neuronavigation and subcortical white matter stimulation. *NeuroImage*. 2005;25(2):424-429. doi:10.1016/j.neuroimage.2004.07.076

25. Nimsky C, Ganslandt O, Hastreiter P, et al. Intraoperative diffusion-tensor MR imaging: shifting of white matter tracts during neurosurgical procedures--initial experience. *Radiology*. 2005;234(1):218-225. doi:10.1148/radiol.2341031984

26. Fernández-Miranda JC, Wang Y, Pathak S, Stefaneau L, Verstynen T, Yeh F-C. Asymmetry, connectivity, and segmentation of the arcuate fascicle in the human brain. *Brain Struct Funct*. 2015;220(3):1665-1680. doi:10.1007/s00429-014-0751-7

27. Martino J, De Witt Hamer PC, Berger MS, et al. Analysis of the subcomponents and cortical terminations of the perisylvian superior longitudinal fasciculus: a fiber dissection and DTI tractography study. *Brain Structure and Function*. 2013;218(1):105-121. doi:10.1007/s00429-012-0386-5

28. Panesar SS, Belo JTA, Yeh F-C, Fernandez-Miranda JC. Structure, asymmetry, and connectivity of the human temporo-parietal aslant and vertical occipital fasciculi. *Brain Struct Funct*. 2019;224(2):907-923. doi:10.1007/s00429-018-1812-0

29. Wang X, Pathak S, Stefaneanu L, Yeh F-C, Li S, Fernandez-Miranda JC. Subcomponents and connectivity of the superior longitudinal fasciculus in the human brain. *Brain Struct Funct*. 2016;221(4):2075-2092. doi:10.1007/s00429-015-1028-5

30. De Benedictis A, Duffau H. Brain hodotopy: from esoteric concept to practical surgical applications. *Neurosurgery*. 2011;68(6):1709-1723; discussion 1723. doi:10.1227/NEU.0b013e3182124690

31. Maier-Hein KH, Neher PF, Houde J-C, et al. The challenge of mapping the human connectome based on diffusion tractography. *Nat Commun*. 2017;8(1):1349. doi:10.1038/s41467-017-01285-x

32. Duffau H. Mapping the connectome in awake surgery for gliomas: an update. *J Neurosurg Sci*. 2017;61(6):612-630. doi:10.23736/S0390-5616.17.04017-6

33. Duffau H. The error of Broca: From the traditional localizationist concept to a connectomal anatomy of human brain. *J Chem Neuroanat*. 2018;89:73-81. doi:10.1016/j.jchemneu.2017.04.003

34. Filley CM. White matter and behavioral neurology. *Ann N Y Acad Sci*. 2005;1064:162-183. doi:10.1196/annals.1340.028

35. Schmahmann JD, Smith EE, Eichler FS, Filley CM. Cerebral white matter: neuroanatomy, clinical neurology, and neurobehavioral correlates. *Ann N Y Acad Sci*. 2008;1142:266-309. doi:10.1196/annals.1444.017

36. Fodor JA, Pylyshyn ZW. Connectionism and cognitive architecture: a critical analysis. *Cognition*. 1988;28(1-2):3-71.

37. Young MP, Scannell JW, Burns GA, Blakemore C. Analysis of connectivity: neural systems in the cerebral cortex. *Rev Neurosci*. 1994;5(3):227-250.

38. Fuster JM. The cognit: a network model of cortical representation. *Int J Psychophysiol*. 2006;60(2):125-132. doi:10.1016/j.ijpsycho.2005.12.015

39. Honey CJ, Kötter R, Breakspear M, Sporns O. Network structure of cerebral cortex shapes functional connectivity on multiple time scales. *Proc Natl Acad Sci USA*. 2007;104(24):10240-10245. doi:10.1073/pnas.0701519104

40. Reijneveld JC, Ponten SC, Berendse HW, Stam CJ. The application of graph theoretical analysis to complex networks in the brain. *Clin Neurophysiol*. 2007;118(11):2317-2331. doi:10.1016/j.clinph.2007.08.010

41. Duffau H. Awake mapping of the brain connectome in glioma surgery: Concept is stronger than technology. *Eur J Surg Oncol*. 2015;41(9):1261-1263. doi:10.1016/j.ejso.2015.05.009

42. Duffau H. Introduction. Surgery of gliomas in eloquent areas: from brain hodotopy and plasticity to functional neurooncology. *Neurosurg Focus*. 2010;28(2):Intro. doi:10.3171/2010.3.FOCUS.APR2010.INTRO

43. ffytche DH, Catani M. Beyond localization: from hodology to function. *Philos Trans R Soc Lond, B, Biol Sci*. 2005;360(1456):767-779. doi:10.1098/rstb.2005.1621

44. Ffytche DH. The hodology of hallucinations. *Cortex*. 2008;44(8):1067-1083. doi:10.1016/j.cortex.2008.04.005

45. Duffau H, Gatignol P, Mandonnet E, Peruzzi P, Tzourio-Mazoyer N, Capelle L. New insights into the anatomo-functional connectivity of the semantic system: a study using cortico-subcortical electrostimulations. *Brain*. 2005;128(Pt 4):797-810. doi:10.1093/brain/awh423

46. Duffau H. The anatomo-functional connectivity of language revisited. New insights provided by electrostimulation and tractography. *Neuropsychologia*. 2008;46(4):927-934. doi:10.1016/j.neuropsychologia.2007.10.025

47. Horwitz B, Braun AR. Brain network interactions in auditory, visual and linguistic processing. *Brain Lang*. 2004;89(2):377-384. doi:10.1016/S0093-934X(03)00349-3

48. Herbet G, Zemmoura I, Duffau H. Functional Anatomy of the Inferior Longitudinal Fasciculus: From Historical Reports to Current Hypotheses. *Front Neuroanat*. 2018;12:77. doi:10.3389/fnana.2018.00077

49.  Nakamura H, Makino K, Yano S, Kuratsu J-I, Kumamoto Brain Tumor Research Group. Epidemiological study of primary intracranial tumors: a regional survey in Kumamoto prefecture in southern Japan--20-year study. *Int J Clin Oncol*. 2011;16(4):314-321. doi:10.1007/s10147-010-0178-y

50.  Ostrom QT, Gittleman H, Fulop J, et al. CBTRUS Statistical Report: Primary Brain and Central Nervous System Tumors Diagnosed in the United States in 2008-2012. *Neuro-oncology*. 2015;17 Suppl 4:iv1-iv62. doi:10.1093/neuonc/nov189

51.  Louis DN, Perry A, Reifenberger G, et al. The 2016 World Health Organization Classification of Tumors of the Central Nervous System: a summary. *Acta Neuropathol*. 2016;131(6):803-820. doi:10.1007/s00401-016-1545-1

52.  Ohgaki H, Kleihues P. The definition of primary and secondary glioblastoma. *Clin Cancer Res*. 2013;19(4):764-772. doi:10.1158/1078-0432.CCR-12-3002

53.  Yuan B, Zhang N, Yan J, Cheng J, Lu J, Wu J. Tumor grade-related language and control network reorganization in patients with left cerebral glioma. *Cortex*. 2020;129:141-157. doi:10.1016/j.cortex.2020.04.015

54.  Bauchet L. Epidemiology of Diffuse Low Grade Gliomas. In: Duffau H, ed. *Diffuse Low-Grade Gliomas in Adults*. Springer International Publishing; 2017:13-53. doi:10.1007/978-3-319-55466-2_2

55.  Claus EB, Black PM. Survival rates and patterns of care for patients diagnosed with supratentorial low-grade gliomas: data from the SEER program, 1973-2001. *Cancer*. 2006;106(6):1358-1363. doi:10.1002/cncr.21733

56.  Mandonnet E, Delattre J-Y, Tanguy M-L, et al. Continuous growth of mean tumor diameter in a subset of grade II gliomas. *Ann Neurol*. 2003;53(4):524-528. doi:10.1002/ana.10528

57.  Pallud J, Fontaine D, Duffau H, et al. Natural history of incidental World Health Organization grade II gliomas. *Ann Neurol*. 2010;68(5):727-733. doi:10.1002/ana.22106

58.  Pallud J, Blonski M, Mandonnet E, et al. Velocity of tumor spontaneous expansion predicts long-term outcomes for diffuse low-grade gliomas. *Neuro-oncology*. 2013;15(5):595-606. doi:10.1093/neuonc/nos331

59.  Pignatti F, van den Bent M, Curran D, et al. Prognostic factors for survival in adult patients with cerebral low-grade glioma. *J Clin Oncol*. 2002;20(8):2076-2084. doi:10.1200/JCO.2002.08.121

60.  Claus EB, Horlacher A, Hsu L, et al. Survival rates in patients with low-grade glioma after intraoperative magnetic resonance image guidance. *Cancer*. 2005;103(6):1227-1233. doi:10.1002/cncr.20867

61.  Smits A, Jakola AS. Clinical Presentation, Natural History, and Prognosis of Diffuse Low-Grade Gliomas. *Neurosurg Clin N Am*. 2019;30(1):35-42. doi:10.1016/j.nec.2018.08.002

62.  Duffau H. Diffuse low-grade gliomas and neuroplasticity. *Diagnostic and Interventional Imaging*. 2014;95(10):945-955. doi:10.1016/j.diii.2014.08.001

63.  de Groot M, Reijneveld JC, Aronica E, Heimans JJ. Epilepsy in patients with a brain tumour: focal epilepsy requires focused treatment. *Brain*. 2012;135(4):1002-1016. doi:10.1093/brain/awr310

64.  Pallud J, McKhann GM. Diffuse Low-Grade Glioma-Related Epilepsy. *Neurosurg Clin N Am*. 2019;30(1):43-54. doi:10.1016/j.nec.2018.09.001

65.  Klein M, Duffau H, De Witt Hamer PC. Cognition and resective surgery for diffuse infiltrative glioma: an overview. *J Neurooncol*. 2012;108(2):309-318. doi:10.1007/s11060-012-0811-x

66. Duffau H. Toward an "active" cognitive assessment in patients with diffuse low-grade glioma. *World Neurosurg*. 2014;82(1-2):e129-131. doi:10.1016/j.wneu.2014.03.023

67. Cochereau J, Herbet G, Duffau H. Patients with incidental WHO grade II glioma frequently suffer from neuropsychological disturbances. *Acta Neurochir (Wien)*. 2016;158(2):305-312. doi:10.1007/s00701-015-2674-3

68. Duffau H, Capelle L. Preferential brain locations of low-grade gliomas. *Cancer*. 2004;100(12):2622-2626. doi:10.1002/cncr.20297

69. Mandonnet E, Capelle L, Duffau H. Extension of paralimbic low grade gliomas: toward an anatomical classification based on white matter invasion patterns. *J Neurooncol*. 2006;78(2):179-185. doi:10.1007/s11060-005-9084-y

70. Capelle L, Fontaine D, Mandonnet E, et al. Spontaneous and therapeutic prognostic factors in adult hemispheric World Health Organization Grade II gliomas: a series of 1097 cases: clinical article. *J Neurosurg*. 2013;118(6):1157-1168. doi:10.3171/2013.1.JNS121

71. Jung T-Y, Jung S, Moon J-H, Kim I-Y, Moon K-S, Jang W-Y. Early prognostic factors related to progression and malignant transformation of low-grade gliomas. *Clinical Neurology and Neurosurgery*. 2011;113(9):752-757. doi:10.1016/j.clineuro.2011.08.002

72. Murphy ES, Leyrer CM, Parsons M, et al. Risk Factors for Malignant Transformation of Low-Grade Glioma. *International Journal of Radiation Oncology*Biology*Physics*. 2018;100(4):965-971. doi:10.1016/j.ijrobp.2017.12.258

73. Kansal AR, Torquato S, Harsh GR IV, Chiocca EA, Deisboeck TS. Simulated brain tumor growth dynamics using a three-dimensional cellular automaton. *J Theor Biol*. 2000;203(4):367-382. doi:10.1006/jtbi.2000.2000

74. Larjavaara S, Mäntylä R, Salminen T, et al. Incidence of gliomas by anatomic location. *Neuro Oncol*. 2007;9(3):319-325. doi:10.1215/15228517-2007-016

75. Parisot S, Darlix A, Baumann C, et al. A Probabilistic Atlas of Diffuse WHO Grade II Glioma Locations in the Brain. *PLoS One*. 2016;11(1). doi:10.1371/journal.pone.0144200

76. Metellus P, Coulibaly B, Colin C, et al. Absence of IDH mutation identifies a novel radiologic and molecular subtype of WHO grade II gliomas with dismal prognosis. *Acta Neuropathol*. 2010;120(6):719-729. doi:10.1007/s00401-010-0777-8

77. Gozé C, Rigau V, Gibert L, Maudelonde T, Duffau H. Lack of complete 1p19q deletion in a consecutive series of 12 WHO grade II gliomas involving the insula: a marker of worse prognosis? *J Neurooncol*. 2009;91(1):1-5. doi:10.1007/s11060-008-9680-8

78. Laigle-Donadey F, Martin-Duverneuil N, Lejeune J, et al. Correlations between molecular profile and radiologic pattern in oligodendroglial tumors. *Neurology*. 2004;63(12):2360-2362.

79. Stockhammer F, Misch M, Helms H-J, et al. IDH1/2 mutations in WHO grade II astrocytomas associated with localization and seizure as the initial symptom. *Seizure*. 2012;21(3):194-197. doi:10.1016/j.seizure.2011.12.007

80. Freyschlag CF, Krieg SM, Kerschbaumer J, et al. Imaging practice in low-grade gliomas among European specialized centers and proposal for a minimum core of imaging. *J Neurooncol*. 2018;139(3):699-711. doi:10.1007/s11060-018-2916-3

81. Thust SC, Heiland S, Falini A, et al. Glioma imaging in Europe: A survey of 220 centres and recommendations for best clinical practice. *Eur Radiol*. 2018;28(8):3306-3317. doi:10.1007/s00330-018-5314-5

82. Dodo T, Okada T, Yamamoto A, et al. T1-weighted MR imaging of glioma at 3T: a comparative study of 3D MPRAGE vs. conventional 2D spin-echo imaging. *Clin Imaging*. 2016;40(6):1257-1261. doi:10.1016/j.clinimag.2016.08.016

83. Corell A, Carstam L, Smits A, Henriksson R, Jakola AS. Age and surgical outcome of low-grade glioma in Sweden. *Acta Neurol Scand*. 2018;138(4):359-368. doi:10.1111/ane.12973

84. Chen X, Dai J, Jiang T. Supratentorial WHO grade II glioma invasion: a morphologic study using sequential conventional MRI. *Br J Neurosurg*. 2010;24(2):196-201. doi:10.3109/02688690903518239

85. Ribba B, Kaloshi G, Peyre M, et al. A tumor growth inhibition model for low-grade glioma treated with chemotherapy or radiotherapy. *Clin Cancer Res*. 2012;18(18):5071-5080. doi:10.1158/1078-0432.CCR-12-0084

86. Castillo M, Smith JK, Kwock L, Wilber K. Apparent diffusion coefficients in the evaluation of high-grade cerebral gliomas. *AJNR Am J Neuroradiol*. 2001;22(1):60-64.

87. Fouke SJ, Benzinger T, Gibson D, Ryken TC, Kalkanis SN, Olson JJ. The role of imaging in the management of adults with diffuse low grade glioma: A systematic review and evidence-based clinical practice guideline. *J Neurooncol*. 2015;125(3):457-479. doi:10.1007/s11060-015-1908-9

88. Zhang L, Min Z, Tang M, Chen S, Lei X, Zhang X. The utility of diffusion MRI with quantitative ADC measurements for differentiating high-grade from low-grade cerebral gliomas: Evidence from a meta-analysis. *J Neurol Sci*. 2017;373:9-15. doi:10.1016/j.jns.2016.12.008

89. Chenevert TL, Stegman LD, Taylor JM, et al. Diffusion magnetic resonance imaging: an early surrogate marker of therapeutic efficacy in brain tumors. *J Natl Cancer Inst*. 2000;92(24):2029-2036. doi:10.1093/jnci/92.24.2029

90. Zhang H, Ma L, Shu C, Wang Y-B, Dong L-Q. Diagnostic accuracy of diffusion MRI with quantitative ADC measurements in differentiating glioma recurrence from radiation necrosis. *J Neurol Sci*. 2015;351(1-2):65-71. doi:10.1016/j.jns.2015.02.038

91. Larsson HBW, Hansen AE, Berg HK, Rostrup E, Haraldseth O. Dynamic contrast-enhanced quantitative perfusion measurement of the brain using T1-weighted MRI at 3T. *J Magn Reson Imaging*. 2008;27(4):754-762. doi:10.1002/jmri.21328

92. Thomsen H, Steffensen E, Larsson E-M. Perfusion MRI (dynamic susceptibility contrast imaging) with different measurement approaches for the evaluation of blood flow and blood volume in human gliomas. *Acta Radiol*. 2012;53(1):95-101. doi:10.1258/ar.2011.110242

93. Jahng G-H, Li K-L, Ostergaard L, Calamante F. Perfusion magnetic resonance imaging: a comprehensive update on principles and techniques. *Korean J Radiol*. 2014;15(5):554-577. doi:10.3348/kjr.2014.15.5.554

94. Law M, Yang S, Wang H, et al. Glioma grading: sensitivity, specificity, and predictive values of perfusion MR imaging and proton MR spectroscopic imaging compared with conventional MR imaging. *AJNR Am J Neuroradiol*. 2003;24(10):1989-1998.

95. Law M, Yang S, Babb JS, et al. Comparison of cerebral blood volume and vascular permeability from dynamic susceptibility contrast-enhanced perfusion MR imaging with glioma grade. *AJNR Am J Neuroradiol*. 2004;25(5):746-755.

96. Fernandez-Miranda JC, Pathak S, Engh J, et al. High-definition fiber tractography of the human brain: neuroanatomical validation and neurosurgical applications. *Neurosurgery*. 2012;71(2):430-453. doi:10.1227/NEU.0b013e3182592faa

97. Potgieser ARE, Wagemakers M, van Hulzen ALJ, de Jong BM, Hoving EW, Groen RJM. The role of diffusion tensor imaging in brain tumor surgery: a review of the literature. *Clin Neurol Neurosurg*. 2014;124:51-58. doi:10.1016/j.clineuro.2014.06.009

98. Abhinav K, Yeh F-C, Mansouri A, Zadeh G, Fernandez-Miranda JC. High-definition fiber tractography for the evaluation of perilesional white matter tracts in high-grade glioma surgery. *Neuro-oncology*. 2015;17(9):1199-1209. doi:10.1093/neuonc/nov113

99. Gimenez U, Perles-Barbacaru A-T, Millet A, et al. Microscopic DTI accurately identifies early glioma cell migration: correlation with multimodal imaging in a new glioma stem cell model. *NMR Biomed*. 2016;29(11):1553-1562. doi:10.1002/nbm.3608

100. Celtikci P, Fernandes-Cabral DT, Yeh F-C, Panesar SS, Fernandez-Miranda JC. Generalized q-sampling imaging fiber tractography reveals displacement and infiltration of fiber tracts in low-grade gliomas. *Neuroradiology*. 2018;60(3):267-280. doi:10.1007/s00234-018-1985-5

101. Bürgel U, Mädler B, Honey CR, Thron A, Gilsbach J, Coenen VA. Fiber tracking with distinct software tools results in a clear diversity in anatomical fiber tract portrayal. *Cent Eur Neurosurg*. 2009;70(1):27-35. doi:10.1055/s-0028-1087212

102. Farquharson S, Tournier J-D, Calamante F, et al. White matter fiber tractography: why we need to move beyond DTI. *J Neurosurg*. 2013;118(6):1367-1377. doi:10.3171/2013.2.JNS121294

103. Feigl GC, Hiergeist W, Fellner C, et al. Magnetic resonance imaging diffusion tensor tractography: evaluation of anatomic accuracy of different fiber tracking software packages. *World Neurosurg*. 2014;81(1):144-150. doi:10.1016/j.wneu.2013.01.004

104. Pujol S, Wells W, Pierpaoli C, et al. The DTI Challenge: Toward Standardized Evaluation of Diffusion Tensor Imaging Tractography for Neurosurgery. *J Neuroimaging*. 2015;25(6):875-882. doi:10.1111/jon.12283

105. Valk PE, Bailey DL, Townsend DW. *Positron Emission Tomography: Basic Science and Clinical Practice*. 1st ed. 2003. 3rd printing 2004 edition. Springer; 2004.

106. Phelps ME, ed. *PET: Physics, Instrumentation, and Scanners*. Springer-Verlag; 2006. doi:10.1007/0-387-34946-4

107. Smits A, Baumert BG. The Clinical Value of PET with Amino Acid Tracers for Gliomas WHO Grade II. *Int J Mol Imaging*. 2011;2011:372509. doi:10.1155/2011/372509

108. Näslund O, Smits A, Förander P, et al. Amino acid tracers in PET imaging of diffuse low-grade gliomas: a systematic review of preoperative applications. *Acta Neurochir (Wien)*. 2018;160(7):1451-1460. doi:10.1007/s00701-018-3563-3

109. Ius T, Angelini E, Thiebaut de Schotten M, Mandonnet E, Duffau H. Evidence for potentials and limitations of brain plasticity using an atlas of functional resectability of WHO grade II gliomas: towards a "minimal common brain." *Neuroimage*. 2011;56(3):992-1000. doi:10.1016/j.neuroimage.2011.03.022

110. Jakola AS, Unsgård G, Myrmel KS, et al. Low grade gliomas in eloquent locations - implications for surgical strategy, survival and long term quality of life. *PLoS ONE*. 2012;7(12):e51450. doi:10.1371/journal.pone.0051450

111. Jakola AS, Unsgård G, Myrmel KS, et al. Surgical strategies in low-grade gliomas and implications for long-term quality of life. *J Clin Neurosci*. 2014;21(8):1304-1309. doi:10.1016/j.jocn.2013.11.027

112. Chammas M, Saadeh F, Maaliki M, Assi H. Therapeutic Interventions in Adult Low-Grade Gliomas. :8.

113. McGirt MJ, Chaichana KL, Attenello FJ, et al. Extent of surgical resection is independently associated with survival in patients with hemispheric infiltrating low-grade gliomas. *Neurosurgery*. 2008;63(4):700-707; author reply 707-708. doi:10.1227/01.NEU.0000325729.41085.73

114. Sanai N, Berger MS. Glioma extent of resection and its impact on patient outcome. *Neurosurgery*. 2008;62(4):753-764; discussion 264-266. doi:10.1227/01.neu.0000318159.21731.cf

115. Smith JS, Chang EF, Lamborn KR, et al. Role of extent of resection in the long-term outcome of low-grade hemispheric gliomas. *J Clin Oncol*. 2008;26(8):1338-1345. doi:10.1200/JCO.2007.13.9337

116. Soffietti R, Baumert BG, Bello L, et al. Guidelines on management of low-grade gliomas: report of an EFNS-EANO Task Force. *Eur J Neurol*. 2010;17(9):1124-1133. doi:10.1111/j.1468-1331.2010.03151.x

117. Santini B, Talacchi A, Squintani G, Casagrande F, Capasso R, Miceli G. Cognitive outcome after awake surgery for tumors in language areas. *J Neurooncol*. 2012;108(2):319-326. doi:10.1007/s11060-012-0817-4

118. Duffau H. Is non-awake surgery for supratentorial adult low-grade glioma treatment still feasible? *Neurosurg Rev*. 2018;41(1):133-139. doi:10.1007/s10143-017-0918-9

119. Motomura K, Chalise L, Ohka F, et al. Neurocognitive and functional outcomes in patients with diffuse frontal lower-grade gliomas undergoing intraoperative awake brain mapping. *J Neurosurg*. Published online May 17, 2019:1-9. doi:10.3171/2019.3.JNS19211

120. Oberheim Bush NA, Chang S. Treatment Strategies for Low-Grade Glioma in Adults. *J Oncol Pract*. 2016;12(12):1235-1241. doi:10.1200/JOP.2016.018622

121. Karim AB, Maat B, Hatlevoll R, et al. A randomized trial on dose-response in radiation therapy of low-grade cerebral glioma: European Organization for Research and Treatment of Cancer (EORTC) Study 22844. *Int J Radiat Oncol Biol Phys*. 1996;36(3):549-556. doi:10.1016/s0360-3016(96)00352-5

122. Shaw E, Arusell R, Scheithauer B, et al. Prospective randomized trial of low- versus high-dose radiation therapy in adults with supratentorial low-grade glioma: initial report of a North Central Cancer Treatment Group/Radiation Therapy Oncology Group/Eastern Cooperative Oncology Group study. *J Clin Oncol*. 2002;20(9):2267-2276. doi:10.1200/JCO.2002.09.126

123. van den Bent M, Afra D, de Witte O, et al. Long-term efficacy of early versus delayed radiotherapy for low-grade astrocytoma and oligodendroglioma in adults: the EORTC 22845 randomised trial. *The Lancet*. 2005;366(9490):985-990. doi:10.1016/S0140-6736(05)67070-5

124. Surma-aho O, Niemelä M, Vilkki J, et al. Adverse long-term effects of brain radiotherapy in adult low-grade glioma patients. *Neurology*. 2001;56(10):1285-1290. doi:10.1212/wnl.56.10.1285

125. Douw L, Klein M, Fagel SS, et al. Cognitive and radiological effects of radiotherapy in patients with low-grade glioma: long-term follow-up. *Lancet Neurol*. 2009;8(9):810-818. doi:10.1016/S1474-4422(09)70204-2

126. Lawrie TA, Gillespie D, Dowswell T, et al. Long-term neurocognitive and other side effects of radiotherapy, with or without chemotherapy, for glioma. *Cochrane Database Syst Rev*. 2019;8:CD013047. doi:10.1002/14651858.CD013047.pub2

127. Wen PY, DeAngelis LM. Chemotherapy for low-grade gliomas: emerging consensus on its benefits. *Neurology*. 2007;68(21):1762-1763. doi:10.1212/01.wnl.0000266866.13748.a9

128. Buckner JC, Shaw EG, Pugh SL, et al. Radiation plus Procarbazine, CCNU, and Vincristine in Low-Grade Glioma. *N Engl J Med*. 2016;374(14):1344-1355. doi:10.1056/NEJMoa1500925

129. Brown TJ, Bota DA, van Den Bent MJ, et al. Management of low-grade glioma: a systematic review and meta-analysis. *Neurooncol Pract*. 2019;6(4):249-258. doi:10.1093/nop/npy034

130. Abrey LE. The impact of chemotherapy on cognitive outcomes in adults with primary brain tumors. *J Neurooncol*. 2012;108(2):285-290. doi:10.1007/s11060-012-0807-6

131. Kaloshi G, Benouaich-Amiel A, Diakite F, et al. Temozolomide for low-grade gliomas: predictive impact of 1p/19q loss on response and outcome. *Neurology*. 2007;68(21):1831-1836. doi:10.1212/01.wnl.0000262034.26310.a2

132. Alfonso JCL, Talkenberger K, Seifert M, et al. The biology and mathematical modelling of glioma invasion: a review. *J R Soc Interface*. 2017;14(136). doi:10.1098/rsif.2017.0490

133. Tracqui P, Cruywagen GC, Woodward DE, Bartoo GT, Murray JD, Alvord EC. A mathematical model of glioma growth: the effect of chemotherapy on spatio-temporal growth. *Cell Prolif*. 1995;28(1):17-31. doi:10.1111/j.1365-2184.1995.tb00036.x

134. Giese A, Westphal M. Glioma invasion in the central nervous system. *Neurosurgery*. 1996;39(2):235-250; discussion 250-252.

135. Swanson KR, Alvord EC, Murray JD. A quantitative model for differential motility of gliomas in grey and white matter. *Cell Prolif*. 2000;33(5):317-329. doi:10.1046/j.1365-2184.2000.00177.x

136. Swanson KR, Alvord EC, Murray JD. Virtual brain tumours (gliomas) enhance the reality of medical imaging and highlight inadequacies of current therapy. *Br J Cancer*. 2002;86(1):14-18. doi:10.1038/sj.bjc.6600021

137. Swanson KR, Bridge C, Murray JD, Alvord EC. Virtual and real brain tumors: using mathematical modeling to quantify glioma growth and invasion. *J Neurol Sci*. 2003;216(1):1-10. doi:10.1016/j.jns.2003.06.001

138. Jbabdi S, Mandonnet E, Duffau H, et al. Simulation of anisotropic growth of low-grade gliomas using diffusion tensor imaging. *Magn Reson Med*. 2005;54(3):616-624. doi:10.1002/mrm.20625

139. Engwer C, Hillen T, Knappitsch M, Surulescu C. Glioma follow white matter tracts: a multiscale DTI-based model. *J Math Biol*. 2015;71(3):551-582. doi:10.1007/s00285-014-0822-7

140. Konukoglu E, Clatz O, Bondiau P-Y, Delingette H, Ayache N. Extrapolating glioma invasion margin in brain magnetic resonance images: suggesting new irradiation margins. *Med Image Anal*. 2010;14(2):111-125. doi:10.1016/j.media.2009.11.005

141. Wakana S, Caprihan A, Panzenboeck MM, et al. Reproducibility of quantitative tractography methods applied to cerebral white matter. *Neuroimage*. 2007;36(3):630-644. doi:10.1016/j.neuroimage.2007.02.049

142. Verhoeven JS, Sage CA, Leemans A, et al. Construction of a stereotaxic DTI atlas with full diffusion tensor information for studying white matter maturation from childhood to adolescence using tractography-based segmentations. *Hum Brain Mapp*. 2010;31(3):470-486. doi:10.1002/hbm.20880

143. Cahill D, Turcan S. Origin of Gliomas. *Semin Neurol*. 2018;38(1):5-10. doi:10.1055/s-0037-1620238

144. Schwartz MS, Morris J, Sarid J. Overexpression of oncogene products can cause tumor progression without parenchymal infiltration in the rat brain. *Cancer Res*. 1991;51(13):3595-3601.

145. Giese A, Loo MA, Rief MD, Tran N, Berens ME. Substrates for astrocytoma invasion. *Neurosurgery*. 1995;37(2):294-301; discussion 301-302.

146. Harsh GR, Wilson CB. *Neuroepithelial Tumors of the Adult Brain*. Vol Youmans JR (ed): Neurological Surgery. ed 3. W.B. Saunders Co.; 1990.

147. Sarubbo S, De Benedictis A, Merler S, et al. Towards a functional atlas of human white matter. *Hum Brain Mapp*. 2015;36(8):3117-3136. doi:10.1002/hbm.22832

148. Smits A, Zetterling M, Lundin M, et al. Neurological Impairment Linked with Cortico-Subcortical Infiltration of Diffuse Low-Grade Gliomas at Initial Diagnosis Supports Early Brain Plasticity. *Front Neurol*. 2015;6. doi:10.3389/fneur.2015.00137

149. Duffau H. A two-level model of interindividual anatomo-functional variability of the brain and its implications for neurosurgery. *Cortex*. 2017;86:303-313. doi:10.1016/j.cortex.2015.12.009

150. Latini F. New insights in the limbic modulation of visual inputs: the role of the inferior longitudinal fasciculus and the Li-Am bundle. *Neurosurg Rev*. 2015;38(1):179-189; discussion 189-190. doi:10.1007/s10143-014-0583-1

151. Latini F, Hjortberg M, Aldskogius H, Ryttlefors M. The Classical Pathways of Occipital Lobe Epileptic Propagation Revised in the Light of White Matter Dissection. *Behav Neurol*. 2015;2015:872645. doi:10.1155/2015/872645

152. Latini F, Mårtensson J, Larsson E-M, et al. Segmentation of the inferior longitudinal fasciculus in the human brain: A white matter dissection and diffusion tensor tractography study. *Brain Res*. 2017;1675:102-115. doi:10.1016/j.brainres.2017.09.005

153. Latini F, Trevisi G, Fahlström M, et al. New insights into the anatomy, connectivity and clinical implications of the middle longitudinal fasciculus. *Front Neuroanat*. 2020;14. doi:10.3389/fnana.2020.610324

154. Liewald D, Miller R, Logothetis N, Wagner H-J, Schüz A. Distribution of axon diameters in cortical white matter: an electron-microscopic study on three human brains and a macaque. *Biol Cybern*. 2014;108(5):541-557. doi:10.1007/s00422-014-0626-2

155. Partadiredja G, Miller R, Oorschot DE. The number, size, and type of axons in rat subcortical white matter on left and right sides: a stereological, ultrastructural study. *J Neurocytol*. 2003;32(9):1165-1179. doi:10.1023/B:NEUR.0000021910.65920.41

156. Stikov N, Campbell JSW, Stroh T, et al. In vivo histology of the myelin g-ratio with magnetic resonance imaging. *NeuroImage*. 2015;118:397-405. doi:10.1016/j.neuroimage.2015.05.023

157. Berntsson SG, Falk A, Savitcheva I, et al. Perfusion and diffusion MRI combined with ^{11}C-methionine PET in the preoperative evaluation of suspected adult low-grade gliomas. *J Neurooncol*. 2013;114(2):241-249. doi:10.1007/s11060-013-1178-3

158. Latini F, Larsson E-M, Ryttlefors M. Rapid and Accurate MRI Segmentation of Peritumoral Brain Edema in Meningiomas. *Clin Neuroradiol*. 2017;27(2):145-152. doi:10.1007/s00062-015-0481-0

159. Evans AC, Marrett S, Neelin P, et al. Anatomical mapping of functional activation in stereotactic coordinate space. *Neuroimage*. 1992;1(1):43-53.

160. Klein S, Staring M, Murphy K, Viergever MA, Pluim JPW. elastix: a toolbox for intensity-based medical image registration. *IEEE Trans Med Imaging*. 2010;29(1):196-205. doi:10.1109/TMI.2009.2035616

161. Van Essen DC, Smith SM, Barch DM, et al. The WU-Minn Human Connectome Project: an overview. *Neuroimage*. 2013;80:62-79. doi:10.1016/j.neuroimage.2013.05.041

162. Andersson JLR, Skare S, Ashburner J. How to correct susceptibility distortions in spin-echo echo-planar images: application to diffusion tensor imaging. *Neuroimage*. 2003;20(2):870-888. doi:10.1016/S1053-8119(03)00336-7

163. Sotiropoulos SN, Moeller S, Jbabdi S, et al. Effects of image reconstruction on fiber orientation mapping from multichannel diffusion MRI: Reducing the noise floor using SENSE. *Magnetic Resonance in Medicine*. 2013;70(6):1682-1689. doi:10.1002/mrm.24623

164. Andersson JLR, Sotiropoulos SN. An integrated approach to correction for off-resonance effects and subject movement in diffusion MR imaging. *Neuroimage*. 2016;125:1063-1078. doi:10.1016/j.neuroimage.2015.10.019

165. Yeh F-C, Wedeen VJ, Tseng W-YI. Generalized q-sampling imaging. *IEEE Trans Med Imaging*. 2010;29(9):1626-1635. doi:10.1109/TMI.2010.2045126

166. Yeh F-C, Verstynen TD, Wang Y, Fernández-Miranda JC, Tseng W-YI. Deterministic diffusion fiber tracking improved by quantitative anisotropy. *PLoS ONE*. 2013;8(11):e80713. doi:10.1371/journal.pone.0080713

167. Desikan RS, Ségonne F, Fischl B, et al. An automated labeling system for subdividing the human cerebral cortex on MRI scans into gyral based regions of interest. *Neuroimage*. 2006;31(3):968-980. doi:10.1016/j.neuroimage.2006.01.021

168. Schurz M, Tholen MG, Perner J, Mars RB, Sallet J. Specifying the brain anatomy underlying temporo-parietal junction activations for theory of mind: A review using probabilistic atlases from different imaging modalities. *Human Brain Mapping*. 2017;38(9):4788-4805. doi:10.1002/hbm.23675

169. Yeh F-C, Tseng W-YI. NTU-90: a high angular resolution brain atlas constructed by q-space diffeomorphic reconstruction. *Neuroimage*. 2011;58(1):91-99. doi:10.1016/j.neuroimage.2011.06.021

170. Yeh F-C, Wedeen VJ, Tseng W-YI. Generalized q-sampling imaging. *IEEE Trans Med Imaging*. 2010;29(9):1626-1635. doi:10.1109/TMI.2010.2045126

171. Yeh F-C, Liu L, Hitchens TK, Wu YL. Mapping immune cell infiltration using restricted diffusion MRI. *Magn Reson Med*. 2017;77(2):603-612. doi:10.1002/mrm.26143

172. Latini F, Fahlström M, Berntsson SG, Larsson E-M, Smits A, Ryttlefors M. A novel radiological classification system for cerebral gliomas: The Brain-Grid. *PLoS ONE*. 2019;14(1):e0211243. doi:10.1371/journal.pone.0211243

173. Yeh F-C, Zaydan IM, Suski VR, et al. Differential tractography as a track-based biomarker for neuronal injury. *Neuroimage*. 2019;202:116131. doi:10.1016/j.neuroimage.2019.116131

174. Riva M, Fava E, Gallucci M, et al. Monopolar high-frequency language mapping: can it help in the surgical management of gliomas? A comparative clinical study. *J Neurosurg*. 2016;124(5):1479-1489. doi:10.3171/2015.4.JNS14333

175. Rossi M, Sani S, Nibali MC, Fornia L, Bello L, Byrne RW. Mapping in Low-Grade Glioma Surgery: Low- and High-Frequency Stimulation. *Neurosurg Clin N Am*. 2019;30(1):55-63. doi:10.1016/j.nec.2018.08.003

176. Verst SM, de Aguiar PHP, Joaquim M a. S, Vieira VG, Sucena ABC, Maldaun MVC. Monopolar 250-500 Hz language mapping: Results of 41 patients. *Clin Neurophysiol Pract*. 2019;4:1-8. doi:10.1016/j.cnp.2018.11.002

177. Gogos AJ, Young JS, Morshed RA, Hervey-Jumper SL, Berger MS. Awake glioma surgery: technical evolution and nuances. *J Neurooncol*. 2020;147(3):515-524. doi:10.1007/s11060-020-03482-z

178. Gerard IJ, Kersten-Oertel M, Petrecca K, Sirhan D, Hall JA, Collins DL. Brain shift in neuronavigation of brain tumors: A review. *Med Image Anal*. 2017;35:403-420. doi:10.1016/j.media.2016.08.007

179. Ohue S, Kumon Y, Nagato S, et al. Evaluation of Intraoperative Brain Shift Using an Ultrasound-Linked Navigation System for Brain Tumor Surgery. *Neurol Med Chir(Tokyo)*. 2010;50(4):291-300. doi:10.2176/nmc.50.291

180. Rasmussen I-A, Lindseth F, Rygh OM, et al. Functional neuronavigation combined with intra-operative 3D ultrasound: Initial experiences during surgical resections close to eloquent brain areas and future directions in automatic brain shift compensation of preoperative data. *Acta Neurochir (Wien)*. 2007;149(4):365-378. doi:10.1007/s00701-006-1110-0

181. Latini F, Mårtensson J, Larsson E-M, et al. Segmentation of the inferior longitudinal fasciculus in the human brain: A white matter dissection and diffusion tensor tractography study. *Brain Research*. 2017;1675:102-115. doi:10.1016/j.brainres.2017.09.005

182. Sreedharan RM, Menon AC, James JS, Kesavadas C, Thomas SV. Arcuate fasciculus laterality by diffusion tensor imaging correlates with language laterality by functional MRI in preadolescent children. *Neuroradiology*. 2015;57(3):291-297. doi:10.1007/s00234-014-1469-1

183. Kaplan EL, Meier P. Nonparametric Estimation from Incomplete Observations. *Journal of the American Statistical Association*. 1958;53(282):457-481. doi:10.1080/01621459.1958.10501452

184. Carter JV, Pan J, Rai SN, Galandiuk S. ROC-ing along: Evaluation and interpretation of receiver operating characteristic curves. *Surgery*. 2016;159(6):1638-1645. doi:10.1016/j.surg.2015.12.029

185. Cox DR. Regression Models and Life-Tables. *Journal of the Royal Statistical Society: Series B (Methodological)*. 1972;34(2):187-202. doi:10.1111/j.2517-6161.1972.tb00899.x

186. Sporns O, Tononi G, Kötter R. The Human Connectome: A Structural Description of the Human Brain. *PLoS Comput Biol*. 2005;1(4). doi:10.1371/journal.pcbi.0010042

187. Sporns O. The human connectome: a complex network: The human connectome. *Annals of the New York Academy of Sciences*. 2011;1224(1):109-125. doi:10.1111/j.1749-6632.2010.05888.x

188. Kong NW, Gibb WR, Tate MC. Neuroplasticity: Insights from Patients Harboring Gliomas. *Neural Plast*. 2016;2016. doi:10.1155/2016/2365063

189. Duffau H. Higher-Order Surgical Questions for Diffuse Low-Grade Gliomas: Supramaximal Resection, Neuroplasticity, and Screening. *Neurosurg Clin N Am*. 2019;30(1):119-128. doi:10.1016/j.nec.2018.08.009

190. Herbet G, Maheu M, Costi E, Lafargue G, Duffau H. Mapping neuroplastic potential in brain-damaged patients. *Brain*. 2016;139(3):829-844. doi:10.1093/brain/awv394

191. Cohen L, Henry C, Dehaene S, et al. The pathophysiology of letter-by-letter reading. *Neuropsychologia*. 2004;42(13):1768-1780. doi:10.1016/j.neuropsychologia.2004.04.018

192. Mandonnet E, Gatignol P, Duffau H. Evidence for an occipito-temporal tract underlying visual recognition in picture naming. *Clin Neurol Neurosurg*. 2009;111(7):601-605. doi:10.1016/j.clineuro.2009.03.007

193. Zemmoura I, Herbet G, Moritz-Gasser S, Duffau H. New insights into the neural network mediating reading processes provided by cortico-subcortical electrical mapping. *Hum Brain Mapp*. 2015;36(6):2215-2230. doi:10.1002/hbm.22766

194. Makris N, Papadimitriou GM, Kaiser JR, Sorg S, Kennedy DN, Pandya DN. Delineation of the Middle Longitudinal Fascicle in Humans: A Quantitative, In Vivo, DT-MRI Study. *Cerebral Cortex*. 2009;19(4):777-785. doi:10.1093/cercor/bhn124

195. Makris N, Preti MG, Wassermann D, et al. Human middle longitudinal fascicle: segregation and behavioral-clinical implications of two distinct fiber connections linking temporal pole and superior temporal gyrus with the angular gyrus or superior parietal lobule using multi-tensor tractography. *Brain Imaging and Behavior*. 2013;7(3):335-352. doi:10.1007/s11682-013-9235-2

196. Makris N, Zhu A, Papadimitriou GM, et al. Mapping temporo-parietal and temporo-occipital cortico-cortical connections of the human middle longitudinal fascicle in subject-specific, probabilistic, and stereotaxic Talairach spaces. *Brain Imaging and Behavior*. 2017;11(5):1258-1277. doi:10.1007/s11682-016-9589-3

197. Menjot de Champfleur N, Lima Maldonado I, Moritz-Gasser S, et al. Middle longitudinal fasciculus delineation within language pathways: A diffusion tensor imaging study in human. *European Journal of Radiology*. 2013;82(1):151-157. doi:10.1016/j.ejrad.2012.05.034

198. Suzuki Y, Enatsu R, Kanno A, Ochi S, Mikuni N. The auditory cortex network in the posterior superior temporal area. *Clinical Neurophysiology*. 2018;129(10):2132-2136. doi:10.1016/j.clinph.2018.07.014

199. Tremblay P, Perron M, Deschamps I, et al. The role of the arcuate and middle longitudinal fasciculi in speech perception in noise in adulthood. *Human Brain Mapping*. 2019;40(1):226-241. doi:10.1002/hbm.24367

200. Kalyvas A, Koutsarnakis C, Komaitis S, et al. Mapping the human middle longitudinal fasciculus through a focused anatomo-imaging study: shifting the paradigm of its segmentation and connectivity pattern. *Brain Struct Funct*. 2020;225(1):85-119. doi:10.1007/s00429-019-01987-6

201. Maldonado IL, de Champfleur NM, Velut S, Destrieux C, Zemmoura I, Duffau H. Evidence of a middle longitudinal fasciculus in the human brain from fiber dissection. *Journal of Anatomy*. 2013;223(1):38-45. doi:10.1111/joa.12055

202. Wang Y, Fernández-Miranda JC, Verstynen T, Pathak S, Schneider W, Yeh F-C. Rethinking the Role of the Middle Longitudinal Fascicle in Language and Auditory Pathways. *Cerebral Cortex*. 2013;23(10):2347-2356. doi:10.1093/cercor/bhs225

203. Wang F, Sun T, Li X-G, Liu N-J. Diffusion tensor tractography of the temporal stem on the inferior limiting sulcus. *Journal of Neurosurgery*. 2008;108(4):775-781. doi:10.3171/JNS/2008/108/4/0775

204. Dell'acqua F, Scifo P, Rizzo G, et al. A modified damped Richardson-Lucy algorithm to reduce isotropic background effects in spherical deconvolution. *Neuroimage*. 2010;49(2):1446-1458. doi:10.1016/j.neuroimage.2009.09.033

205. De Witt Hamer PC, Moritz-Gasser S, Gatignol P, Duffau H. Is the human left middle longitudinal fascicle essential for language? A brain electrostimulation study. *Hum Brain Mapp*. 2011;32(6):962-973. doi:10.1002/hbm.21082

206. Berrios GE. Musical hallucinations. A historical and clinical study. *Br J Psychiatry*. 1990;156:188-194. doi:10.1192/bjp.156.2.188

207. Hugdahl K. Auditory Hallucinations as Translational Psychiatry: Evidence from Magnetic Resonance Imaging. *Balkan Med J*. 2017;34(6):504-513. doi:10.4274/balkanmedj.2017.1226

208. Hugdahl K. "Hearing voices": auditory hallucinations as failure of top-down control of bottom-up perceptual processes. *Scand J Psychol*. 2009;50(6):553-560. doi:10.1111/j.1467-9450.2009.00775.x

209. Lagemann T, Rentzsch J, Montag C, et al. Early orbitofrontal hyperactivation in obsessive-compulsive disorder. *Psychiatry Res*. 2012;202(3):257-263. doi:10.1016/j.pscychresns.2011.10.002

210. Orjuela Rojas JM, Lizarazo Rodríguez IL. The Stuck Song Syndrome: A Case of Musical Obsessions. *Am J Case Rep*. 2018;19:1329-1333. doi:10.12659/AJCR.912402

211. Zungu-Dirwayi N, Hugo F, van Heerden BB, Stein DJ. Are musical obsessions a temporal lobe phenomenon? *J Neuropsychiatry Clin Neurosci*. 1999;11(3):398-400. doi:10.1176/jnp.11.3.398

212. Duma CM, Kim BS, Chen PV, et al. Upfront boost Gamma Knife "leading-edge" radiosurgery to FLAIR MRI-defined tumor migration pathways in 174 patients with glioblastoma multiforme: a 15-year assessment of a novel therapy. *J Neurosurg*. 2016;125(Suppl 1):40-49. doi:10.3171/2016.7.GKS161460

213. Schiff D. Low-grade Gliomas. *Continuum (Minneap Minn)*. 2017;23(6, Neuro-oncology):1564-1579. doi:10.1212/CON.0000000000000537

214. Marín O, Rubenstein JLR. Cell Migration in the Forebrain. *Annual Review of Neuroscience*. 2003;26(1):441-483. doi:10.1146/annurev.neuro.26.041002.131058

215. Zhan JS, Gao K, Chai RC, et al. Astrocytes in Migration. *Neurochem Res*. 2017;42(1):272-282. doi:10.1007/s11064-016-2089-4

216. Olivier C, Cobos I, Villegas EMP, et al. Monofocal origin of telencephalic oligodendrocytes in the anterior entopeduncular area of the chick embryo. *Development*. 2001;128(10):1757-1769.

217. González-Arnay E, González-Gómez M, Meyer G. A Radial Glia Fascicle Leads Principal Neurons from the Pallial-Subpallial Boundary into the Developing Human Insula. *Front Neuroanat*. 2017;11. doi:10.3389/fnana.2017.00111

218. Malatesta P, Hartfuss E, Götz M. Isolation of radial glial cells by fluorescent-activated cell sorting reveals a neuronal lineage. *Development*. 2000;127(24):5253-5263.

219. Heins N, Malatesta P, Cecconi F, et al. Glial cells generate neurons: the role of the transcription factor Pax6. *Nat Neurosci*. 2002;5(4):308-315. doi:10.1038/nn828

220. Ge W-P, Jia J-M. Local production of astrocytes in the cerebral cortex. *Neuroscience*. 2016;323:3-9. doi:10.1016/j.neuroscience.2015.08.057

221. Tripathi RB, Clarke LE, Burzomato V, et al. Dorsally- and ventrally-derived oligodendrocytes have similar electrical properties but myelinate preferred tracts. *J Neurosci*. 2011;31(18):6809-6819. doi:10.1523/JNEUROSCI.6474-10.2011

222. Ono K, Yasui Y, Rutishauser U, Miller RH. Focal Ventricular Origin and Migration of Oligodendrocyte Precursors into the Chick Optic Nerve. *Neuron*. 1997;19(2):283-292. doi:10.1016/S0896-6273(00)80939-3

223. Spassky N, Goujet-Zalc C, Parmantier E, et al. Multiple Restricted Origin of Oligodendrocytes. *J Neurosci*. 1998;18(20):8331-8343. doi:10.1523/JNEUROSCI.18-20-08331.1998

224. Cuddapah VA, Robel S, Watkins S, Sontheimer H. A neurocentric perspective on glioma invasion. *Nat Rev Neurosci*. 2014;15(7):455-465. doi:10.1038/nrn3765

225. Fathallah-Shaykh HM, DeAtkine A, Coffee E, et al. Diagnosing growth in low-grade gliomas with and without longitudinal volume measurements: A retrospective observational study. *PLoS Med*. 2019;16(5). doi:10.1371/journal.pmed.1002810

226. Painter KJ, Hillen T. Mathematical modelling of glioma growth: The use of Diffusion Tensor Imaging (DTI) data to predict the anisotropic pathways of cancer invasion. *Journal of Theoretical Biology*. 2013;323:25-39. doi:10.1016/j.jtbi.2013.01.014

227. Giacci MK, Bartlett CA, Huynh M, Kilburn MR, Dunlop SA, Fitzgerald M. Three dimensional electron microscopy reveals changing axonal and myelin morphology along normal and partially injured optic nerves. *Scientific Reports*. 2018;8(1):3979. doi:10.1038/s41598-018-22361-2

228. Lee H-H, Yaros K, Veraart J, et al. Along-axon diameter variation and axonal orientation dispersion revealed with 3D electron microscopy: implications for quantifying brain white matter microstructure with histology and diffusion MRI. *Brain Struct Funct*. 2019;224(4):1469-1488. doi:10.1007/s00429-019-01844-6

229. Schmithorst VJ, Holland SK, Dardzinski BJ. Developmental differences in white matter architecture between boys and girls. *Hum Brain Mapp*. 2007;29(6):696-710. doi:10.1002/hbm.20431

230. Coelho S, Pozo JM, Costantini M, et al. Histological data of axons, astrocytes, and myelin in deep subcortical white matter populations. *Data Brief*. 2019;23. doi:10.1016/j.dib.2019.103762

231. Benjamini D, Komlosh ME, Holtzclaw LA, Nevo U, Basser PJ. White matter microstructure from nonparametric axon diameter distribution mapping. *Neuroimage*. 2016;135:333-344. doi:10.1016/j.neuroimage.2016.04.052

232. Mathiisen TM, Lehre KP, Danbolt NC, Ottersen OP. The perivascular astroglial sheath provides a complete covering of the brain microvessels: an electron microscopic 3D reconstruction. *Glia*. 2010;58(9):1094-1103. doi:10.1002/glia.20990

233. Wolburg H, Noell S, Mack A, Wolburg-Buchholz K, Fallier-Becker P. Brain endothelial cells and the glio-vascular complex. *Cell Tissue Res*. 2009;335(1):75-96. doi:10.1007/s00441-008-0658-9

234. Mukherjee P, Miller JH, Shimony JS, et al. Diffusion-tensor MR imaging of gray and white matter development during normal human brain maturation. *AJNR Am J Neuroradiol*. 2002;23(9):1445-1456.

235. Qiu D, Tan L-H, Zhou K, Khong P-L. Diffusion tensor imaging of normal white matter maturation from late childhood to young adulthood: voxel-wise evaluation of mean diffusivity, fractional anisotropy, radial and axial diffusivities, and correlation with reading development. *Neuroimage*. 2008;41(2):223-232. doi:10.1016/j.neuroimage.2008.02.023

236. Suzuki Y, Matsuzawa H, Kwee IL, Nakada T. Absolute eigenvalue diffusion tensor analysis for human brain maturation. *NMR Biomed*. 2003;16(5):257-260. doi:10.1002/nbm.848

237. Takahashi M, Ono J, Harada K, Maeda M, Hackney DB. Diffusional anisotropy in cranial nerves with maturation: quantitative evaluation with diffusion MR imaging in rats. *Radiology*. 2000;216(3):881-885. doi:10.1148/radiology.216.3.r00se41881

238. Burgess PK, Kulesa PM, Murray JD, Alvord EC. The interaction of growth rates and diffusion coefficients in a three-dimensional mathematical model of gliomas. *J Neuropathol Exp Neurol*. 1997;56(6):704-713.

239. Duffau H. Functional Mapping before and after Low-Grade Glioma Surgery: A New Way to Decipher Various Spatiotemporal Patterns of Individual Neuroplastic Potential in Brain Tumor Patients. *Cancers*. 2020;12(9). doi:10.3390/cancers12092611

240. Duffau H. Does post-lesional subcortical plasticity exist in the human brain? *Neuroscience Research*. 2009;65(2):131-135. doi:10.1016/j.neures.2009.07.002

241. Latini F, Fahlström M, Hesselager G, Zetterling M, Ryttlefors M. Differences in the preferential location and invasiveness of diffuse low-grade gliomas and their impact on outcome. *Cancer Med*. 2020;9(15):5446-5458. doi:10.1002/cam4.3216

242. Sanai N, Polley M-Y, Berger MS. Insular glioma resection: assessment of patient morbidity, survival, and tumor progression. *J Neurosurg*. 2010;112(1):1-9. doi:10.3171/2009.6.JNS0952

243. Wang J, Liang Y, Chen H, et al. Structural changes in white matter lesion patients and their correlation with cognitive impairment. *Neuropsychiatr Dis Treat*. 2019;15:1355-1363. doi:10.2147/NDT.S194803

244. Onay A, Yapıcı Eser H, Ulaşoğlu Yıldız Ç, Aslan S, Talı ET. A combined VBM and DTI study of schizophrenia: bilateral decreased insula volume and cerebral white matter disintegrity corresponding to subinsular white matter projections unlinked to clinical symptomatology. *Diagn Interv Radiol*. 2017;23(5):390-397. doi:10.5152/dir.2017.16519

245. Wu T, Wang X, Wu Q, et al. Anterior insular cortex is a bottleneck of cognitive control. *Neuroimage*. 2019;195:490-504. doi:10.1016/j.neuroimage.2019.02.042

246. Duffau H. Awake surgery for incidental WHO grade II gliomas involving eloquent areas. *Acta Neurochir (Wien)*. 2012;154(4):575-584; discussion 584. doi:10.1007/s00701-011-1216-x

247. Lima GL de O, Zanello M, Mandonnet E, Taillandier L, Pallud J, Duffau H. Incidental diffuse low-grade gliomas: from early detection to preventive neuro-oncological surgery. *Neurosurg Rev*. 2016;39(3):377-384. doi:10.1007/s10143-015-0675-6

248. Pallud J, Audureau E, Blonski M, et al. Epileptic seizures in diffuse low-grade gliomas in adults. *Brain*. 2014;137(Pt 2):449-462. doi:10.1093/brain/awt345

249. Rudà R, Bello L, Duffau H, Soffietti R. Seizures in low-grade gliomas: natural history, pathogenesis, and outcome after treatments. *Neuro Oncol*. 2012;14(Suppl 4):iv55-iv64. doi:10.1093/neuonc/nos199

250. Douw L, van Dellen E, de Groot M, et al. Epilepsy is related to theta band brain connectivity and network topology in brain tumor patients. *BMC Neurosci*. 2010;11:103. doi:10.1186/1471-2202-11-103

251. Bosma I, Douw L, Bartolomei F, et al. Synchronized brain activity and neurocognitive function in patients with low-grade glioma: A magnetoencephalography study. *Neuro Oncol*. 2008;10(5):734-744. doi:10.1215/15228517-2008-034

252. Bartolomei F, Bosma I, Klein M, et al. How do brain tumors alter functional connectivity? A magnetoencephalography study. *Ann Neurol*. 2006;59(1):128-138. doi:10.1002/ana.20710

253. Ponten SC, Bartolomei F, Stam CJ. Small-world networks and epilepsy: graph theoretical analysis of intracerebrally recorded mesial temporal lobe seizures. *Clin Neurophysiol*. 2007;118(4):918-927. doi:10.1016/j.clinph.2006.12.002

254. Ghinda CD, Duffau H. Network Plasticity and Intraoperative Mapping for Personalized Multimodal Management of Diffuse Low-Grade Gliomas. *Frontiers in Surgery*. 2017;4:3. doi:10.3389/fsurg.2017.00003

255. Fuchs E, Flügge G. Adult Neuroplasticity: More Than 40 Years of Research. *Neural Plast*. 2014;2014. doi:10.1155/2014/541870

256. Wang S, Young KM. White matter plasticity in adulthood. *Neuroscience*. 2014;276:148-160. doi:10.1016/j.neuroscience.2013.10.018

257. Jones DK, Cercignani M. Twenty-five pitfalls in the analysis of diffusion MRI data. *NMR Biomed*. 2010;23(7):803-820. doi:10.1002/nbm.1543

258. Jones DK, Knösche TR, Turner R. White matter integrity, fiber count, and other fallacies: the do's and don'ts of diffusion MRI. *Neuroimage*. 2013;73:239-254. doi:10.1016/j.neuroimage.2012.06.081

259. Jones DK. Determining and visualizing uncertainty in estimates of fiber orientation from diffusion tensor MRI. *Magn Reson Med*. 2003;49(1):7-12. doi:10.1002/mrm.10331

260. Behrens TEJ, Berg HJ, Jbabdi S, Rushworth MFS, Woolrich MW. Probabilistic diffusion tractography with multiple fibre orientations: What can we gain? *Neuroimage*. 2007;34(1):144-155. doi:10.1016/j.neuroimage.2006.09.018

261. Mårtensson J, Nilsson M, Ståhlberg F, et al. Spatial analysis of diffusion tensor tractography statistics along the inferior fronto-occipital fasciculus with application in progressive supranuclear palsy. *MAGMA*. 2013;26(6):527-537. doi:10.1007/s10334-013-0368-5

262. Vos SB, Jones DK, Viergever MA, Leemans A. Partial volume effect as a hidden covariate in DTI analyses. *Neuroimage*. 2011;55(4):1566-1576. doi:10.1016/j.neuroimage.2011.01.048

263. Panesar SS, Yeh F-C, Jacquesson T, Hula W, Fernandez-Miranda JC. A Quantitative Tractography Study Into the Connectivity, Segmentation and Laterality of the Human Inferior Longitudinal Fasciculus. *Front Neuroanat*. 2018;12:47. doi:10.3389/fnana.2018.00047

264. Stadlbauer A, Salomonowitz E, Strunk G, Hammen T, Ganslandt O. Age-related degradation in the central nervous system: assessment with diffusion-tensor imaging and quantitative fiber tracking. *Radiology*. 2008;247(1):179-188. doi:10.1148/radiol.2471070707

265. Beaulieu C. The basis of anisotropic water diffusion in the nervous system - a technical review. *NMR Biomed*. 2002;15(7-8):435-455. doi:10.1002/nbm.782

266. Tournier J-D, Mori S, Leemans A. Diffusion tensor imaging and beyond. *Magn Reson Med*. 2011;65(6):1532-1556. doi:10.1002/mrm.22924

267. Thomason ME, Dougherty RF, Colich NL, et al. COMT genotype affects prefrontal white matter pathways in children and adolescents. *Neuroimage*. 2010;53(3):926-934. doi:10.1016/j.neuroimage.2010.01.033

268. Hoeft F, Barnea-Goraly N, Haas BW, et al. More is not always better: increased fractional anisotropy of superior longitudinal fasciculus associated with poor visuospatial abilities in Williams syndrome. *J Neurosci*. 2007;27(44):11960-11965. doi:10.1523/JNEUROSCI.3591-07.2007

269. Soares JM, Marques P, Alves V, Sousa N. A hitchhiker's guide to diffusion tensor imaging. *Front Neurosci*. 2013;7. doi:10.3389/fnins.2013.00031

270. Conti Nibali M, Rossi M, Sciortino T, et al. Preoperative surgical planning of glioma: limitations and reliability of fMRI and DTI tractography. *J Neurosurg Sci*. 2019;63(2):127-134. doi:10.23736/S0390-5616.18.04597-6

271. Duffau H. Diffusion tensor imaging is a research and educational tool, but not yet a clinical tool. *World Neurosurg*. 2014;82(1-2):e43-45. doi:10.1016/j.wneu.2013.08.054

272. Aghi MK, Nahed BV, Sloan AE, Ryken TC, Kalkanis SN, Olson JJ. The role of surgery in the management of patients with diffuse low grade glioma: A systematic review and evidence-based clinical practice guideline. *J Neurooncol*. 2015;125(3):503-530. doi:10.1007/s11060-015-1867-1

273. Duffau H. Diffuse low-grade glioma, oncological outcome and quality of life: a surgical perspective. *Curr Opin Oncol*. 2018;30(6):383-389. doi:10.1097/CCO.0000000000000483

274. Duffau H. The role of surgery in low-grade gliomas: do timing and extent of resection matter? *CNS Oncol*. Published online July 18, 2017. doi:10.2217/cns-2017-0009

275. McKhann GM, Duffau H. Low-Grade Glioma: Epidemiology, Pathophysiology, Clinical Features, and Treatment. *Neurosurg Clin N Am*. 2019;30(1):xiii-xiv. doi:10.1016/j.nec.2018.10.001

# Acta Universitatis Upsaliensis

*Digital Comprehensive Summaries of Uppsala Dissertations
from the Faculty of Medicine* 1744

Editor: The Dean of the Faculty of Medicine

A doctoral dissertation from the Faculty of Medicine, Uppsala
University, is usually a summary of a number of papers. A few
copies of the complete dissertation are kept at major Swedish
research libraries, while the summary alone is distributed
internationally through the series Digital Comprehensive
Summaries of Uppsala Dissertations from the Faculty of
Medicine. (Prior to January, 2005, the series was published
under the title "Comprehensive Summaries of Uppsala
Dissertations from the Faculty of Medicine".)